Seismic Acquisition in a Shallow Marine Sea Ice Covered Environment: The Significance of Survey Geometry and Possible Impacts on Pinnipeds

Helene Meling Stemland

Thesis for the degree

Master of Science

DEPARTMENT OF EARTH SCIENCE

UNIVERSITY OF BERGEN

May 2017

Abstract

Seismic surveying of Arctic environments is important for both economic and environmental reasons. The world energy demand is increasing, and new areas need to be explored to cover the demand. One of the new areas where hydrocarbons are expected to be found is the Arctic. At the same time, the Arctic is severely affected by climate change. Rising temperatures lead to melting ice, and methods for monitoring the ice are needed.

The seismic method can be used both for mapping the subsurface, and for monitoring the properties of ice. Therefore, studies about the use of seismic in Arctic environments are needed. The seismic method does, however, not have a good reputation amongst everyone. Claims have been made that seismic surveying may harm marine animals, due to the high sounds involved when conducting seismic surveys in Arctic environments. In addition, seismic surveying in Arctic environments is challenging. Harsh weather conditions and remoteness means that special equipment is needed for Arctic surveying. The wavefield in a sea ice covered environment is also complex, especially if the water depth is limited. There is a high presence of dispersive surface waves that cannot be removed with conventional processing techniques. Data was acquired in such an environment on Svalbard in 2016.

This master thesis therefore studies the effect on the seismic data quality of changing source type (detonating cord versus air gun), source depth (on top of ice, or at different depths in the water), receiver depth (hydrophones at different depths), and air gun pressure (from 90 to 160 bar) in a seismic survey. The thesis also compares frequency spectra, sound pressure levels, sound exposure levels and wave propagation underwater with theory about hearing damages in pinnipeds (seals). From this, the potential seismic surveys have to harm pinnipeds is discussed.

The results reveal that survey geometry can have a large impact on the quality of the seismic data. Stronger reflections and less noise are obtained in the records when an air gun rather than a detonating cord is used, and when the source and receiver are located deeper in the water. The results also reveal that pinnipeds probably cannot hear many of the frequencies used in seismic acquisition, especially when the source is an air gun located deep in the water. The results show that sound pressure levels and sound exposure levels that may be harmful to a pinniped are only found very close to a seismic source. Sound levels decrease rapidly away from a seismic source, but the attenuation is not constant in a shallow marine environment with sea ice cover. This makes it difficult to conclude if, where and how a pinniped will be affected by seismic surveys in such an environment.

Acknowledgements

This thesis has been written at the Department of Earth Science at the University of Bergen, under supervision of Professor Tor Arne Johansen and senior engineer Bent Ole Ruud. First of all, I would like to thank my supervisor and co-supervisor for their help and useful feedback when writing this thesis. Their input has been greatly appreciated. Especially Bent Ole's suggestions for improvements of the thesis in the final few weeks have been very helpful.

The rest of Professor Tor Arne Johansen's research group also deserve a thank you for their feedback and comments on my presentations throughout the year.

Participation in the field work part of the UNIS course AG-335/835 (Arctic Seismic Exploration) gave me great insight into how seismic surveying of the Arctic works in practice. I would like to thank all participants for making it a fun and educational trip, with many discussions that have helped me in my work with this thesis.

Finally, friends and family deserve a big thank you for their support. Especially my fellow students who have made my years at the University of Bergen unforgettable, as well as my flatmates in Parkveien for helping me unwind during stressful times.

Contents

1. Introduction

1.1. Motivation

The world energy demand has been constantly increasing for the last hundred years, and the demand continues to rise. As the world population rises, combined with an increased living standard for more and more people, the need for energy resources continues to be one of the main issues in the world. Fossil fuels are hydrocarbon energy resources, including coal, oil and natural gas, that have been present on the market for many years. However, fossil fuels are non-renewable, and the easily accessible reserves are starting to become depleted. Renewable energy sources like wind, water, and solar energy are becoming more and more common, but are not yet numerous enough to cover the energy demand of the world. The need for fossil fuels is still present, and will be for many years to come (OECD/IEA, 2016). Thus, new areas need to be explored for hydrocarbons. At the same time, the effects of climate change are becoming more and more obvious. We daily hear about extreme weather situations all over the world, and studies show a clear relation between the world's energy use, and rising temperatures (Hartmann et al., 2013). Finding a balance between covering the world energy demand, while at the same time not changing the Earth's climate, is one of the main challenges the world faces.

One of the new areas where hydrocarbon resources might be found is the Arctic. The Arctic is the large region located north of the Arctic circle, where there is 24 consecutive hours with sun above the horizon, and 24 consecutive hours with sun below the horizon at least once a year (National Snow and Ice Data Center, n.d.). Understanding the geology and Earth dynamics of the Arctic areas is therefore important for both economic and environmental reasons:

- Economic because a large percentage of the world economy is somehow related to energy, in the sense that energy is needed for almost all services and goods produced in the world. In some countries, e.g. Norway, energy is also directly contributing greatly to the economy through the oil and gas export business (WEF and CERA, 2012, Harriss, 2016). Studies have shown that there is a high probability that large amounts of energy resources can be found in the Arctic, both offshore and onshore. It is, however, difficult to exactly estimate the undiscovered oil and gas resources in the Arctic, and estimates in these studies vary greatly (Gautier et al., 2009, Schenk et al., 2012, Harriss, 2016). Gautier et al. (2009) present estimates from the USGS claiming that approximately 13 percent of the world's undiscovered oil resources, and 30 percent of the world's undiscovered natural gas reserves are located in the Arctic. Figure 1a and 1b show the

estimated remaining oil and gas resources in the Arctic, respectively (Gautier et al., 2009).

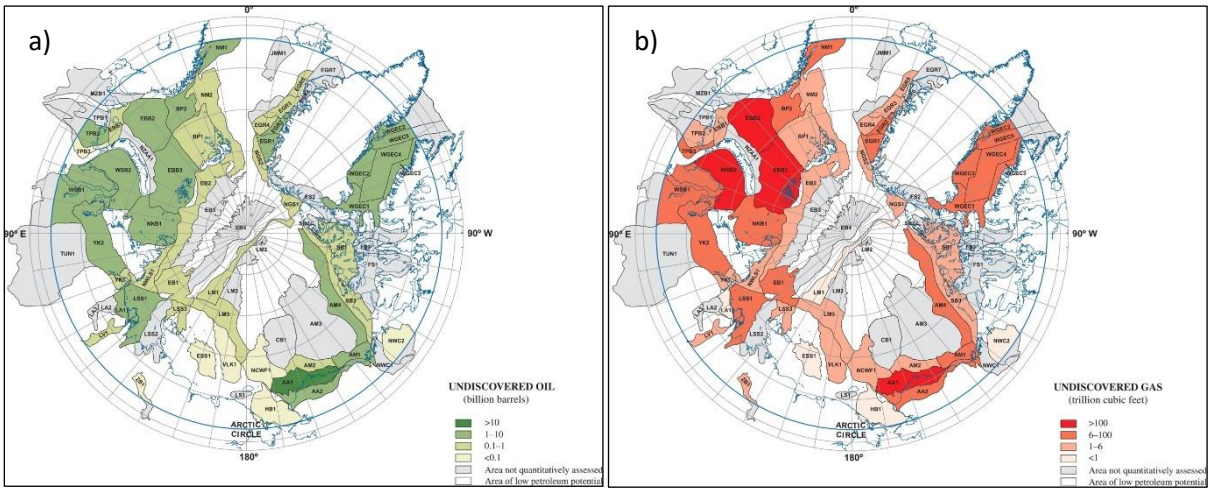

Figure 1: Figures from Gautier et al. (2009). Figure 1a shows the estimated remaining oil resources in the Arctic, and Figure 1b shows the estimated remaining natural gas resources. A darker green or red colour means a higher amount of oil and gas, respectively. Svalbard is located between 10 and 35 degrees East, where the estimates show that both oil and gas can be expected to be found.

- Environmental because the Arctic environment has a great impact on the environment in the rest of the world (Screen and Simmonds, 2010). Temperatures seem to rise faster in the Arctic than the world average (Hartmann et al., 2013). Rising temperatures lead to melting ice, and this melting ice can work as a so-called positive feedback, leading to an amplification of the rise in temperatures, which again leads to further ice melting (Screen and Simmonds, 2010). The Arctic is therefore especially sensitive to changing temperatures, and since rising global temperatures can have huge impacts all around the world, being able to monitor the change in ice cover due to rising temperatures is necessary. To do this, detailed knowledge of methods for measuring ice properties in Arctic environments is needed.

All in all, the conclusion is that detailed knowledge about the Arctic, including geology, weather and ice cover, is important. To acquire this knowledge, good methods for surveying the Arctic must be developed.

There are, however, many challenges associated with surveying and utilizing the Arctic areas for hydrocarbon exploration. First of all, the Arctic environment is unlike any other. The Arctic is an expansive region with many local variations, both onshore and offshore. The common factor is, however, that the Arctic areas have cold, harsh weather conditions. Onshore, the permafrost makes surveying difficult, and offshore, a presence of sea ice makes surveying both

challenging and risky (Hall et al., 2001, Trupp et al., 2009, Johansen et al., 2011, Rice et al., 2013). Special equipment that can handle these extreme weather conditions is necessary in order to avoid accidents (Rice et al., 2013). The Arctic ecosystem is also unique, with a large biodiversity including many animal species that cannot be found any other place on Earth, and that may be affected by climate change (Burek et al., 2008). Second, large parts of the Arctic are located far away from populated areas, with lack of infrastructure for transportation of equipment and possible exploited energy resources. This is yet another challenge related to Arctic hydrocarbon exploration. It is especially important to focus on the challenges that would arise in case of an accident, e.g. an oil spill. It could take a long time to get help to the site of the accident, and harsh weather conditions could make it difficult to clean up. Traditional equipment for this work may not function in as cold conditions as in the Arctic (Venosa and Holder, 2007, Harriss, 2016).

All the factors that make surveying in the Arctic challenging also add costs to the work. To make Arctic exploration feasible, finding ways to reduce the costs is necessary. Doing field work in the Arctic usually requires a large workforce and expensive equipment, and therefore each day of field work can be very expensive. Spending weeks acquiring data using methods that do not work well can result in a large loss of money. In order to reduce these costs, it is crucial with extensive testing and studying of methods and equipment before they are used in the field, as well as detailed planning (Trupp et al., 2009).

One of the widely used methods for surveying the Earth is the seismic method, where sound waves are expelled from a seismic source to propagate through the Earth. Parts of the waves are reflected back from geological boundaries, and these are recorded by a seismic receiver (Steeples et al., 1995, Association of Oil and Gas Producers, 2011). Thus, the seismic method can be used in exploration for hydrocarbons by mapping the subsurface. The seismic method can, however, also be used to monitor changes in ice properties. Since seismic velocities in ice and water are very different (approximately 3000 m/s and 1500 m/s, respectively), areas with melting ice can be identified using the seismic method (Stein et al., 1998, Johansen et al., 2003, Marsan et al., 2012). Figure 2 shows how the seismic velocities of a material change when water gradually freezes (Johansen et al., 2003).

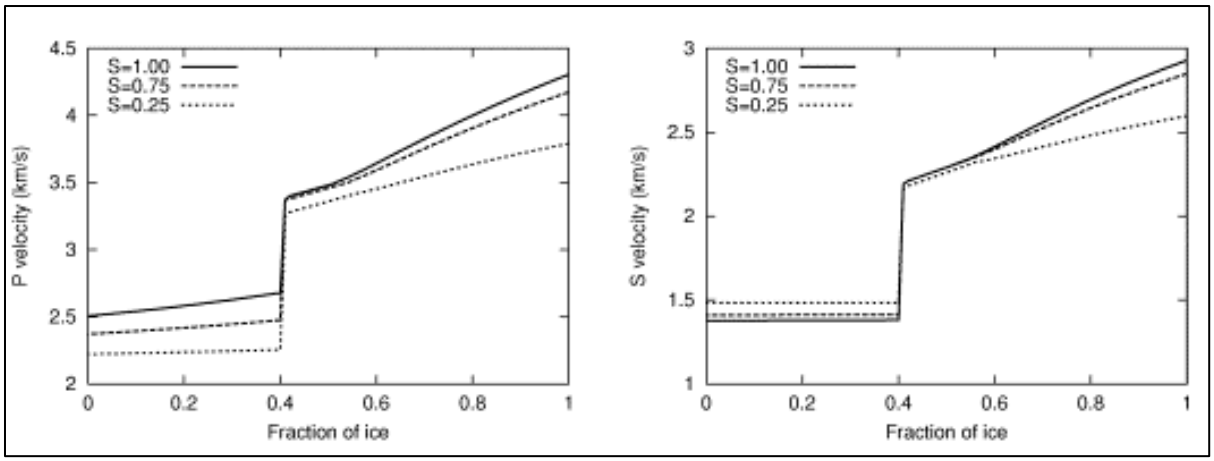

Figure 2: Figure from Johansen et al. (2003). The figure shows what will happen with the seismic velocities in a material when the fraction of ice in a water filled material gradually increases. When water freezes and gradually turns into ice, both Vp and Vs will drastically increase when a certain amount of the water (approximately 40 %) has turned into ice. This is mainly due to the non-existent shear modulus in water, compared with a high shear modulus in ice (see Equation 2 and 3 in section 2.2.).

Historically, the seismic method has been developed from the beginning of the 20th century, gradually becoming more and more advanced. During the 19th century, large advancements in the knowledge about elasticity were made. A book written by Love (1892) summed up what had been found within the field of elasticity up until then, including how Hooke's law could be extended to elasticity, the theory of stress and strain, the elastic parameters that describe a medium, and the existence of P- and S-waves (Chapman, 2004). A paper by Rayleigh (1885) explained the existence of surface waves, and all of the acquired knowledge up until the 20th century led to Lamb (1904) being able to explain the excitation and propagation of P-waves, S-waves, head waves and Rayleigh waves, which is the foundation of the seismic method. Since the paper by Lamb was published in 1904, the theory of, and concepts behind, the seismic method have been improved drastically. New waves have been discovered, and the propagation of waves under different conditions have been explained (Chapman, 2004).

However, the use of seismic in the vicinity of sea ice is less studied. Some of the most commonly used seismic sources and receivers require large open areas without any obstacles, therefore alternative acquisition geometries need to be tested in areas with sea ice cover. The presence of ice has also been shown to affect the seismic records. There is a high presence of surface waves in such areas, which can complicate the wavefield (Proubasta, 1985, Rendleman and Levin, 1990, Del Molino et al., 2008). Another type of environment that has proven to have a complicated wavefield is shallow marine areas, where the water depths are very limited (Richardson et al., 1995, Hermannsen et al., 2015). This also tends to lead to a high presence of surface waves. Based on this, it follows that the wavefield in an area with both of these characteristics, i.e. a shallow marine sea ice covered environment, can be expected to be quite

complicated (Hall et al., 2001). Effort has been made to develop processing routines that can remove these surface waves from the seismic records, but this has appeared to be difficult. Many conventional processing techniques fail when it comes to the removal of surface waves (Proubasta, 1985, Henley, 2003, Henley, 2007, Rovetta et al., 2009a). Therefore, a suggestion is to instead change the acquisition geometry, to see if it is possible to avoid recording these surface waves at all, in that way enhancing the quality of the seismic data.

While the seismic method has been warmly embraced by oil and gas explorers, it does not have a good reputation amongst everyone. One of the concerns that has been raised is regarding the fact that marine seismic acquisition involves the use of high intensity sounds underwater. Most people have experienced that very loud sounds can be hurtful for their ears, and since sounds can travel very well underwater, there has been worry about whether sounds expelled from seismic sources can hurt animals living in the sea, including fishes and marine mammals (Engås et al., 1996, Malakoff, 2002, Gordon et al., 2003). Studies showing inconsistent propagation patterns for sound waves underwater have also raised concerns about whether impacts of sounds can be predicted well enough using simple modelling methods (Richardson et al., 1995, Tolstoy et al., 2004, Farcas et al., 2016). It has been claimed by fishermen that seismic exploration activity scares the fish away from areas where they are fishing, and in that way reducing their stocks, a claim supported by a few studies (e.g. Engås et al. (1996)). There have also been reports of stranded whales where seismic exploration has been blamed as the cause, but without any direct link between the two being proved (Malakoff, 2002). Concern has also been raised about the possible effects of seismic operations on pinnipeds (commonly called seals), who breed and feed in areas were seismic operations might be performed (Harris et al., 2001, Southall et al., 2007). The uncertainties that exist within this field makes it clear that more studies about the effect of seismic on marine animals are needed, to be able to enforce the necessary protection measures.

1.2. Objectives

The purpose of this thesis is twofold. One objective is to give an overview of the impact of acquisition geometry on the quality of seismic data acquired in areas with sea ice. This will be done by comparing seismic records acquired with seismic sources and receivers at different locations. The thesis studies the effect of having a seismic source on top of the ice sheet, or at different depths in the water underneath it. It also studies the effect of having receivers at different depths in the water.

The other main objective of the thesis is to study and highlight any possible harmful effects seismic surveys can have on marine mammals, with a specific focus on pinnipeds. In this thesis, I focus mainly on three things related to this. I compare the frequency spectra from the seismic data with the hearing bandwidth for pinnipeds found in previous studies. I also compare recorded sound pressure levels and sound exposure levels with theory, to look at whether any physical or physiological effects can be expected when seismic exploration is performed. Since P-waves are the only waves that can travel through water, that is the only type of wave that needs to be considered when studying possible impacts of seismic waves on marine life. Last, I will briefly study how the waves are attenuated between the receivers, and from this see if any apparent propagation patterns in a shallow water sea ice covered environment like this can be identified. This is important information to know when assessing where seismic surveys can affect pinnipeds. The thesis is based on seismic data acquired in the Van Mijen fjord on Svalbard in March 2016, and therefore the focus will be on pinnipeds that are common in the waters close to the archipelago of Svalbard.

1.3. Outline

The outline of this thesis is the following:

Chapter 1 presents the motivation and objectives for this thesis.

Chapter 2 presents background theory about seismic waves and seismic wave propagation.

Chapter 3 presents background theory about seismic sources and receivers.

Chapter 4 presents background theory about seismic surveying in an Arctic environment.

Chapter 5 presents background theory about sound propagation underwater, and how pinnipeds will be affected by sounds.

Chapter 6 outlines the data and methods that are used in the work with this thesis.

Chapter 7 presents the results of the work with this thesis.

Chapter 8 discusses the results presented in chapter 7, in light of theory presented in chapter 2 to 5.

Chapter 9 gives the conclusions and discusses future work that can be done within this field.

2. Background – Seismic waves

This chapter will present background theory about seismic waves and wave propagation. The chapter will start by defining seismic waves, and will then go on to presenting the behaviour of a wave within a medium, and at the boundary between two media with different properties. Then these concepts will be used to briefly explain the seismic method, before the chapter ends with a section about the principles behind how a wave will lose energy when it is propagating away from a source.

2.1. Seismic waves

A seismic wave is a package of elastic energy, generated by a disturbance, that propagates through a medium (Kearey et al., 2002). The seismic wave will be periodic and have a certain signature, and the shape of that signature will depend on the strain made by the source that created the wave. The signature will thus vary depending on what kind of source made the strain (Ziolkowski et al., 1982). A seismic wave is defined by many different measures both in the time and frequency domain, including frequency, wavelength and amplitude. When the wave travels, the energy and characteristics of the wave cause certain particle movements (Gelius, 2012a).

Seismic waves can be divided into two types; body waves and surface waves. Body waves are waves that can travel through the interior of the Earth, without being immediately attenuated. These are either compressional waves with particle movement in the same direction as the direction of motion, often called P-waves, or shear waves with particle movement in a direction perpendicular to the direction of motion, often called S-waves. An important difference between the two types of body waves is that due to the different particle movements associated with the waves, P-waves can travel through liquids, while S-waves cannot (Gelius, 2012a).

The other seismic wave type is surface waves, and these waves have particle movements in other directions than the body waves, depending on the layer properties close to the interface where they travel. Surface waves have a more limited area of distribution, and as can be deduced from their name, they will usually only exist close to an interface like a surface. Thus, they do not travel deep into the interior of the Earth, and will not give much information about deep Earth structures (Steeples et al., 1995, Gelius, 2012a). However, they can still affect the seismic records, since the receivers are usually close to the Earth surface. According to Boiero et al. (2013), seismic data acquired in a shallow marine environment often reveals many surface

waves and guided waves (body waves "trapped" in a layer), many of them with well-defined dispersion patterns. Some surface waves that occur in a shallow marine Arctic environment can for example be Scholte waves (a type of oceanic Rayleigh/Stoneley wave) at the sea bottom in very shallow water, and flexural ice waves (an asymmetric Lamb wave) in a rigid ice layer (Del Molino et al., 2008, Boiero et al., 2013). These two surface waves will be explained in further detail in chapter 4.

2.2. Wave propagation

Wave propagation within a medium is described by the wave equation. The elastic wave equation in its most basic form is given by:

$$\nabla^2\varphi = \frac{1}{c^2}\frac{\delta^2\varphi}{\delta t^2}, \tag{1}$$

for an isotropic medium, where c is the velocity and φ is a field variable depending on the wave type that the wave equation is for, for example a P-wave (Krebes, 2004, Gelius, 2012a). Wave propagation will not be discussed in detail in this thesis, but the present paragraph discusses wave propagation briefly. See e.g. Chapman (2004) for a complete discussion. Within a layer, the velocity of a wave will depend on the elastic parameters of that medium, which are the incompressibility or bulk modulus k, the rigidity or shear modulus μ, and the density ρ (Kearey et al., 2002). The velocities of a body wave within a medium are then given by:

$$V_p = \sqrt{\frac{k+\frac{4}{3}\mu}{\rho}}, \tag{2}$$

and

$$V_s = \sqrt{\frac{\mu}{\rho}}. \tag{3}$$

Therefore, the velocity and field variable used in the wave equation will vary depending on the medium, and in a complex medium the wave equation can become quite complicated. Numerical solution of the wave equation is therefore often very time consuming, and for that reason, different approximations for the solution are often used. These approximate the propagation of a wave front through a heterogeneous medium (Krebes, 2004, Gjøystdal et al., 2007). A solution to the elastic wave equation was, however, presented by Press and Ewing (1951) for wave propagation for a model consisting of air, ice and water. Their derivation is partly presented in chapter 4.

2.3. Wave propagation in layered media

2.3.1. The wavefield

The previous section covered how a wave will travel within a medium. What is also important to understand for the scope of this thesis, is what will happen at a boundary between two layers with different properties. To more easily describe travel paths of a wave, the concept of rays is often used. A ray is a theoretical concept where a small pencil of seismic energy that is perpendicular to a specific point on the wavefront at all times is defined as a ray (Kearey et al., 2002). Figure 3 demonstrates this concept.

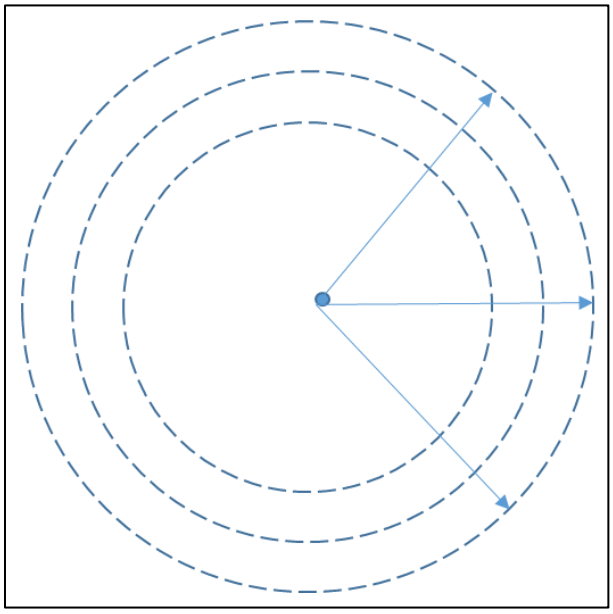

Figure 3: A ray is a theoretical concept used to describe a small pencil of energy that is perpendicular to the wave front at all times. In the figure, the arrows represent rays, and the stippled lines represent wave fronts.

In the first section of this chapter, it was explained how waves can be divided into different groups based on where they travel (e.g. surface waves are distinguished from body waves), and based on what kind of particle motion they cause when they pass (e.g. P-waves are distinguished from S-waves). Due to the behaviour of waves at a layer boundary, it is also possible to characterize waves based on the paths they travel between a source and a receiver (Steeples et al., 1995).

A wave can travel directly from a source to a receiver, and this is called the *direct wave*. However, a wave expelled from a source will usually spread out in all directions, and parts of the wave will eventually travel into a layered medium. At a boundary between two materials with different acoustic impedances, the incoming body wave will be split up. Parts of the wave will then be reflected as *reflected waves*, parts of the wave will travel through the boundary as

transmitted waves, and parts will be mode-converted to other types of waves (e.g. P- to S-waves). *Refracted* waves will also occur, which are waves that travel along the boundary in the layer below an interface, continuously sending up waves with the so-called critical angle (Kearey et al., 2002).

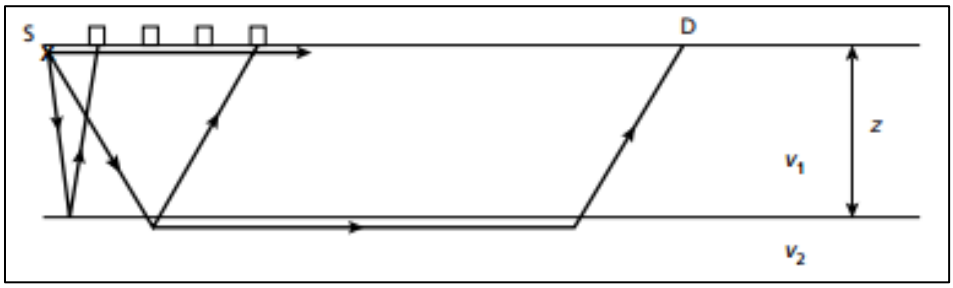

Figure 4: Figure from Kearey et al. (2002). The figure shows the different propagation paths a wave can follow from a source to a receiver. The figure shows a direct wave, two reflected waves and a refracted wave. The mode-converted PS-wave and surface waves are not displayed in the figure.

Figure 4 shows the propagation paths for direct, reflected and refracted waves (Kearey et al., 2002). The next section will explain in more detail how these waves are generated at a boundary.

2.3.2. Behaviour of a wave at a boundary

The amount of energy that will be reflected, and the amount of energy that will be transmitted at a layer boundary depends on the acoustic impedances Z of the layer above (layer 1), and below (layer 2) the boundary. As a measure of this, the amplitude of the reflected ray A_1 relative to the amplitude of the incident ray $A_{incident}$, or the amplitude of the transmitted ray A_2 relative to the amplitude of the incident ray $A_{incident}$, is often used. These are called the reflection and transmission coefficients R and T, respectively, and are given by the following expressions from Kearey et al. (2002):

$$R = A_1/A_{incident}, \quad (4)$$

$$T = A_2/A_{incident}. \quad (5)$$

For the simple case of normally incident rays, the reflection and transmission coefficients can be calculated quite easily, assuming the seismic velocities v_1 and v_2, and densities ρ_1 and ρ_2 of the layers above and below the boundary are known. To do this, the following equations found in Kearey et al. (2002) are used:

$$Z = \rho v, \quad (6)$$

$$R = \frac{\rho 2 v 2 - \rho 1 v 1}{\rho 2 v 2 + \rho 1 v 1} = \frac{Z2 - Z1}{Z2 + Z1}, \quad (7)$$

$$T = \frac{2Z1}{Z2 + Z1}. \quad (8)$$

When the rays are not normally incident, the more complicated Zoeppritz equations have to be applied to compute the reflection and transmission angles and coefficients (Stewart et al., 1999). However, the reflection angle θ of all waves that are created at a boundary can still be computed in a simple way, assuming the layers are non-dipping. Since the ray parameter $\frac{\sin\theta}{v}$, should be constant right above and below a boundary, the angles can be computed using Snell's law:

$$\frac{\sin\theta 1}{v1} = \frac{\sin\theta 2}{v2} \quad (9)$$

(Kearey et al., 2002).

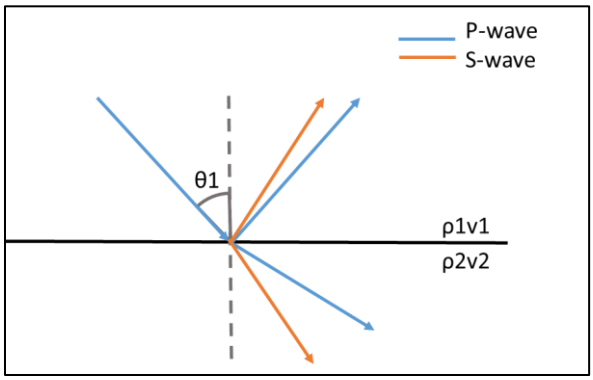

Figure 5: An obliquely incident P-wave is split up into reflected and refracted P- and S-waves according to Snell's law (see Equation 9) when it hits a boundary.

The waves that are created are often referred to as PP-waves (incoming P-wave, outgoing P-wave), PS-waves (incoming P-wave, outgoing S-wave), and SS-waves (incoming S-wave, outgoing S-wave). Reflected and transmitted PP- and PS-waves are displayed in Figure 5.

Due to all the factors mentioned in this chapter, the propagation of a wave through a heterogeneous medium can be very complicated.

2.4. The seismic method

The seismic method, commonly used for exploration of the subsurface, makes use of the principles of wave propagation that have been described earlier in this chapter. Seismic waves are created by an artificial source, and seismic receivers record the waves that return to the receiver (Steeples et al., 1995, Association of Oil and Gas Producers, 2011). The recorded signals can be displayed in a seismogram, where the received signal is plotted against arrival

time. Figure 6 shows a simplified example of such a seismogram, displaying only a direct, reflected, and refracted wave (Kearey et al., 2002).

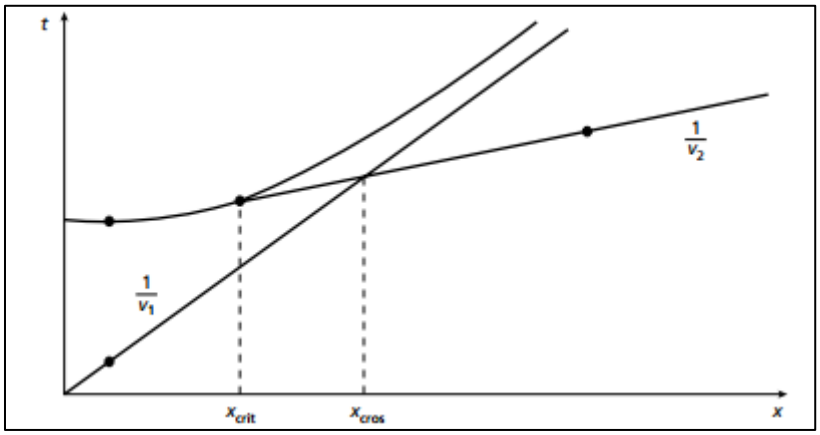

Figure 6: Figure from Kearey et al. (2002). The figure shows how we would expect to see the direct, reflected and refracted wave that were displayed in figure 4 in a simplified seismogram. It can be seen that both direct and refracted waves will be straight events, while reflected waves will be curved events. The direct wave starts in t=0, while the reflected and refracted waves arrive later. At a certain distance away from the source (the crossover distance x_{cros}), the refracted wave arrives before the direct wave. The reflected wave never arrives first.

Based on the previous sections it should be clear that a seismogram will consist of signals from many different types of waves, and can therefore be difficult to interpret. Since the amplitudes of the reflected waves from a boundary between two layers depend directly on the properties of the two layers, the seismic records can be used to interpret the subsurface. The recorded signal should ideally represent the reflection coefficients from all layer boundaries, convolved with the source signal. However, this is only the case if the Earth is horizontally layered, the waves are normally incident, no noise is present, and the source pulse is not changed with depth (Gelius, 2012b).

It has traditionally been most common to make use of PP-waves, but studying PS- or SS-waves are becoming more and more common (Stewart et al., 1999, Boiero et al., 2013). These types of body waves have often been regarded as noise in the seismic records, just like surface and interface waves have. Effort has therefore been made to remove these waves from the seismic records. Studies in recent years have, however, revealed that important information about subsurface properties can be contained in records of these wave types as well, and for that reason studies of these waves are increasing. By making use of several wave types, better quality images of the subsurface can be obtained (Stewart et al., 1999, Boiero et al., 2013).

Due to attenuation effects, sources that generate low frequency waves are usually used in seismic exploration. This is because we want to be able to penetrate deep into the subsurface before the wave is attenuated, and resolution is lost (Ten Kroode et al., 2013). The frequencies

expelled from a seismic source are typically up to 100 Hz, but might contain higher frequencies as well (Hermannsen et al., 2015). With thorough knowledge of how waves behave underground, the seismic records can be interpreted to get a good understanding of the structure of the subsurface. This thorough knowledge is crucial to be able to distinguish the different waves from each other, to distinguish reflections from noise, and to get a realistic interpretation of the covered area (Kearey et al., 2002).

2.5. Attenuation of a travelling body wave

A wave that is travelling through a medium will lose energy, and this is called attenuation. The mechanisms that contribute to attenuation of a body wave give attenuation effects that can be divided into geometrical effects, and absorption effects. In addition to these effects, transmission losses will occur at interfaces as described in subsection 2.3.2, as well as scattering of energy at irregularities (Johnston et al., 1979, Gelius, 2012a). In studies of wave propagation in shallow water the absorption effects are very small, so geometrical spreading effects are most relevant to look at (Hermannsen et al., 2015). Even though surface waves will be attenuated much faster than body waves, a body wave will also be attenuated when travelling away from a seismic source. In water, P-waves are the only body waves that can travel, and thus the attenuation mechanisms that affect P-waves are especially interesting when studying wave propagation in a marine environment (Gausland, 2000).

2.5.1. Geometrical effects

Assuming no absorption loss, the total energy of a seismic wave is constant. Geometrical spreading of a wave front means that the area of the wavefront is increasing with distance away from the source, which means that the energy must be spread out over a larger area. Since intensity is defined as the power transferred per area, spreading of energy over a larger area means a decrease in intensity (Richardson et al., 1995, Kearey et al., 2002). Two models often used to describe geometrical spreading are spherical spreading, and cylindrical spreading. Depending on the source used and the environment where the wave propagation takes place, either one of these models for geometrical spreading can often be used (Richardson et al., 1995). Figure 7 shows waves following the two spreading models. In Figure 7, spherical spreading is shown close to the source (i.e. when radius<water depth), and cylindrical spreading is shown further away from the source (i.e. when radius>water depth). The formulas for these two spreading models can be derived, following the webpage Discovery of Sound in The Sea, developed by University of Rhode Island and Marine Acoustics inc. (2013):

The decrease in energy per unit area due to geometrical spreading is often called the propagation loss PL. The energy level P(r) at a certain distance away from the source (assuming PL is the only energy loss) should therefore be P(r)=P(s)-PL, where P(s) is the initial energy level at the source. Since spreading of energy means a decrease in intensity, propagation loss in decibel, as a function of intensity I, can be given by:

$$PL = 10\log\frac{I_0}{I}, \quad (10)$$

where I_0 is the initial intensity. It would, however, be desirable to have the propagation loss given as a function of distance from the source, to be able to calculate the energy level at any specific position.

A sphere has the area $4\pi r^2$, thus if an energy source leads to spherical spreading, the total power that crosses the sphere is $4\pi r^2 I$. Assuming energy is conserved, meaning that the total power that crosses the sphere of energy at any time is the same, then $4\pi r^2 I = 4\pi r_0^2 I_0$, if r_0 is the radius of the initial sphere, and r is the radius of the sphere after spreading. Removing equal terms gives $I=I_0\frac{r_0^2}{r^2}$, which shows that intensity decreases as the inverse square of the range for spherical spreading. If one assumes r_0=1 m, the propagation loss PL can be expressed as:

$$PL = 10\log\frac{I_0}{I} = 10\log(r^2) = 20\log(r)\ \text{dB}^* \quad (11)$$

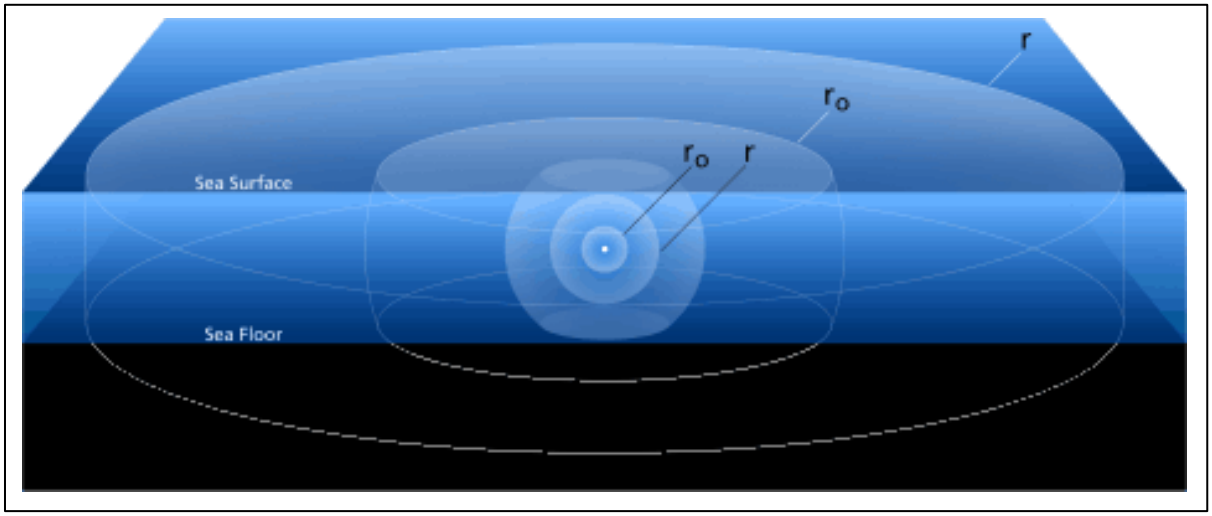

Figure 7: Figure from University of Rhode Island and Marine Acoustics inc. (2013). The figure shows how a wave front will spread out from a point source, assuming spherical spreading when the radius r of the wave is smaller than the water depth, and cylindrical spreading when the radius is larger than the water depth. r_0 is the initial radius, and r is the radius after spreading. These can be inserted into Equation 11 and 12.

* University of Rhode Island and Marine Acoustics inc. (2013) use $\frac{I}{I_0}$ instead of $\frac{I_0}{I}$, but this is assumed to be a misprint.

A similar derivation can be done for cylindrical spreading, by changing the area to the area of a cylinder $2\pi rh$. The same arguments give $2\pi rh=2\pi r_0 h$, which further gives $I=I_0\frac{r_0}{r}$. This shows that intensity decreases as the inverse of the range for cylindrical spreading. If r_0 is again assumed to be 1 m, the propagation loss PL can be expressed as:

$$PL = 10\log\frac{I_0}{I} = 10\log(r) = 10\log(r)\ dB \quad (12)$$

(University of Rhode Island and Marine Acoustics inc., 2013). The only difference in the formulas for spherical and cylindrical is therefore that the value before the log(r) expression is 20 for spherical spreading, and 10 for cylindrical spreading.

2.5.2. Absorption

Absorption, also called intrinsic attenuation, is attenuation caused by the intrinsic properties of a medium (Johnston et al., 1979). The absorbed energy ends up as heat energy that can increase for example the temperature of the material. The amount of absorption in a medium is often given as the dimensionless quality factor $Q = 2\pi\frac{E}{\delta E}$, where E is the total elastic energy, and $\frac{E}{\delta E}$ is the elastic energy lost per cycle (Sato, 1967). The attenuation is thus $\frac{A}{A_0} = \frac{r_0}{r}e^{-\alpha(r-r0)}$, where $\alpha = \frac{\pi f}{Qc}$ (Gelius, 2012a). The amount of absorption that happens when a wave travels through a medium generally depends on the properties of the medium, the fluid saturation, and the surrounding pressure (Johnston et al., 1979). Attenuation due to absorption does not happen as fast as attenuation due to geometrical spreading. In most rocks, Q will be independent of frequency, i.e. the same amount of energy will be lost per cycle for every frequency component. This means that high frequencies will have more oscillations than low frequencies, and therefore they will be attenuated more than low frequencies. That is, Q will increase for higher frequencies (Johnston et al., 1979, Cormier, 1982). High frequencies will thus be attenuated faster than low frequencies in the subsurface, so only low frequency components can penetrate deep into the Earth's interior. It then follows that resolution will decrease with depth, since vertical resolution is given by $\lambda=c/f$, and horizontal resolution is given by the radius of the Fresnel zone $R_f = \sqrt{\frac{\lambda Z}{2}}$ (Gelius, 2012a).

2.5.3. Attenuation of P-waves in water

Gausland (2000) presents a simple general formula for low frequency (<1 kHZ) wave propagation in a water environment, which takes into account geometrical spreading,

absorption, and scattering due to obstacles. The sound pressure P(r) at a distance r from a seismic source is given by the formula:

$$P(r) = P(s)-A\log(r)-Br-C, \quad (13)$$

where A is an attenuation constant depending the type of geometrical spreading of the wave, B is a range dependent attenuation factor (i.e. absorption), and C is attenuation due to obstacles (Gausland, 2000). For short distances and open water, B and C can be neglected as an approximation, and Equation 13 becomes:

$$P(r) = P(s)-A\log(r). \quad (14)$$

This formula for wave attenuation is the same as the formulas derived for spherical and cylindrical spreading in the previous subsection, where A was 20 for spherical spreading, and 10 for cylindrical spreading. Spherical spreading has been shown to be a good approximation for compressional wave propagation in deep water (water depth>>wavelength), while in very shallow water the geometrical spreading loss has been shown to be more complicated, appearing to be larger than cylindrical spreading, but smaller than spherical spreading (Richardson et al., 1995, Hermannsen et al., 2015).

2.6. Summary

This chapter has shown that a seismic wave propagating through a medium will be affected by the properties of that medium. The properties of the medium will determine the velocity, propagation pattern, and attenuation of a wave. Changes in properties can therefore have a large impact on the propagation pattern of a wave. The next chapter will present the sources and receivers that are necessary to be able to use the principles presented in this chapter in seismic surveying.

3. Background – Seismic sources and receivers

A lot of advanced equipment that can be used during seismic surveys exists, but there are only two elements that are absolutely necessary to be able to do seismic exploration; the presence of a seismic source, and the presence of a seismic receiver (Kearey et al., 2002).

The purpose of the source is to create waves that should travel into the medium that is being explored. In some cases, the source can be natural, for example two tectonic plates moving relative to each other, thereby creating an earthquake. In most planned seismic exploration studies the seismic source is, however, artificial. The purpose of the receiver is to record the seismic waves that reach the receiver. The receiver records all waves that reach the receiver, both waves created by an artificial seismic source, and waves created by other sources, often referred to as noise (Kearey et al., 2002).

There are several different types of sources and receivers that can be used in seismic exploration. Which source and which receiver is best suited for a survey can vary depending on several factors, including the purpose of the survey, the surroundings, the weather conditions, and animal life in the area. The combination of source type and receiver type, as well as the positions of the equipment, might affect the quality of the seismic records (Association of Oil and Gas Producers, 2011, Haavik and Landrø, 2016).

3.1. Sources

Two of the seismic sources that are common in seismic exploration are air guns and dynamite. For both sources, the idea is that an explosion of air or dynamite, respectively, will create a pulse that travels away from the source. The wave continues into the subsurface, and is partly reflected at geological boundaries, leading to parts of the seismic wave returning to the surface again (Steeples et al., 1995, Kearey et al., 2002). Other types of sources, such as vibrators, hammers, sparkers and water guns also exist, but are not described in detail in this thesis (Kearey et al., 2002).

The main requirements for a source to be an appropriate seismic source is, according to Kearey et al. (2002), that

- It has sufficient energy, and energy at a wide range of frequencies.
- It is as close to a pulse as possible, containing as little coherent noise as possible.
- It must be possible to recreate the same source waveform several times.
- It must be safe, efficient and environmentally acceptable.

3.1.1. Air guns

The concept of an air gun is that air under high pressure is stored in one or more chambers in a mechanical device. This compressed air is released following a firing command, leading to the air expanding as a bubble in the water. Some of the energy that is released in this process is converted to P-waves that propagate through the water, and further down through the subsurface (Parkes and Hatton, 1986, Dragoset, 2000, Landrø and Amundsen, 2010, Association of Oil and Gas Producers, 2011).

The size of the air gun bubble will increase until the work done by the pressured air on the water is equal to the work done by the hydrostatic pressure. At this time, the pressure within the air gun is much smaller than the hydrostatic pressure (Pascouet, 1991). Therefore, the maximum size of the bubble depends on the initial pressure in the air gun. When this point has been reached, the bubble will rapidly decrease in size until the air gun pressure is yet again higher than the hydrostatic pressure. The bubble will keep oscillating in size, creating so-called bubble pulses, for a while (Parkes and Hatton, 1986, Dragoset, 2000). These bubble pulses are amongst the biggest problems related to processing of seismic data acquired with an air gun. Ideally, we would like to keep only the primary bubble, and to get rid of the oscillations that complicate the signature of the air gun signal (Landrø and Amundsen, 2010).

A second problem with using an air gun as a seismic source is related to the fact that a bubble will propagate in all directions away from an air gun. Since the reflection coefficient between water and air from below is very close to -1, the wave that travels towards the water surface will be almost completely reflected at the sea surface, changing polarity in the process (Landrø and Amundsen, 2010). This behaviour is visualized in Figure 8.

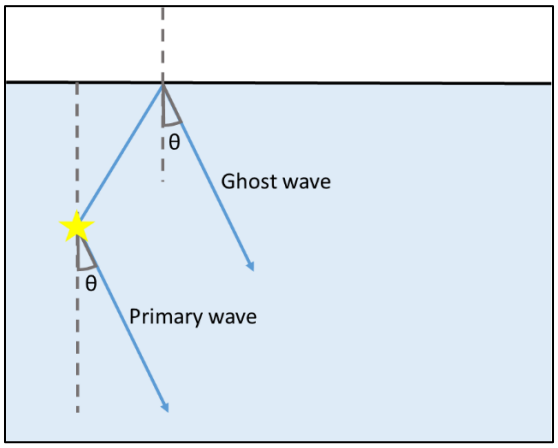

Figure 8: When a wave expelled from a source under water hits the water surface from below, it will be almost 100 % reflected, changing polarity in the process. If the ghost wave is reflected with the same angle as the primary wave, they can interfere at a receiver.

Each of the pulses created by an air gun will therefore have an almost equally large, but oppositely polarized, pulse arriving right after the primary pulse. This pulse is often called a ghost, and is a signal it is desirable to get rid of (Landrø and Amundsen, 2010). At the receiver, the pressure signature of an air gun can often be seen like in Figure 9, from Landrø and Amundsen (2010).

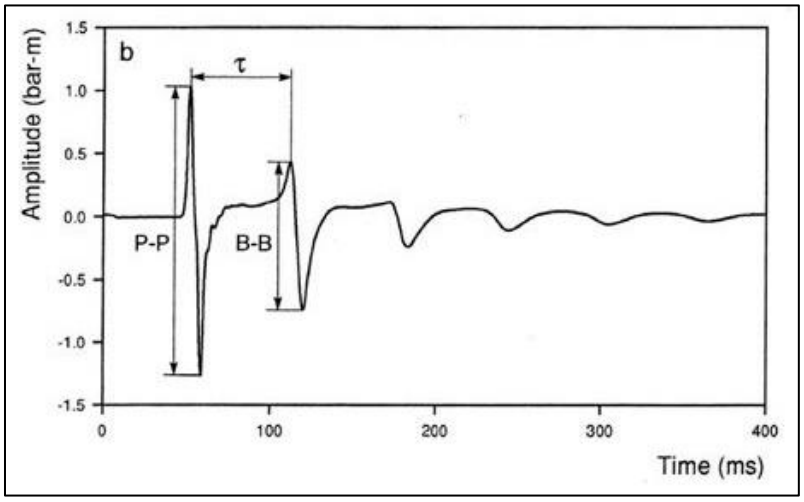

Figure 9: Figure from Landrø and Amundsen (2010). The figure shows the far-field pressure signature from a single 40 in³ air gun. P-P is the peak-to-peak pressure for the primary pulse, and B-B is the peak-to-peak pressure for the bubble pulse. τ is the bubble period.

There are two main ways to remove the effect of the bubble pulses. The most common in commercial surveys is to use an array of air guns that are fired with different volumes of air. The different volumes will give different maximum bubble sizes, leading to different starting times for when the bubble begins to oscillate (Dragoset, 2000). The time between each of the following bubble pulses is called the bubble period, and is described by the Rayleigh-Willis equation:

$$T = k\frac{P^{1/3}V^{1/3}}{(P_{atm}+\rho gD)^{5/6}}. \quad (15)$$

P is the air gun pressure, V is the air gun volume, P_{atm} is the atmospheric pressure, g is the gravitational acceleration, D is the depth of the air gun, and k is a constant that depends on the unit (Gelius, 2012b). From this, it follows that the bubble period will vary for air guns of different volumes.

Therefore, the primary pulse will arrive at the same time for all air guns in the array, and thus interfere constructively. The bubble pulses will arrive at slightly different times, and thus interfere destructively. The primary-to-bubble ratio (P/B ratio) can in that way be increased (Dragoset, 2000).

Another way to increase the P/B ratio is to use an air gun with two chambers, often called a generator-injector (GI) air gun, referring to the chambers called the generator and the injector. Then, the compressed air in the generator is released first. When this air has created a bubble that has reached its maximum size, the compressed air in the injector is released. In that way, air is pushed into the centre of the bubble to increase the internal pressure to the value of the hydrostatic pressure, just when it is about to start collapsing. This prevents the violent collapse of the bubble, and the signal becomes less complicated. This makes the seismic records simpler to interpret (Pascouet, 1991, Sercel, 2016). The processes happening within a GI air gun are shown schematically in Figure 10, that was modified from a figure in Sercel (2016).

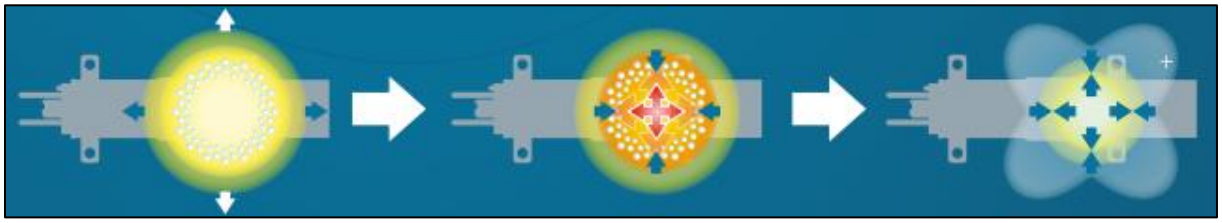

Figure 10: Figure modified from Sercel (2016). The figure shows the principles behind a GI air gun. In the first phase, the generator is fired. When the bubble has reached its maximum size, the injector is fired and injects air into the middle of the bubble. This reduces the oscillation of the bubble since the internal pressure is increased to reduce the difference between air gun pressure and hydrostatic pressure.

There are several advantages with using a GI air gun instead of an array to remove the effect of the bubble pulse. The main advantage is that the seismic acquisition becomes simpler. Since using an array requires use of several air guns that need to be fired at exactly the same time, timing is crucial, and even small mistakes can lower the quality of the acquired seismic. It is easier logistically as well to use only one air gun instead of a whole array (Pascouet, 1991).

3.1.2. Detonating cords

Dynamite is another type of seismic source. In seismic exploration, dynamite is often used in a detonating cord, meaning that the explosives are connected in a line. When dynamite is used to create an explosion, a high-amplitude pressure wave is generated. Parts of this P-wave will travel in air with the velocity of sound in air (approximately 330 m/s), and parts of the wave will travel into the subsurface. This P-wave will have a short rise time, generally much shorter than for a P-wave created by an air gun where the rise time can be controlled more accurately. However, when using detonating cords, the source pulse becomes relatively long. It might be difficult to know the exact signature of the source wavelet when using dynamite as a seismic source, and the signature may also change from explosion to explosion (Sharpe, 1942, Johansen et al., 2011).

The most commonly known type of dynamite is TNT (*trinitrotoluene*). Dynamite can, however, be of several types, but the strength is often converted to the number of grams of TNT that would give the same size of explosion. When the dynamite is ignited at one end of the line, the explosion will travel along the line with a speed of approximately 6900 m/s. This means that when using a 10 m long detonating cord, the whole cord will explode in less than 1.5 ms. The seismic source can thus be regarded as a many point sources fired at almost the same time. This leads to interference, and thus directionality in the direction the explosion travels (Johansen et al., 2011). PETN (*pentaerythritol tetranitrate*) is a type of explosive that is often used in detonating cords. PETN is a stronger explosive than TNT, with a relative effectiveness factor of 1.66 (i.e. 100 g of TNT will give the same strength of explosion as 60 g of PETN) (Jaw and Lee, 2008). Detonating cords are flexible and easy to use, and work well in very low temperatures. They can also be deployed effectively (Johansen et al., 2011).

3.2. Receivers

Devices that record the parts of the seismic wavefield that return to the surface after reflection or refraction are necessary in seismic exploration. These devices detect either the ground motion that the returning waves cause, or the pressure change that arrives with a returning wave. Receivers then convert these signals into electrical signals, and record the arrival times of the waves. The output from the receivers is usually displayed in a seismogram showing the amplitudes of the returning waves versus the time when they returned. Which frequencies a receiver can detect depends on the sampling interval. Usually the range is around 0-500 Hz, but broadband receivers that can detect very high frequencies, necessary for exploring the shallow subsurface, also exist (Steeples et al., 1995). Geophones and hydrophones are such seismic receivers, and as the names suggest, they are to be used on land and in water, respectively (Kearey et al., 2002).

3.2.1. Geophones

Geophones are the most common type of receiver to use on land. The geophone is constructed to detect any ground motion caused by a returning wave, and to convert it into an electrical signal. The principle behind the most common type of geophone is that a magnet is fastened to a frame on the ground, so that the magnet will move if the ground moves. A coil is also hanging freely from the frame. Since movement of a coil in the presence of a magnet will induce a current, a current can be detected whenever the ground moves (Kearey et al., 2002).

The principle behind a geophone sounds simple enough, but there are several issues present when using a geophone to record ground movements caused by passing waves. For example, one single geophone can only measure ground movement in one direction. Thus, when using a geophone to measure ground motion, several geophones are needed to be able to measure ground motion in all directions. "3C geophone" stands for "three component geophone", and such geophones are often used to avoid that problem. The response from the different geophone components must be interpreted separately, and can later be used together to get a complete image of the ground motion (Steeples et al., 1995, Kearey et al., 2002).

Also, choosing which component of motion to measure (displacement, velocity or acceleration) can be difficult. One must choose which parts of the wavefield to focus on when recording, processing and interpreting the seismograms. Geophones that are used above the water column (e.g. on top of sea ice) are often optimized for registering ground motion in the vertical direction. This is because that is the main direction P-wave particle movement, and S-waves cannot travel through water. In places where the focus is on registering P-waves, it can thus be more convenient to use several vertical component geophones instead of geophones that register ground movement in all directions (Kearey et al., 2002, Association of Oil and Gas Producers, 2011).

3.2.2. Hydrophones

Hydrophones are the most common seismic receivers to use in water. Instead of measuring ground motion like a geophone, a hydrophone records transient pressure changes. Transient pressure changes could indicate the arrival of a compressional wave (Kearey et al., 2002). Contrary to geophones, hydrophones do not measure in a specific direction. Pressure is a scalar quantity, and only the total pressure at a location will be recorded. This makes it simple to measure the strength of the total wavefield, but at the same time it makes it difficult to distinguish between the different parts of the wavefield, for example primary reflections and multiples (Hoffe et al., 2000). Unlike geophones, hydrophones do not have a resonant frequency. However, hydrophones that are made to be used in combination with geophones can be made with a response that corresponds to a typical resonance frequency of a geophone, for simpler use of combinations of geophones and hydrophones in shallow-water areas (DTCC, n.d.).

Hydrophones are commonly used in an array called a marine streamer. Since hydrophones are made to be used in water, connecting them to large cables that can be towed behind a marine

vessel is a good way to get seismic coverage of large areas in a time-effective way. Typically, the length of a streamer will be 3-9 kilometres long, with receivers 25 meters apart, and up to 16 streamers can be connected to one marine vessel (Association of Oil and Gas Producers, 2011, Gelius, 2012a). From these numbers, it is clear that very large areas without any obstructions such as land, drilling rigs, or sea ice must be present to be able to use marine streamers. This is not always the case, and in areas without open water, alternative setups must be used. In those cases, hydrophones can be used separately instead, as nodes hanging down into the water at variable depths.

3.2.3. OBS

OBS stands for ocean bottom seismometer. This means that instead of being placed either on land (i.e. a geophone) or in the water column (i.e. a hydrophone), an OBS is placed on the water bottom. A 4C OBS is a device that has four components, and these are the same components as in a 3C geophone and a hydrophone, all placed inside a frame (Seabed Geosolutions, 2015). The 3C geophone records displacements, and the hydrophone records pressure changes. The device also contains a computer that records and stores output from the four components. Because of this, an OBS can be recording continuously on the sea bottom for a relatively long time, depending on the design of the OBS (Seabed Geosolutions, 2015).

The OBS is lowered to the sea bottom, and is pulled up again when the acquisition is done (Seabed Geosolutions, 2015). Placing the seismic receiver on the sea bottom instead of on land, ice, or in the water column, can have several advantages. One is that if the seismometer is placed on the sea bottom, there is no water column between the reflector and the receiver. Thus, both PP- and PS-waves can be recorded. This can make it easier to interpret the lithology of the subsurface, for example determining the presence of liquid hydrocarbons (Stewart et al., 1999, Hoffe et al., 2000). Also, the distance between source and receiver can be adjusted easier than when using a marine streamer, so that a wide-azimuth coverage of an area can be obtained (Bouska, 2008). Third, the presence of both a 3C geophone and a hydrophone can help distinguishing the principal reflections from the ghost (Hoffe et al., 2000).

However, since the OBS must be placed on the sea bottom, a disadvantage with using it is that moving it around can be very time consuming. On the other hand, in narrow areas that can be difficult to access using marine streamers, for example in fjords, close to sea ice, or close to drilling rigs, the OBS can cover areas that the other types of receivers cannot (Bouska, 2008).

3.3. Summary

From what has been presented in this chapter it should be clear that the main principles behind different seismic sources and receivers, respectively, are similar. Seismic sources are devices that create and send out seismic waves, and seismic receivers are devices that record the seismic waves. There are other sources and receivers than the ones mentioned in this chapter (e.g. Vibroseises and snowstreamers (Eisen et al., 2015)) that can be used in an Arctic environment, but the ones mentioned here are the ones relevant for the scope of this thesis. Since the focus here will be on seismic exploration in the vicinity of sea ice, the use of some of these sources and receivers in such situations will be further presented and discussed in the following chapters. It should also be clear after reading this chapter that the placement of sources and receivers can have an impact on the quality of the seismic data acquired.

4. Background – Arctic seismic surveying

As described in the introduction, seismic surveying of Arctic areas is important for both economic and environmental reasons. At the same time, seismic acquisition in Arctic environments can be very challenging. This chapter will introduce some of the challenges that are typically associated with seismic surveying in a shallow marine sea ice covered environment.

4.1. Seismic acquisition in an Arctic environment

Special equipment and acquisition geometries might be needed in areas with a presence of sea ice. Harsh weather conditions and sea ice makes it necessary with solid and well adapted equipment that can work in very low temperatures (Trupp et al., 2009, Rice et al., 2013). Traditional marine streamer surveys can only be conducted if large ice breakers are available, extreme caution is taken to avoid the sea ice, or in the very short Arctic summer (Rypdal et al., 2012). The presence of sea ice makes it possible to either find sources and receivers that can be put on top of the ice, or lowered down below the ice.

Many Arctic areas are also very remote and can be difficult to access, but one of the biggest challenges is that the wavefield in Arctic areas is not very well understood, and is assumed to be quite complicated. If the acquisition is performed in an area with shallow water as well, the wavefield becomes even more complicated. Both the presence of sea ice and shallow water give rise to several different types of surface waves, which give a complex wavefield, and hence a seismic record that can be difficult to process and interpret properly (Rendleman and Levin, 1990, Henley, 2007, Johansen et al., 2011).

4.2. Wavefield in an Arctic shallow water environment

The wavefield in Arctic areas may include many different types of waves, and can be quite complex. Shallow water depth and a presence of sea ice can complicate the wavefield, and in addition, both the upper sediment layers and ice can be highly varying media (Press and Ewing, 1951a, Rendleman and Levin, 1990, Johansen et al., 2011).

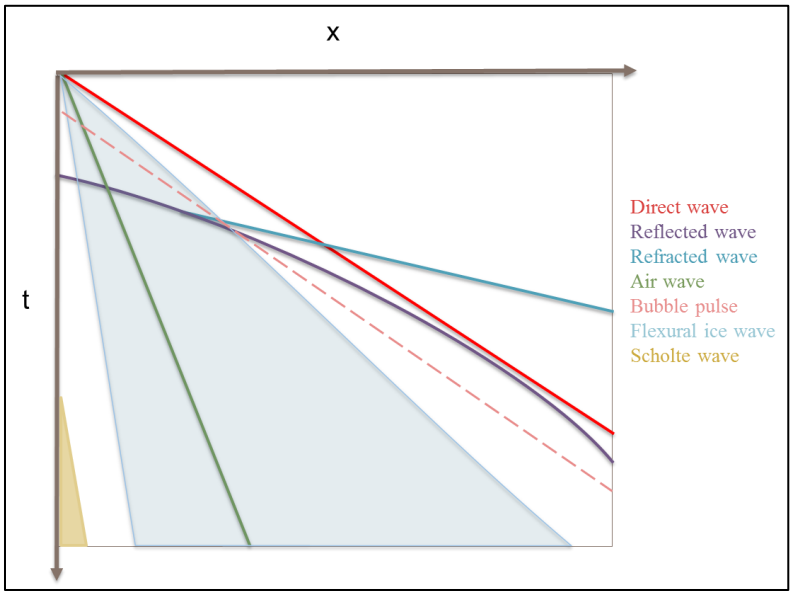

Figure 11: Schematic figure of a typical seismogram from a shallow marine Arctic survey, including body waves (direct, reflected and refracted P-waves), source-induced waves (air wave and bubble pulse), and surface waves (flexural ice waves and Scholte waves). Not all waves will be present in all seismograms from such areas. Which types of waves are present in each survey, will depend on the characteristics of that survey.

The waves that would typically be present in the records from a shallow marine Arctic survey are shown in Figure 11. The same waves as in a traditional seismic survey are usually found, i.e. direct, reflected and refracted P- and S-waves, but other events will be present as well. Various types of source-induced waves, i.e. bubble pulses and air waves (see subsection 3.1.1 and 3.1.2.), are common to find in seismic records from areas both with and without sea ice. However, a high presence of surface waves is typical for such an environment, and they can complicate the wavefield (Johansen et al., 2011). Surface waves will typically travel close to an interface, but have coupled waves that make it possible to record them further away from the interface (Press and Ewing, 1951b). Examples of such surface waves can be flexural ice waves and Scholte waves.

As explained in section 2.2, wave propagation can be described by the wave equation:

$$\nabla^2\varphi = \frac{1}{c^2}\frac{\delta^2\varphi}{\delta t^2}. \quad (16)$$

Press and Ewing (1951a) derive the solutions of the wave equations in an air-ice-sea environment (Figure 12). In that case, the wave equations are:

$$\nabla^2\varphi_1 = \frac{1}{v_{p1}^2}\frac{\delta^2\varphi_1}{\delta t^2} \quad \text{in the ice,} \quad (17)$$

$$\nabla^2\psi_1 = \frac{1}{v_{s1}^2}\frac{\delta^2\psi_1}{\delta t^2} \quad \text{in the ice,} \quad (18)$$

$$\nabla^2\varphi_2 = \frac{1}{v_{p2}^2}\frac{\delta^2\varphi_2}{\delta t^2} \quad \text{in the water.} \quad (19)$$

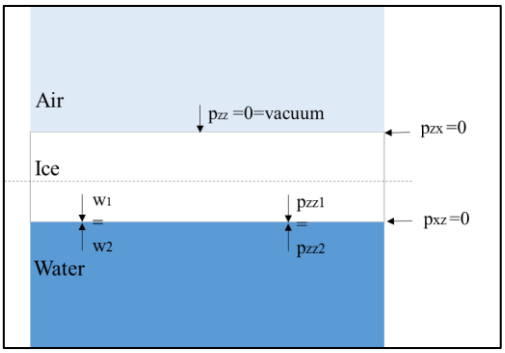

Figure 12: The boundary conditions used by Press and Ewing (1951a) is shown in the figure showing an infinite vacuum layer, a finite ice layer, and an infinite water layer. There is no pressure from the air on the ice (pzz), the pressure and displacement from the ice on the water and from the water on the ice are similar (pzz1, w1, pzz2, w2), and there is no shear pressure (pzx, pxz).

φ and ψ are the elastic potentials for P- and S-waves, respectively. These are defined from the horizontal and vertical displacements, and thus displacement can be derived from the potentials. This means that for a P-wave, pressure will be proportional to the potential. The solutions become:

$$\varphi_1 = [A\sinh(\xi z) + B\cosh(\xi z)]e^{i(kx-\omega t)}, \quad (20)$$

$$\psi_1 = [C\sinh(\eta z) + D\cosh(\eta z)]e^{i(kx-\omega t)}, \quad (21)$$

$$\varphi_2 = Ee^{-\varsigma z}e^{i(kx-\omega t)}, \quad (22)$$

where

$$\xi^2 = k^2\left(1-\frac{c^2}{v_{p1}^2}\right), \quad (23)$$

$$\eta^2 = k^2\left(1-\frac{c^2}{v_{s1}^2}\right), \quad (24)$$

$$\varsigma^2 = k^2\left(1-\frac{c^2}{v_{p2}^2}\right)^*, \quad (25)$$

for the boundary conditions given by Press and Ewing (1951a), where p means pressure, and w means vertical displacement (Figure 12).

* In Press and Ewing (1951a), Equation 25 is given as $\varsigma^2 = k\left(1-\frac{c^2}{v_{p2}^2}\right)$, but this is assumed to be a misprint.

A, B, C, D and E are constants that can be found from different boundary conditions. ω is the angular frequency, k is the wave number, c=ω/k is the phase velocity, and z is the depth. The subscript 1 means that the property is in ice, and the subscript 2 means that the property is in water. v_p means the P-wave velocity, and v_s means the S-wave velocity. Press and Ewing (1951a) give a thorough derivation of all the waves present in the wavefield based on these three wave equations, for the three cases of small wavelengths compared to ice thickness, large wavelengths compared to ice thickness, and wavelengths similar to the ice thickness. They assume that the wave equation reduces to different wave modes for each of these conditions. The whole derivation by Press and Ewing (1951a) is too detailed for this thesis, but two of the waves that can be found in an Arctic environment will be presented in the next subsections.

4.2.1. The flexural ice wave

The most relevant regarding seismic exploration is the case where the wavelengths are large compared to ice thickness. Then it can be shown that an asymmetrical Lamb wave will travel as a flexural wave in the ice (Press and Ewing, 1951a).

The flexural ice wave is a surface wave that is evident on seismic records from areas with shallow water depth and ice cover. The rigidity of ice leads to a horizontally travelling wave within the ice layer, when a vertical disturbance is inflicted on the ice surface. The wave makes the whole ice sheet move, and therefore the flexural ice wave will have coupled waves travelling in the water as well (Press and Ewing, 1951a, Henley, 2007). An analogy to what happens can be to think about a drum skin. Applying a vertical disturbance to the drum skin in one place will lead to a horizontally travelling disturbance, making the whole drum skin move vertically (Proubasta, 1985). Figure 13 shows how the flexural ice wave will make the whole ice sheet move asymmetrically around the horizontal plane.

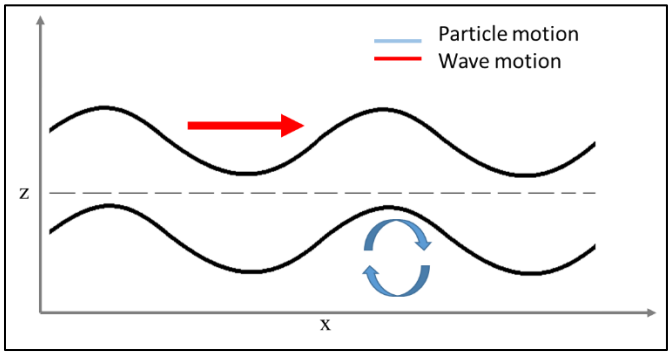

Figure 13: Schematic figure of a flexural ice wave. The figure shows the particle and wave motion of a flexural ice wave. The flexural ice wave is a Lamb wave that is asymmetric around the horizontal plane. The flexural ice wave makes the whole ice sheet move due to the rigidity of ice.

The wave is dispersive, meaning that different frequency components will travel with different phase velocities. On a seismic record of offset versus time, the flexural ice wave will therefore appear as a broad fan, as was seen in Figure 12. The amplitudes of the flexural ice wave are often high compared to reflections from the subsurface, and thus they tend to mask the reflections on a seismic record (Rendleman and Levin, 1990, Henley, 2007). Varying ice thickness and temperature can affect the generation of flexural ice waves (Kohnen, 1974, Rovetta et al., 2009a).

Since the flexural ice wave tends to mask reflections on a seismic record, it is usually considered to be noise. Several filtering techniques have been tested to remove the flexural ice wave, including the radon transform (RT), slant stack (τ-p), and frequency-wavenumber (f-k) filtering (Henley, 2003, Henley, 2007, Rovetta et al., 2009a, Jensen, 2016). These have had limited success in removing the flexural ice wave. It has been suggested that changing the acquisition geometry to avoid the flexural ice wave from being created at all could be a better approach to the problem (Rendleman and Levin, 1990, Henley, 2007, Del Molino et al., 2008).

Press and Ewing (1951b) show that when a seismic source is placed in air, a wave train of flexural waves with constant frequency and the velocity of sound in air (~330 m/s) can be observed. They relate the existence of this wave train to a coupling between air waves and surface waves when the phase velocity of the surface wave is close to the velocity of sound in air. They refer to these waves as air-coupled flexural waves.

4.2.2. The Scholte wave

The Scholte wave is another type of surface wave that is often encountered in seismic records from shallow marine areas with sea ice cover. The model used by Press and Ewing (1951a) assume infinite air and water layers, with a finite ice layer between them. If a water bottom is added to the model, the solutions become more complicated, and a Scholte wave will occur. Just like the flexural ice wave, the Scholte wave will have coupled waves travelling in the water. If the water depth is less than the wavelengths of the two surface waves, a coupling between the Scholte- and flexural ice waves may also occur (Senior Engineer Bent Ole Ruud 2017, personal communication, 02.05.17).

Scholte waves are interface waves that occur at the water bottom, at the interface between the solid subsurface and liquid water. The wave is elliptically polarized, with a particle movement resembling the particle movement of a Rayleigh/Stoneley wave (Boiero et al., 2013). The Scholte wave usually travels with very low velocities, and is often dispersive. Studies have

shown that the waves are generally contained within the low-frequency range 2-20 Hz (Boiero et al., 2013). The reason why the Scholte wave is dispersive is partly due to sediment layering, and partly due to limited water depth (Bohlen et al., 2004, Kugler et al., 2005). As previously mentioned, low frequency components of a wave will not be attenuated as quickly as higher frequencies, and can thus penetrate relatively deep into the subsurface. High frequency components of a Scholte wave can on the other hand only penetrate 1-2 wavelengths into the subsurface. Since the propagation velocity in sediments generally increases with depth, the low frequency components will thus travel in higher velocity layers than the higher frequencies, and therefore with a higher phase velocity (Dosso and Brooke, 1995, Boiero et al., 2013). This is opposite of the flexural ice wave, where the high frequencies will travel with the highest phase velocities. If the subsurface is homogenous, and the water depth is much larger than the wavelength, the Scholte wave will generally not be dispersive. This is also opposite of the flexural ice wave, which is dispersive by nature (Del Molino et al., 2008).

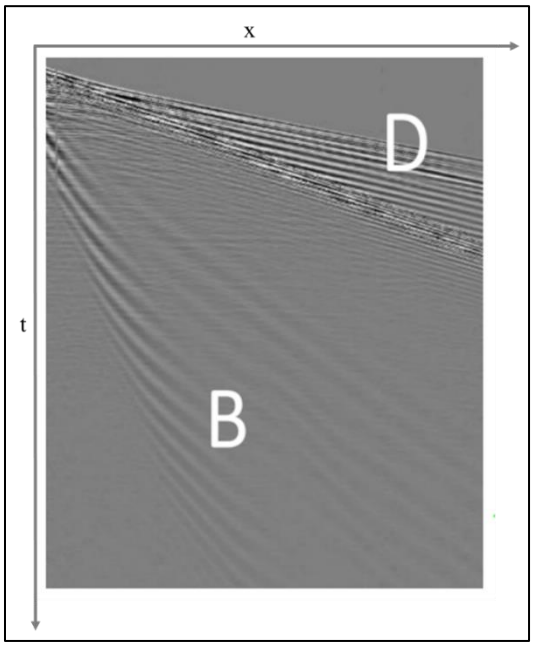

Figure 14: Figure modified from Boiero et al. (2014). The figure shows a common receiver plot for a shallow water towed streamer. The event marked with B is believed to be the dispersive Scholte wave, and the event marked with D is believed to be guided P-waves. We see that we can expect Scholte waves to have steep slopes relative to guided P-waves.

Figure 14 is modified from Boiero et al. (2014), and shows how we can expect to see the Scholte waves in a common receiver gather from a hydrophone streamer. Since the velocity of the wave is very low, the gradient is expected to be steep.

Just like the flexural wave, the Scholte wave has often been regarded as noise in the seismic records, but studies have shown that Scholte waves can be used to obtain important information about the subsurface. Since there is a relation between how deep one frequency component of

the Scholte wave will penetrate, and the phase velocity the frequency component will travel with, studies have indicated that the shear wave velocity profile of the shallow subsurface can be estimated based on the dispersion characteristics of the Scholte wave. This is done in practice by finding the dispersion characteristics of Scholte waves from experimental data, and estimating the properties of the subsurface by adjusting a model of the subsurface to match the dispersion characteristics (Dosso and Brooke, 1995, Socco et al., 2010, Boiero et al., 2013).

4.3. Summary

When performing seismic exploration in Arctic areas, several special considerations must be made. The presence of sea ice makes it necessary to use seismic equipment fitted for those conditions, meaning that instead of using marine streamers, seismic sources and receivers need to be placed either on top of the sea ice, or in the water column below the sea ice. If the equipment is placed on top of the sea ice, land seismic equipment such as detonating cords and geophones can be used. If the equipment is lowered into the water below the sea ice, marine seismic equipment such as air guns, hydrophones and OBS can be used (Hall et al., 2001, Del Molino et al., 2008). Studies have indicated that the seismic wavefield created during seismic acquisition in areas with sea ice can vary depending the equipment used, and the combination of them (Rendleman and Levin, 1990, Del Molino et al., 2008). However, more studies of the effect of this need to be done, and this is partly what this thesis will look at in the following chapters. The seismic wavefield from an area with shallow water depth and sea ice cover has been seen to include some surface waves. This is for example flexural ice waves in the ice, and Scholte waves at the seabed-water interface. These surface waves also have coupled waves travelling in the water. Surface waves are often considered as noise in the seismic records, but can contain important information if they are interpreted correctly (Boiero et al., 2013). Depending on the goal of the seismic study, effort can be made to either remove these surface waves, or to interpret them correctly.

5. Background – Sound propagation and pinniped hearing

5.1. Sound propagation

The seismic waves most often used in seismic surveys are compressional waves, as these can penetrate through the interior of the Earth. Also, as opposed to S-waves, they can travel through water. As explained in chapter 2, P-waves are quantified by many different measures, both in the time and frequency domain. The compressional particle movement associated with P-waves makes it possible to hear them when they hit an ear, assuming that the wave consists of frequencies within the hearing bandwidth of the receiver. Therefore, P-waves are often referred to as sound waves. The particle displacement A associated with a passing wave is given through the relation:

$$A = \frac{P}{\omega \rho_0 c}. \tag{26}$$

P is the pressure, ω is the angular frequency, ρ_0 is the specific density, and c is the velocity of the medium the wave travels through. The amount of displacement will determine how high sound level is perceived (Association of Oil and Gas Producers, 2008). Sound propagation underwater is a subject that has been extensively studied, but the literature can be confusing and difficult to compare. There are many different notions used within the subject, and many different relationships between e.g. frequencies, sound pressures, and intensities that need to be understood. Also, different terms tend to be used by different authors. The following subsection is meant to give a clarification of the concepts used, and is largely based on the review paper written by Gausland (2000).

5.1.1. Sound pressure level (SPL)

Sound levels are often given as sound pressure levels (SPLs). Sounds are usually measured by their effective sound pressure P_e, which can be measured in many different ways in a seismic record. When comparing sound pressures, adjustments due to different measuring methods might therefore be necessary.

- P_e(rms) is when P_e is measured as the root mean square of the pressure.
- P_e(0-p) is when P_e is measured as the value of the largest positive pressure in the signal.
- P_e(p-p) is when P_e is measured as the difference between the largest negative pressure and the largest positive pressure in the signal.
- P_e(f) is when P_e is given as a function of frequency.

(Gausland, 2000).

Sound pressure is given in either Newton/m^2 or Pascal, but when talking about sounds, it often makes more sense to talk about the intensity of the sound, since intensity takes the medium that the sounds travel in into account as well. The formula to compute intensity from sound pressure is given by:

$$I = \frac{{P_e}^2}{\rho_0 c}. \quad (27)$$

The denominator in Equation 27 is the acoustic impedance, with ρ_0 being the density of the surrounding medium, and c being the sound velocity in the surrounding medium. Since the formula for intensity takes the acoustic impedance of the medium where the sound travels into account, sounds in different media can thus be compared easier by referring to intensities instead of sound pressures (Gausland, 2000).

In addition to different elastic properties, different media can also have different reference pressure levels P_0 or reference intensity levels I_0. This must also be taken into account when talking about sound levels, so a given sound level must be given relative to a reference pressure level. This can be done by converting the intensities I or sound pressures P_e to decibel levels using the formulas given below:

$$\text{Intensity level: } dB = 10\log\frac{I}{I_0}, \quad (28)$$

or

$$\text{Sound pressure level } dB = 20\log\frac{P_e}{P_0}. \quad (29)$$

It is important to highlight the fact that a decibel level is not a unit for measuring sound, but rather a relative measure used for giving sound levels (Gausland, 2000).

If we, as an example, look at the case where it is desirable to compare sounds travelling in air and in water, we can find that a sound needs to be approximately 62 dB louder under water than in air to hear the same sound level. This is due to different acoustic impedances in the two media, and different reference pressure levels:

- The acoustic impedance in air is approximately 415 Pa*s/m^3, and the acoustic difference in water is approximately $1.54*10^6$ Pa*s/m^3. This corresponds to a difference of 35.6 dB between air and water.

- The reference pressure in air is approximately 20.4 μPa, and the reference pressure level in water is approximately 1 μPa. This corresponds to a difference of 26 dB between air and water.

(Gausland, 2000).

5.1.2. Sound exposure level (SEL)

It has been claimed that impulse sources such as seismic air guns should have sound levels expressed as sound exposure levels (SELs) instead of as SPLs (e.g. Farcas et al. (2016)). While SPL gives a decibel value for sound, it takes no account of the duration of the sound, or that there might be several sounds following each other. It has been shown that a sound with a certain SPL can be perceived similar to a sound with a different SPL if the sound has a long duration, or occurs several times in a row. The idea is that it is the total sound energy received that matters, often referred to as the equal energy hypothesis (Gordon et al., 2003). SEL is a measure that takes into account the duration of a sound, and also the fact that a pulse can be repeated several times.

The formula for SEL is given by Southall et al. (2007) as

$$\text{SEL} = 10\log\frac{\sum_{n=1}^{N}\int_0^T p_n^2(t)dt}{p_0^2}. \quad (30)$$

N is the number of pulses, T is the duration of each pulse, p is the instantaneous effective pressure, and p_0 is the reference pressure. As can be seen from the formula, the SEL sums the integral of the squared effective sound pressure over time for all pulses, and gives a sound level in dB re 1 μPa^2s for measurements underwater. The formula assumes that there is no recovery of hearing loss between the pulses, therefore only pulses that occur within a given time frame (e.g. without a 12 hour break) are summed together.

5.2. Hearing

How a sound is perceived by a marine mammal depends both on the sound pressure of the signal, the intensity, and the frequencies that the signal consist of. Hearing is the trait of being able to perceive a sound, and is one of the primary sensory modalities for most vertebrates, both terrestrial and marine (Southall et al., 2007). Hearing is also one of the senses that are most useful in water, since sounds tend to travel very well in water, while sight is rapidly degraded. Sounds have been recorded as far as half the Earth away from a strong sound source (Shockley et al., 1982, Harris et al., 2001). Different receivers have different frequency bandwidths that

they can hear, e.g. a human will usually hear sounds within the frequency range of 20 Hz to 20 kHz (Richardson et al., 1995). A receiver will not hear all frequencies within this range equally well, e.g. for humans the frequency that is usually heard best is 1 kHz (Southall et al., 2007).

In addition to only being able to a hear a limited frequency range, there is also a lower limit of how low SPLs a receiver can detect, and an upper limit of how high SPLs a receiver can detect without being harmed. The first is often referred to as the hearing threshold, and the latter is often called the threshold of damage. For humans, the low limit is 0 dB in air or 62 dB in water, and the threshold of direct damage is 160 dB in air or 222 dB in water. The hearing threshold of marine mammals can be assumed to be 20 dB lower than humans, i.e. it can be assumed that marine mammals would hear sounds of approximately 42 dB re 1 µPa in water (Gausland, 2000). Whether a receiver can detect a specific sound also depends on the amount of background noise present (Richardson et al., 1995). Since whether a signal can be heard or not depends both on the frequency of the signal and the SPL, measuring hearing thresholds can be quite difficult. One method to measure hearing thresholds is to study the response of receivers when they are exposed to sounds with different frequencies, at different SPLs. The lowest SPL that gives a response for each specific frequency can be assumed to be give the audiogram of the receiver (Gordon et al., 2003, Southall et al., 2007). Example of such audiograms for several different pinniped species are displayed in Figure 15 (Kastelein et al., 2002).

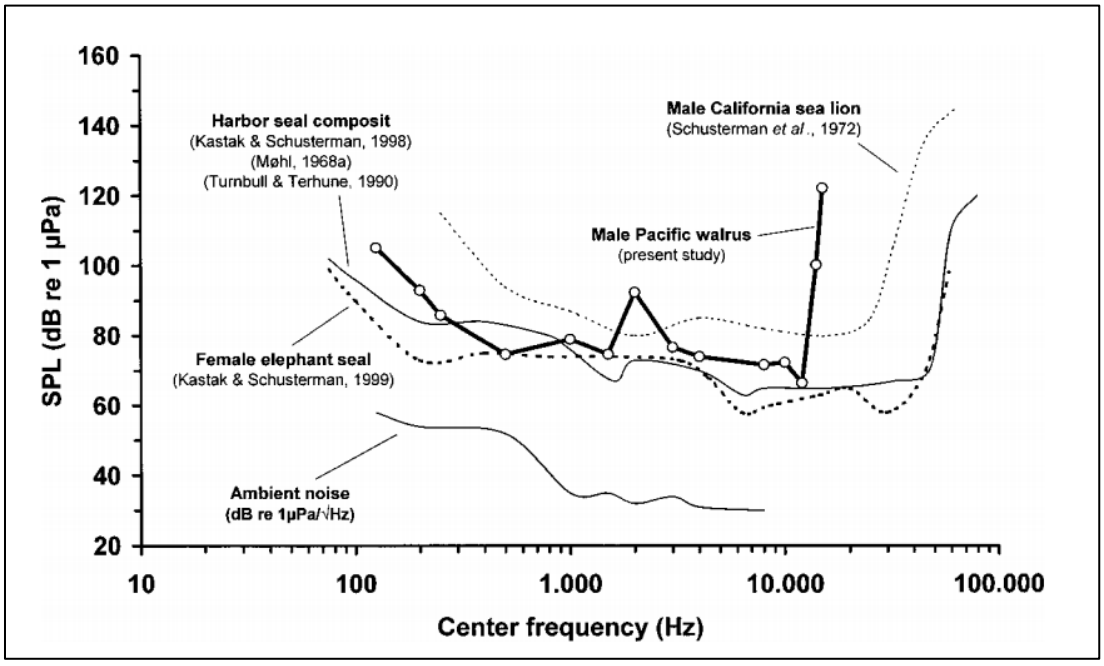

Figure 15: Figure from Kastelein et al. (2002). The figure shows the audiograms for several different pinniped species, based on results from several studies by Kastelein, Kastak, Schusterman, Møhl, Turnbull and Terhune.

An audiogram can be used to make a frequency-weighting function, where the SPLs that are needed to hear different frequencies are determined relative to each other. The result can be plotted as a curve where the best-heard frequency is weighted as 0 dB, and all other frequencies that need a higher SPL to be heard are weighted with a negative decibel value (Southall et al., 2007, National Marine Fisheries Service, 2016). Figure 16 shows examples of curves of such theoretical frequency-weighting functions for two pinniped families.

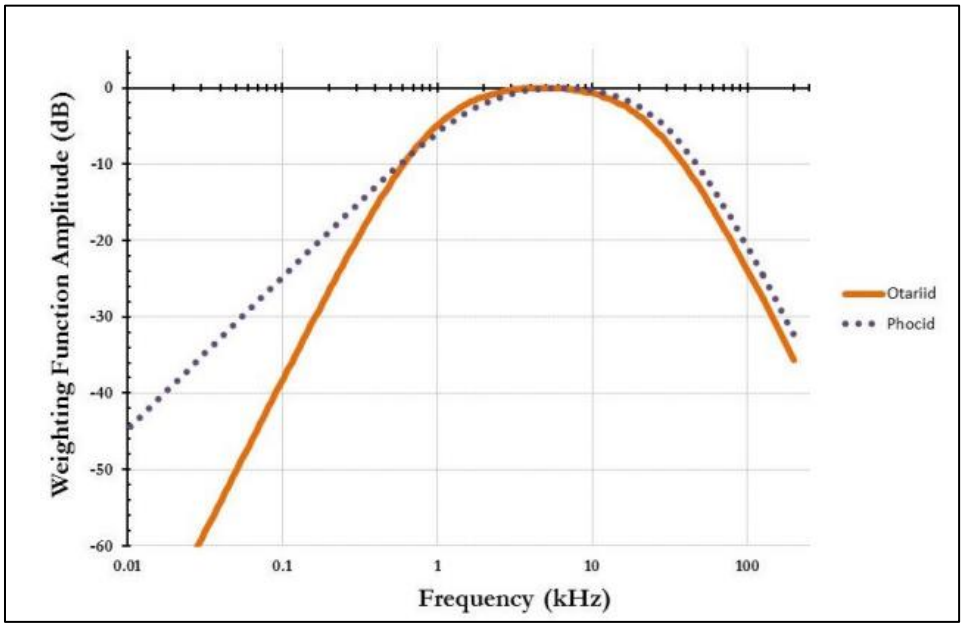

Figure 16: Figure from National Marine Fisheries Service (2016). Simplified frequency-weighting curve for in water. Individual differences between different pinniped species have been observed, so a simplified curve like this is probably not accurate. We can see that for frequencies below approximately 200 Hz, the hearing sensitivity of Phocid pinnipeds is between 20 and 45 dB lower than at 3 kHz to 8 kHz.

For pinnipeds, this curve is often called an M-weighting curve, while for humans A-weighting curves are often used to deemphasize frequencies below 1 kHz and above 6 kHz (Southall et al., 2007, National Marine Fisheries Service, 2016). The technical guidance from National Marine Fisheries Service (2016) contains formulas for weighting-functions for several different types of marine mammals (table ES2, p. 3).

5.3. Pinnipeds and hearing damage

The ears are the parts of the body that incorporate the trait of hearing, and they usually consist of three parts: the inner, the middle and the outer ear. Pinnipeds are mammals thought to have developed from terrestrial animals, thus there are several similarities between the human ear and the pinniped ear. However, since seals are marine mammals and thus spend time both above and under water, they need to hear in both environments. Adaptions in the anatomy of their ears have led to efficient underwater hearing, in addition to the possibility to hear in air. It has been

suggested that the part of the ear that promotes underwater hearing is the middle ear. Studies have shown that the middle ear in pinnipeds is larger and denser than the middle ear in terrestrial animals, and that it might function as a variable transformer allowing hearing both in air and underwater (Kastak and Schusterman, 1998, Southall et al., 2007).

If a receiver is exposed to very high SPLs, the hearing threshold can be changed. This is called a threshold shift, and a threshold shift can be either temporary (TTS) or permanent (PTS). TTS or PTS in seals can, according to Southall et al. (2007), be induced by physical consequences related to the arrival of the wave. Whether this leads to a temporary change in sensitivity in the tissue in the ears, or a permanent damage to the tissue in the ears, can depend on the intensity or the duration of the exposure. This is why it has been suggested to use the SEL instead of the SPL when assessing the possible harmful effects of noise exposure (Southall et al., 2007, Kvadsheim et al., 2017). As was explained above, if we follow the equal energy hypothesis, the threshold shift should be proportional to the product of intensity and time (Gordon et al., 2003). Sounds from seismic sources are amongst the strongest anthropogenic noise sources that exist, and studies about how and where these can cause TTS or PTS are therefore necessary (Hermannsen et al., 2015).

The effects intense sounds can have on marine mammals can be divided into four groups: physical and physiological effects, perceptual effects, behavioural effects, and indirect effects (Gordon et al., 2003). These need to be treated separately, since each effect can come into play at very different sound levels and distances from a noise source. Thus, different spatial zones around a sound source can be defined, based on how the sound is perceived there. The first is where a sound will be detected (zone of audibility), the second is where a sound will cause behavioural change (zone of responsiveness), the third is where a sound will make it difficult to detect other sounds (zone of masking), and the last is where a sound will physically harm an animal (zone of hearing loss, discomfort or injury) (Richardson et al., 1995, Davis et al., 1998, Gordon et al., 2003, Tougaard et al., 2009, Kvadsheim et al., 2017). A method that is often used to make sure seismic operations do not harm marine mammals, is to determine the extent of these zones, and to use this to make so-called “seismic shut down zones”. These zones determine when seismic operations should be shut down if marine mammals are observed within the zone (Tolstoy et al., 2004, Tougaard et al., 2009, Hermannsen et al., 2015).

Investigating the effects of man-made noise on marine mammals can be difficult. There are relatively few pinniped individuals held captive, and the behaviour of those individuals is often altered since they are used to taking part in noise exposure experiments (Gordon et al., 2003,

Southall et al., 2007). Background noise is usually present during noise impact studies, and this may also affect the results of the studies (Kastelein et al., 2009). Behavioural responses may also be difficult to interpret objectively, and they may vary depending on the experiences of the specific animal (Gordon et al., 2003). Nevertheless, the studies are harmless to the animals, as opposed to what studies of TTS or PTS might be. When studying physical effects of noise exposure, ethical and legal considerations make the studies difficult to obtain (Southall et al., 2007). Therefore, there is an uncertainty involved in determining how certain sound levels will affect an animal.

5.4. Pinnipeds on Svalbard

The Norwegian polar institute is registering observations of pinnipeds on Svalbard, and according to them there are six types of pinnipeds living on Svalbard. This includes the walrus (*Odobenus Rosmarus*), the bearded seal (*Erignathus Barbatus*), the harbour seal (*Phoca Vitulina*), the ringed seal (*Pusa Hispida*), the harp seal (*Phoca Groenlandica*), and the hooded seal (*Cystophora Cristata*) (Aanes et al., 2011). Whales (*cetaceans*) are the other family of marine mammals living in the waters close to Svalbard.

Pinnipeds can be divided into the families *Phocidae* (true seals/earless seals), *Otariidae* (eared seals/sea lions and fur seals), and *Odobenidae* (walruses), where all the seals on Svalbard belong to the *Phocidae* family (Aanes et al., 2011, Reichmuth et al., 2013). According to the Norwegian polar institute, three of these species require special caution by people roaming in their habitat. These are the ringed seal, the bearded seal, and the harbour seal. The ringed seal spends a lot of time on the sea ice in the fjords of Svalbard in the period when they are giving birth and molting, from mid-March to June (Krafft et al., 2006, Aanes et al., 2011). It has been claimed that activities in the fjords of Svalbard in that period, including for example seismic surveys, could be harmful to the ringed seal (Enger et al., 1987, Aanes et al., 2011).

5.4.1. Frequency range

The science available does not give exact exposure criteria for when harm occurs for every species and every sound source, and there is a special lack of studies for the low frequencies (<1000 Hz) most common in seismic surveys (Richardson et al., 1995, Kastak and Schusterman, 1998). Table 1 sums up a few studies where frequency ranges for pinnipeds have been tested in a controlled facility.

Author	Species	Studied frequency range	Best heard frequency	Lowest heard frequency
Kastelein et al. (2002)	Pacific walrus	125 Hz to 15 kHz	12 kHz (at 67 dB re 1 µPa, rms)	125 Hz (at 106 dB re 1 µPa, rms)
Kastelein et al. (2009)	Harbour seal	125 Hz to 100 kHz	1 kHz (at 54 and 56 dB re 1 µPa, rms)	125 Hz (at 77 dB re 1 µPa, rms)

Table 1: A summary of two studies where low frequency hearing capacities of pinnipeds have been tested in a controlled facility. Frequencies down to 125 Hz were tested, and were heard quite well, however with a 23-39 dB lower hearing sensitivity than the best heard frequency.

Southall et al. (2007) suggested that pinnipeds in general can hear frequencies in the range of 75 Hz to 75 kHz in water, and 75 Hz to 30 kHz in air. These values were for many years accepted as the standard criteria for assessing hearing damages in seals, but were recently updated in a technical guidance from NMFS (National Marine Fisheries Services). Then, the hearing range was extended to 50 Hz to 86 kHz for *Phocid* pinnipeds in water, as was seen in Figure 16 (National Marine Fisheries Service, 2016). The science is too uncertain to draw any definite conclusions, but nothing indicates that they can hear frequencies below this limit of 50 Hz.

Air gun pulses mainly contain frequencies below 100 Hz, but according to Hermannsen et al. (2015), some frequency components up to 10 kHz have been recorded in shallow water surveys. This suggests that frequencies that pinnipeds can hear well are also possibly found in seismic signals. The presence of high frequencies during seismic surveys have also been reported by e.g. Landrø et al. (2011) and Goold and Fish (1998). Goold and Fish (1998) recorded SPLs up to 90 dB re 1µPa, rms, at frequencies up to 22kHz during an air gun array survey.

5.4.2. TTS- and PTS-onset

When it comes to sound levels, Southall et al. (2007) claim that TTS-onset in marine mammals will happen when the hearing threshold is temporarily raised 6 dB compared to the normal hearing threshold. The relationship between TTS and PTS is complicated, but Southall et al. (2007) developed a way of extrapolating data from TTS-onset to PTS-onset. They assumed that PTS-onset happens if a TTS of 40 dB occurs. It is important to note that 1 dB of TTS does not necessarily mean 1 dB of raised SPL. Based on this, as well as knowledge about hearing capabilities of marine mammals, Southall et al. (2007) calculated a precautionary criterion of 6 dB of extra noise exposure after TTS-onset to be the SPL when PTS-onset occurs. Table 2 summarizes some studies where the effect of sound exposure has been studied for several species of marine mammals.

Author	Species	SPL	Duration	Comment
Southall et al. (2007)	Harbour seal	152 dB re 1µPa, rms	25 minutes	TTS-onset
Finneran et al. (2003)	California sea lions	<183 dB re 1µPa, p-p	Pulse	No TTS
Blackwell et al. (2004)	Ringed seal	<151 dB re 1 µPa, rms	Offshore construction work	No behaviour change
Harris et al. (2001)	Ringed seal	>190 dB re 1 µPa, rms	Air gun pulses	Small avoidance behaviour
Crum and Mao (1996)	Marine mammals	<190 dB re 1 µPa, rms	Sonar pulses	Decompression sickness unlikely
Davis et al. (1998)	Marine mammals	202 dB re 1 µPa, p-p	100 pulses of 0.1 s	TTS-onset, extrapolated from the Ward DRC
Gordon et al. (2003)	Marine mammals	195 dB re 1 µPa, p-p	100 pulses of 0.1 s	TTS-onset, extrapolated from the Ward DRC
Richardson et al. (1995)	Marine mammals	178 dB re 1 µPa, p-p	100 pulses of 0.2 s	TTS-onset, extrapolated from the Ward DRC
Richardson et al. (1995)	Marine mammals	244 dB re 1 µPa, p-p	1 pulse of 0.025 s	TTS-onset, extrapolated from the Ward DRC

Table 2: A summary of studies where the effect of sound exposure on marine mammals have been studied. The mentioned DRC are damage risk criteria developed by Ward (1968) for humans, by considering how exposure to 100 pulses of varying duration would lead to TTS in humans.

There is clearly some uncertainty involved in determining damage thresholds for pinnipeds, but the distance from the seismic source where 180-190 dB re 1µPa, rms, is found is often used as the radii of the seismic shut down zone (Gausland, 2000, Tolstoy et al., 2004). The recent technical guidance by National Marine Fisheries Service (2016) claim that SPLs of 212 dB re 1µPa, p-p, or SELs of 170 dB re1µPas^2 are needed for TTS-onset for impulsive sounds, and SPLs of 218 dB re 1µPa, p-p, or SELs of 185 dB re1µPas^2 are needed for PTS-onset for impulsive sounds in *Phocids*.

5.5. Summary

This chapter has given an overview of the propagation of sound waves in water, and the impact sound waves might have on pinnipeds. A sound wave will be characterized both by the frequency components it consists of, and the sound level of the wave. SPLs are given in decibel, and must be given relative to a reference pressure (1 µPa in water). The challenges related to measuring hearing bandwidths for marine mammals means that few studies are available. However, the studies that do exist indicate that seals cannot hear low frequencies very well, but that frequencies down to 50 Hz may be heard if the sound levels are very high (National Marine

Fisheries Service, 2016). In seismic operations, it is most common to use low frequencies, but higher frequencies can also be observed in some cases (Hermannsen et al., 2015). From these studies, it is therefore assumed that seals can hear at least some of the frequency components used in seismic operations. The SPL that seems to be the limit for when harm can occur is approximately 180 dB re 1µPa, rms, but the nature of the pulse will also have a lot to say. The duration and number of exposures may have a large impact on the harmful effects of loud sounds, and if the pulse is repeated several times, it might be better to require that the SEL should be below this limit.

6. Methods and data

A seismic survey was conducted in the Van Mijen fjord, close to the settlement of Sveagruva on Spitsbergen, Svalbard, in March 2016. The location of the survey area is displayed in Figure 17. The survey will hereafter be referred to as the "2016 Svea survey".

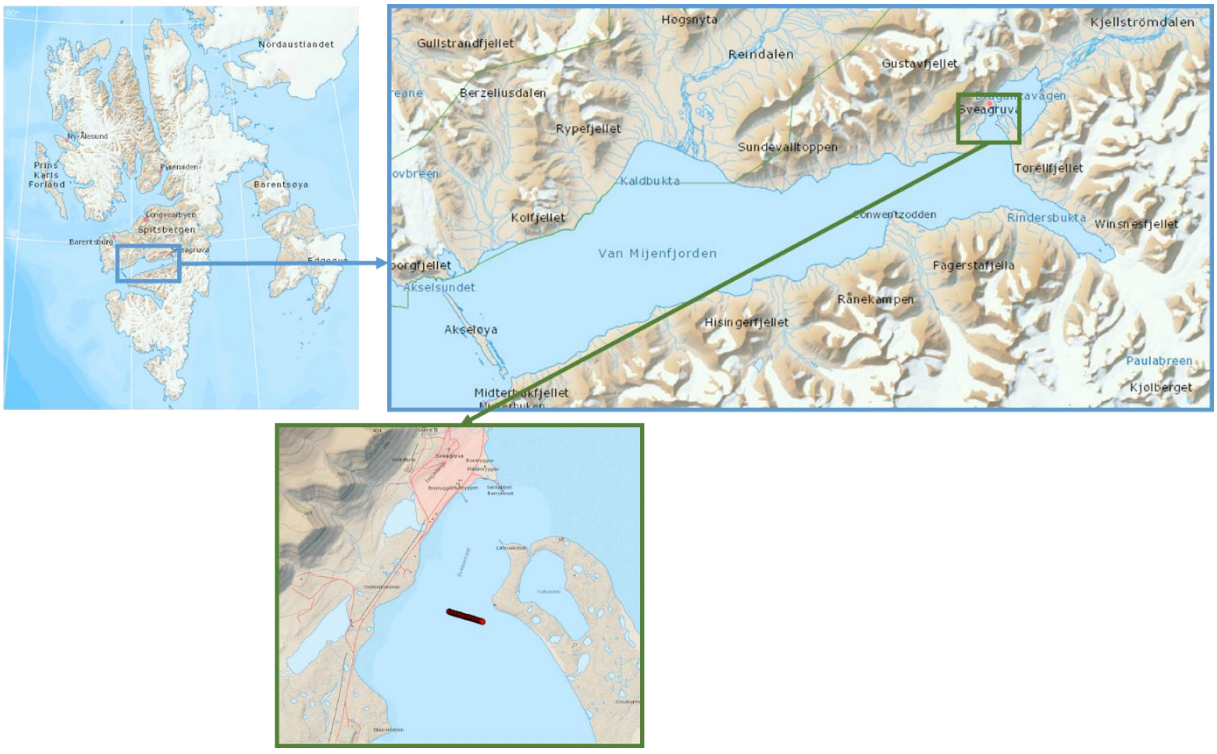

Figure 17: The survey area was in the Van Mijen fjord on Spitsbergen. The upper window shows the inner Van Mijen fjord, while the lower window shows the area closest to Sveagruva. The coordinates of the spread are marked with red dots in the lower window.

In the survey, different seismic sources and receivers were used to be able to study and compare the seismic data from different combinations of equipment. The survey was a 2D acquisition, and the spread was 450 meters long. Air guns and detonating cords were used as seismic sources, and geophones, hydrophones and ocean bottom seismometers (OBS) were used as seismic receivers. In this thesis, the seismic data from the 2016 Svea survey have been investigated, to produce the results that will be presented in chapter 7. Similar acquisitions were conducted in the Van Mijen fjord in March 2013 and February 2017 as well, where I participated in the latter.

6.1. Survey geometry

Detailed information about the layout of sources and receivers during the 2016 Svea survey is important to know to be able to understand the differences in the seismic data, caused by

differences in survey geometry. “Location” will be used to refer to horizontal position along the spread, and “depth” will be used to refer to vertical position in the water.

6.1.1. Receiver geometry

The receiver geometry in the survey was similar to the schematic Figure 18 below.

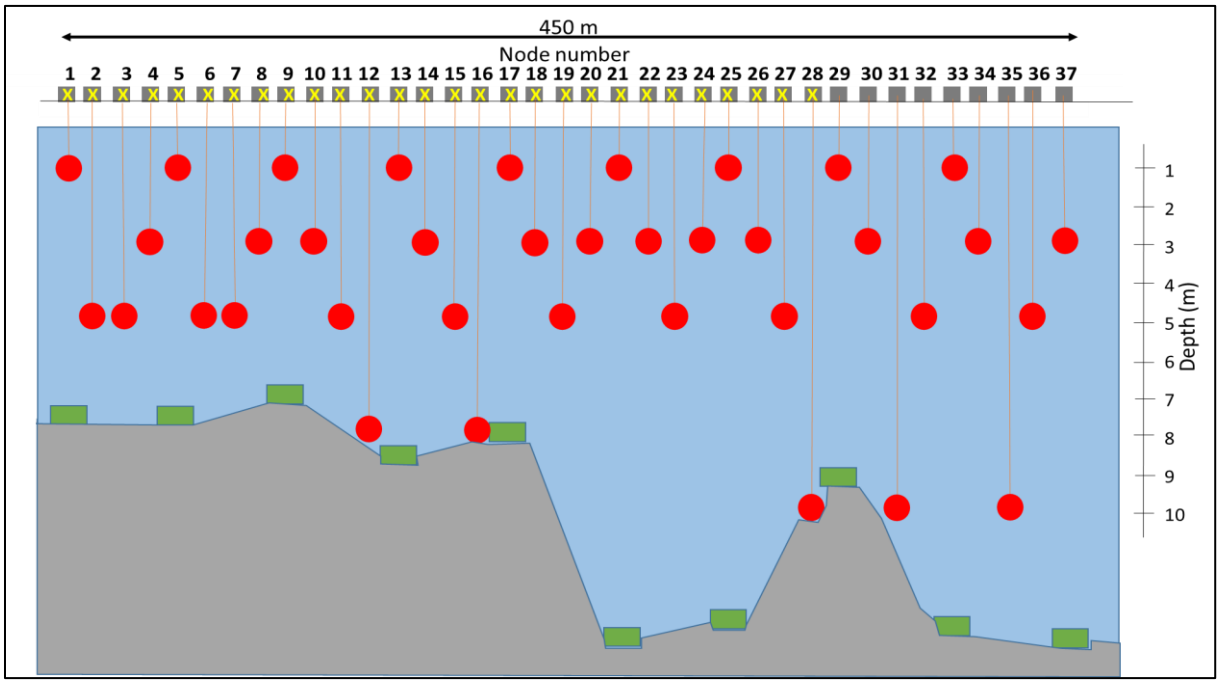

Figure 18: Schematic figure of the receiver geometry in Svea in 2016. Grey box represents a node, yellow cross represents a geophone, red circle represents a hydrophone, and green box represents an OBS.

Four different types of receivers were used, including hydrophones (of the type Unite, manufactured by DTCC), EDR and DAR 4C OBSs (of the type Trilobit, manufactured by Seabed Geosolutions), gimballed geophone strings, and 3C geophones. Some of these can be seen in Figure 19. A spread with a total length of 450 m was measured up, and 37 stations were distributed evenly along the line, meaning that the distance between each station was approximately 12.5 m. At each station, one or two nodes were placed. Each node worked as a recording device with four exits that receivers and external batteries could be connected to. All receivers were placed in positions that were later given relative to the nodes.

- One Unite hydrophone was lowered down into the water from one node at each station, giving a total of 37 Unite hydrophones at different depths (9 Unite hydrophones at 1 m depth, 12 Unite hydrophones at 3 m depth, 11 Unite hydrophones at 5 m depth, and 5 Unite hydrophones at various deeper depths).
- The geophone strings were laid out on top of the ice, parallel to the spread. They were laid out in two directions opposite to each other, with the centre at the node. This was

done from node 1 to 28, giving a total of 56 gimballed geophone strings. From some nodes, 3C geophones were connected to three of the exits.

- The OBSs were placed on the sea bottom by lowering them down using ropes. The OBSs were placed approximately 4 nodes apart from each other, with the first one below node 1, and the last one below node 37, giving a total of 10 OBSs with 50 m distance between each.

Figure 19: Some of the seismic receivers that were used during the acquisition were gimballed geophone strings (grey, upper left), Unite hydrophones (black, red and blue, lower left), and Trilobits (orange, right). In the picture to the left, a node connected to a battery is also visible.

The seismic profile was obtained with a sampling rate of 1 ms in the receivers.

6.1.2. Source geometry

In the 2016 Svea survey, two types of sources were used, including detonating cords with 40 g PETN per meter (equivalent to 66 g TNT per meter, of the type Nobelcord manufactured by Orica Mining Services), and mini GI air guns (manufactured by Sercel). Several shots were fired to test and calibrate the sources, and to orientate the Trilobits. The Trilobits had a Galperin setup, so to find the vertical and horizontal components, some shots that were recorded at both the geophones and the Trilobits had to be fired.

During the main part of the survey, a total of 104 shots were fired. Details about each of the shots are attached in Appendix II, but a brief summary will be given in the next paragraphs.

6.1.2.1. Detonating cord shots

A total of 43 shots were fired with detonating cords at different locations.

- One shot was fired close to each of the 37 nodes (except node 18), using a 5 m long detonating cord laid out parallel to the spread, on top of the ice, in front of the node. This gave a total of 36 shots, 12.5 meters apart along the spread.
- 5 shots were also fired outside the spread, with detonating cords of 10 m length, at every 50 m from node 37 + 50 m to node 37 + 250 m.
- 2 shots with detonating cords of 12.5 m length were fired at node 37 + 250 m.

The detonating cords were laid out as lines, and could therefore not be placed exactly at the node. A detonating cord is ignited at one end (usually the end closest to the start of the spread), and the explosion travels with a velocity of approximately 6900 m/s. Therefore, the cord can be interpreted as several point sources fired at almost, but not exactly, the same time. The difference in time Δt between shots with a distance Δd between them is $\Delta t=\frac{\Delta d}{v}$, where v=6900 m/s. The waves from the point sources will interfere, and create a directionality in the direction the explosion travels. The main amplitude lobe is pointing down and in that direction (Johansen et al., 2011). Since this will lead most of the energy in that direction, the detonating cord was placed in front of the receivers (e.g. the detonating cord said to be fired at node 9, is a detonating cord starting at node 9 – 5 m, and ending at node 9).

6.1.2.2. Air gun shots

23 shots were fired using a mini GI air gun lowered down into the water at node 17, and 38 shots were fired with the same air gun lowered down into the water from node 1 – 50 m. The air gun had two chambers with 15 in^3 volume in each. The air gun was alternating between being at 3 m and 5 m depth when it was at node 17, and 1.5 m and 3 m depth when it was at node 1 – 50 m:

- Node 17: 5 shots at 5 m depth, 10 shots at 3 m depth, and 8 shots at 5 m depth.
- Node 1 – 50 m: 3 shots at 3 m depth, 6 shots at 1.5 m depth, 6 shots at 3 m depth, 8 shots at 1.5 m depth, 6 shots at 3 m depth, 6 shots at 1.5 m depth, and 3 shots at 3 m depth.

The pressure of the air gun was also varying between the shots, from 90 bar to 160 bar.

6.2. Data investigation

The seismic data was stored in several segy files. The files mainly used in the work with this thesis were line_shots_h.segy, which included all hydrophone responses for all detonating cord shots, and airgun_shots_h.segy, which included all hydrophone responses for all air gun shots.

The seismic data was plotted and further investigated in MATLAB R2015B, using the add-on SeisLab 3.01. Depending on the purpose, the seismic traces were sometimes scaled, and other times not. Ormsby filters with varying cut-off values were also applied to the data, to highlight different events. The data was not processed heavily, and neither NMO-correction nor stacking was done. No interpretation of the subsurface based on the seismic data was therefore attempted. Several MATLAB scripts were written to investigate the data, and an explanation of how to get access to the scripts is attached in Appendix I. In addition to scripts for plotting the seismic data, MATLAB scripts for converting the seismic data to pressure values, and for computing decibel levels at different receiver locations were written. Also, MATLAB scripts for studying the wave propagation in the survey area were written. Additionally, the Schlumberger processing tool Vista 2016 was briefly used for looking at the seismic data.

6.2.1. Plotting of seismic data

Each of the steps described in this subsection was applied to both the detonating cord records, and the air gun records. The first thing that was done, was to plot the seismic data. The seismic data was plotted in MATLAB using the two scripts called *shotplot.m* and *receiverplot.m*. These scripts plot a common shot gather (i.e. receiver responses at all receivers for one single shot), and a common receiver gather (i.e. receiver responses at one single receiver for all shots), respectively. The user must specify in the input parameters which receiver(s) and/or which shot(s) the script should plot. The output is seismic records that can be used to study the events that occur in the seismic data, either in the form of wiggle plots, or colour plots. Different filters can be applied to look for specific wave types, individual scaling of traces can be turned on or off, and the limits of the colour scale can be set.

Functions that analyse the frequency contents of the plots made using *receiverplot.m* and *shotplot.m* were added to the previous scripts, by using the SeisLab function s_spectrum. Then, amplitude spectra are created by the scripts, in addition to the seismic plots. Since the sampling rate was 1 ms, all frequencies displayed in the amplitude spectra are contained in the range 0 to 500 Hz. The frequency spectra can either show the frequency content of the response at a single receiver for one or more shots, or the frequency content from a single shot at one or more receivers.

A script called *pressuretime.m* was written to convert the amplitude values (counts) contained in the segy files to pressure values (mBar). The user must specify which shot(s) and/or receiver(s) to pick the amplitudes from. The script converts the amplitudes to pressures by

multiplying all the counts with the gain, which is 6.742e-5 mV/count. Further, the sensitivity of the hydrophones was given by the manufacturer as 14.0 mV/mBar. Thus, to convert to mBar, the amplitude values need to be multiplied with $\frac{6.742e{-}5\ \mathrm{mV/count}}{14.0\ \mathrm{mV/mBar}}$=4.816e-6 mBar/count. Since positive amplitudes correspond to negative pressures, a multiplication with -1 is also required to get positive pressure values. The script then plots pressure versus time in a figure.

Two scripts called *SPL.m* and *SPLairgun.m* then use the pressure values from the previous script, and extract the maximum and minimum pressure value registered at each receiver for each shot. The sum of absolute maximum pressure, and absolute minimum pressure is the peak-to-peak pressure, and the scripts use the peak-to-peak pressures in Equation 29: dB = $20\log\frac{P_e}{P_0}$, to compute the SPL that this pressure would correspond to.

The maximum SPL registered at each receiver for each shot is stored in matrices called decibels and decibelsAirgun, respectively. decibels is a 37x37 matrix, where each row contains the maximum SPL from all detonating cord shots at one receiver, and each column contains the maximum SPL from one detonating cord shot at all receivers. decibelsAirgun is a 37x61 matrix, where the same is happening, but for the air gun shots instead. The last thing that happens in the *SPL.m* and *SPLairgun.m,* is that the SPLs are extracted from the matrices to make figures where the maximum SPL at all receivers for one shot is displayed. The generated figures can be compared with Figure 18, where each circle in the generated figure represents the location of a hydrophone. The strength of the SPL at the hydrophone is illustrated using colour codes. This means that when running *SPL.m,* 37 figures will be made, and when running *SPLairgun.m,* 61 figures will be made. The first figure made by *SPL.m* will show the SPLs caused by detonating cord shot 1, the second figure will show the SPLs caused by detonating cord shot 2, and so on.

The SELs for each receiver can also be computed. Instead of using the peak-to-peak pressure that was used for computing SPL, the rms pressure can be computed using the formula

$$p_{rms} = \sqrt{\frac{1}{S}\sum_{n=1}^{N} p_n^2}, \tag{31}$$

where N is the number of traces, p is the instantaneous pressure, and S is the number of samples in each trace.

The computed rms pressure can then be used in Equation 30: SEL = $10\log\frac{\sum_{n=1}^{N}\int_0^T p_{rms,n}^2(t)dt}{p_0^2}$, to compute the sound exposure level. In the formula, the duration of each sound is set constantly equal to the window that was used for computing the rms pressure. Thus, the integral becomes definite, and can be simplified in the MATLAB script.

Since the SPLs vary between the different receivers, some kind of mechanism apparently leads to attenuation between the receivers. As was described in the background theory, a formula that has been proposed to describe the propagation loss when seismic waves are travelling in water is Equation 14: P(r)=P(s)-Alog(r). In this formula, A vary depending on the type of spreading that occurs (Gausland, 2000). An attempt was made at determining a constant A that fits our seismic data. This was done using the MATLAB script *AlogR.m,* and the node 17 air gun data. The script uses the recorded SPLs at each receiver, and the distances from the air gun to each receiver to calculate A and P(s), using linear regression.

Linear regression means that experimental x- and y-values are used to compute best fitted a- and b-values in a formula of the form y=ax+b. When comparing this with Equation 14, we see that linear regression can be used in this case if y=P(r), x=log(r), a=-A and b=P(s). The maximum SPL at each receiver for each shot can be used as P(r), and the distance between the source and the receiver as r. The best fitting A and P(s) is calculated for each shot. The script plots the best fitted curve for each shot, as well as the experimental data, in the same figure. In addition to this, the script calculates the "coefficient of determination", R^2, to be able to say something about the match between the model and the experimental data.

6.2.2. Data comparisons

The data was investigated further by comparing the figures that were made. To study the effect of changing survey geometry on the quality of the seismic data, the following figures were compared:

- To study the effect of changing source type, common shot plots and frequency spectra from shots with the two types of sources (detonating cords and air guns) were compared. The pressure figures were also studied, to compare the different signatures caused by the different sources.
- To study the effect of source depth, the air gun data was used. The detonating cords were laid out on top of the ice for all shots, and the source depth was thus constant for all detonating cord shots. Common shot plots from shots where the air gun was located

at different depths in the water (1.5 m, 3 m or 5 m), but with the same air gun pressure, were compared with each other. Common receiver plots from the air gun shots were also studied, since each trace in a common receiver plot represents one shot. With knowledge about which shots were fired at which depth and with which pressure, differences between the individual traces could be studied. The frequency spectra from air gun shots at different depths were also compared with each other.

- To study the effect of receiver depth, both air gun data and detonating cord data were studied separately. For each of the source types, common receiver plots where the hydrophone was located at different depths in the water (1 m, 3 m, 5 m, 8 m or 10 m) were compared with each other. In addition to this, some common shot plots were studied, since each shot plot contains 37 traces, i.e. one trace from each receiver. Differences between individual traces within a common shot plot are thus believed to be caused by different receiver depths. The frequency spectra from receivers at different depths were also compared with each other.
- To study the effect of source pressure, common shot plots from air gun shots fired at the same depth, but with different pressures, were compared with each other. This was only done for the air gun data, since detonating cords of 5 m length were used in the majority of the detonating cord shots. Both whole common shot gathers, and single receivers were studied.

To study the effect seismic can have on pinnipeds, SPLs and SELs were computed for both detonating cord shots and air gun shots, and the results were compared to further study the effect of using air guns or detonating cords. The A-values in P(r)=P(s)-Alog(r) were also compared with theory about wave propagation underwater, and both SPL, SEL, frequency spectra and wave propagation were compared with theory about hearing in pinnipeds.

6.3. Quality of the data

Regarding the quality of the data, it can be concluded that the quality is quite good, but that some error sources may have affected the data. The effects of changing acquisition geometry can be studied using these data, as well as the approximate frequency contents and sound levels of the signals. For studying the wave propagation patterns in water in detail, more data should probably be available, but the data should be good enough to map the subsurface in the covered area quite well. For determining exactly how and where seismic will affect pinnipeds, the amount of data may be too scarce. Some of the main error sources are the following:

- There may be some noise in the seismic data, caused by e.g. weather conditions.
- The hydrophones may have vibrated or moved due to water currents or wind conditions, and therefore not have been exactly at the depth they were reported to be at.
- Time errors may be present in the seismic records.
- The receivers may have distorted the signals during recording. This will be further discussed in chapter 8.3.2.
- When computing the A-values for studying wave propagation, it is assumed that the wave was travelling directly from the source to the receiver. As will be discussed in chapter 8, this was not necessarily the case during the survey.
- Detailed information about the study area, regarding ice, water and subsurface properties was not available.
- The data comparisons were done by visual inspection of the data, thus the results of this may be influenced by my background. This may be especially relevant when the data are used to discuss the impact seismic can have on marine mammals.

7. Results

In this chapter, the results of the work described in the previous chapter will be presented. The chapter will start with an analysis of the seismic data from the detonating cord shots, followed by an analysis of the seismic data from the air gun shots. Both single traces, common shot plots, common receiver plots, and frequency spectra will be presented. Only the responses recorded by Unite hydrophone receivers will be studied. Next, figures showing the pressure signatures for different shots and receivers will be presented. Then will follow the results of computing SPLs and SELs, which have been used to compute A-values. These are presented at last.

7.1. Detonating cord shots

During the 2016 Svea survey, 43 shots were fired with detonating cords of 5 m, 10 m and 12.5 m length. The shots were recorded by several types of receivers, including Unite hydrophone receivers.

7.1.1. Common shot plots

Plots displaying the response from one single shot at all receivers, were made for each shot. In a common shot plot, each trace represents one receiver, therefore each of the common shot plots from the hydrophone data contains 37 traces. Some of these will be presented in the current subsection. Note the varying time axis between the figures.

Figure 20 shows the common shot plot from the shot at node 37 + 50 m. The common shot plot was made to be able to study the seismic data, and to be able to identify some of the events.

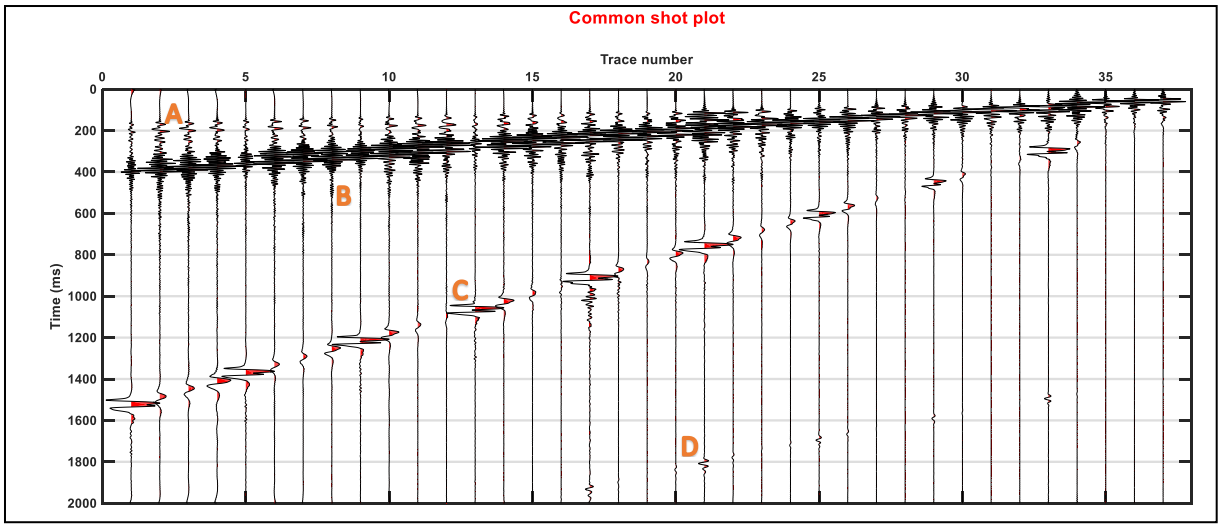

Figure 20: Common shot plot for detonating cord shot 37. The shot was fired on top of the ice, 50 m outside the spread (at node 37 + 50 m). The plot is Ormsby-filtered (5-10-100-110 Hz). Refracted waves (A), reflected waves (B), air waves (C) and refracted air waves (D) are visible. Differences between individual traces that correspond to different receiver depths can be observed.

Several events can be seen in this figure:

- A relatively narrow event is seen as the first arrival. The event is straight, and does not start at t=0, but appears after a certain time. It is travelling with a velocity of approximately 4000 m/s. The velocity and shape of the event makes me assume that this is probably a wave that has been travelling in some of the upper sediment layers, before being refracted. The event is marked with "A" in Figure 20.
- A thick "package" of parallel events appear after the first arrival. The fact that these events start close to t=0, and have a velocity of approximately 1500 m/s, makes me assume that these are probably guided P-waves travelling in the water column, as were described by e.g. Boiero et al. (2013). A P-wave has probably been reflected from the water bottom and water surface several times, creating several multiples. Since the wavelengths are large, they are probably caused by an interaction between ice, water and sediments. This would explain the many parallel events arriving at very similar times. The velocity of approximately 1500 m/ fits well with the known seismic P-wave velocity in water. It can be seen that the event is weaker at the traces from the shallower receivers than at the traces from the deeper receivers. The event is marked with "B" in Figure 20.

  In a shot plot that has been filtered using an Ormsby filter (0-5-30-40 Hz), the difference in strength of these P-wave reflections at different receivers can be seen clearer:

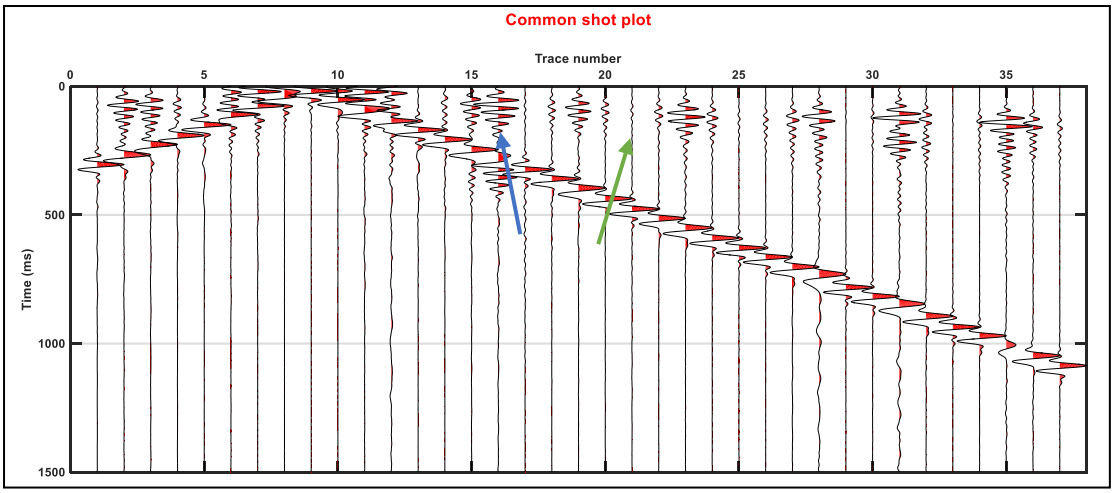

Figure 21: Common shot plot for detonating cord shot 9. The shot was fired on top of the ice, in front of node 9. The plot is Ormsby-filtered (0-5-30-40 Hz). The differences between the individual traces are more visible than in Figure 20. The arrows point at the trace from Unite 16 (receiver at 8 m depth, blue arrow) and Unite 21 (receiver at 1 m depth, green arrow). The reflections seem to be stronger the deeper the receivers are.

The arrows in Figure 21 point at a trace from a receiver at 8 m depth (blue arrow), and from a receiver at 1 m depth (green arrow). There are strong differences in the amplitude strength between the traces.

- An event with approximate velocity of 325 m/s is also identified in the common shot plot. The velocity of P-waves in air is usually approximately 330 m/s, which means that this event has almost the same velocity as the P-wave velocity in air. This makes me assume that the event has something to do with the P-wave in air, and that it is an air-coupled flexural wave. This is a wave that is travelling in the water, due to a coupling with an air wave. The coupled air wave will in the following text often be referred to as the air wave, but it is important to note that when the air wave is recorded in water, it is actually the air-coupled flexural wave we record. The air wave shows the opposite tendency of the reflected P-waves, and appears stronger on the traces from the shallower receivers than on the traces from the deeper receivers. The air wave appears to be dispersive (Figure 22). The event is marked with "C" in Figure 20.
- Some oscillations can be observed arriving before and after the air wave. The oscillations cover relatively large parts of the seismic records. This, in combination with knowing that the source was placed on top of ice, makes me assume that this is the flexural ice wave. The velocities are ranging from velocities lower than the air wave, up to the velocity of the P-waves travelling in the water. Stronger oscillations are observed at the traces from the shallow receivers than from the deep receivers. The waves are dispersive, and are not that easily visible, due to the large amplitude of the air wave.

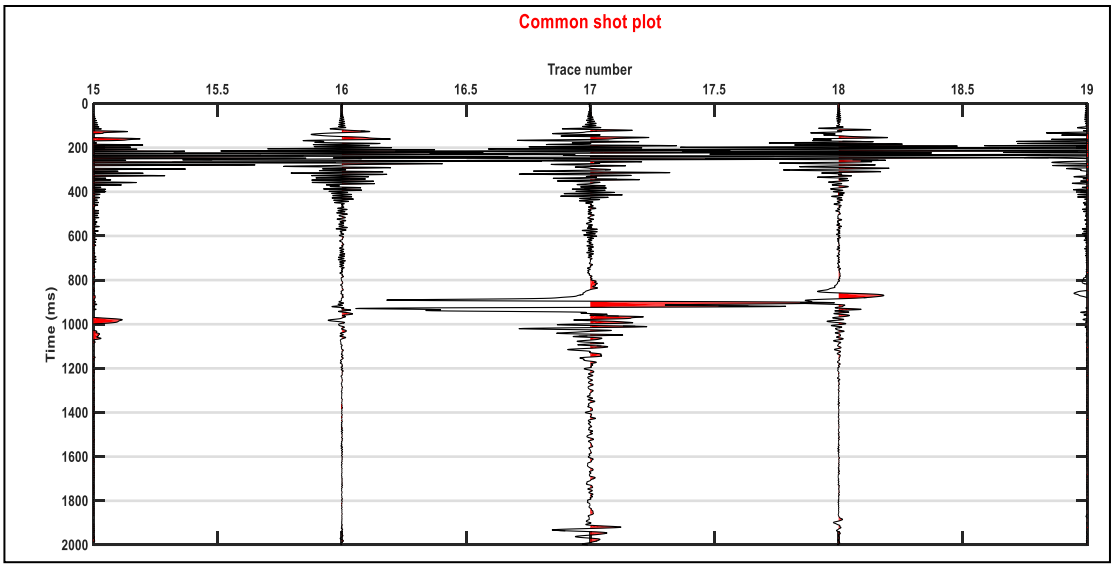

Figure 22: Parts of the common shot plot for detonating cord shot 37. The shot was fired on top on the ice, at node 37 + 50 m. The plot is unfiltered. Only traces 16, 17 and 18 are displayed, i.e. the receiver responses at Unite 16 (receiver at 8 m depth), Unite 17 (receiver at 1 m depth) and Unite 18 (receiver at 3 m depth). The event at approximately 900 ms is the air wave, and the oscillations before and after are the flexural ice wave. Both events are stronger the shallower the receiver is.

When we zoom into only a few traces in the common shot plot, as in Figure 22, we can see that when comparing the responses at receivers 16, 17 and 18, which are located at 8 m, 1 m, and 3 m depth, respectively, both the air wave and the flexural ice wave decrease in strength when the receiver is located deeper in the water.

- In some of the shot plots from shots near the end of the spread (including the one in Figure 20), an event is seen arriving approximately 1 second after the air wave. In Figure 20, the event arrives 1050 ms after the air wave. The event has a similar slope as the air wave, which makes me assume that this is the coupled wave of a refracted air wave, coming from topography in the area. The event shows the same behaviour as the air wave, and appears stronger on the shallower receivers. The event is marked with "D" in Figure 20.
- One thing to note is that we do *not* see a direct wave in Figure 20. In a typical seismogram, we would expect to see a straight event starting at t=0, travelling with a constant velocity towards the receiver. In the case where the source is located on top of the ice sheet, and the receiver is located in the water, we would expect this wave to travel with a velocity between approximately 3000 m/s and 1500 m/s, since those are the P-wave velocities in ice and water, respectively.

If a heavy low-pass filter (Ormsby-filter 0-1-5-8 Hz) is applied to the common shot plots, yet another event can be identified, in addition to the waves identified in Figure 20. This scenario

is shown in the common shot plot for detonating cord shot 1, shown in Figure 23. Then, a dispersive event, travelling with very low velocities (approximately 43 m/s), can be seen. The event can be seen arriving at very late times, up to 4 seconds after the shot was fired. The dispersive nature of the event, combined with the very low velocities, makes me assume that this event is a Scholte wave.

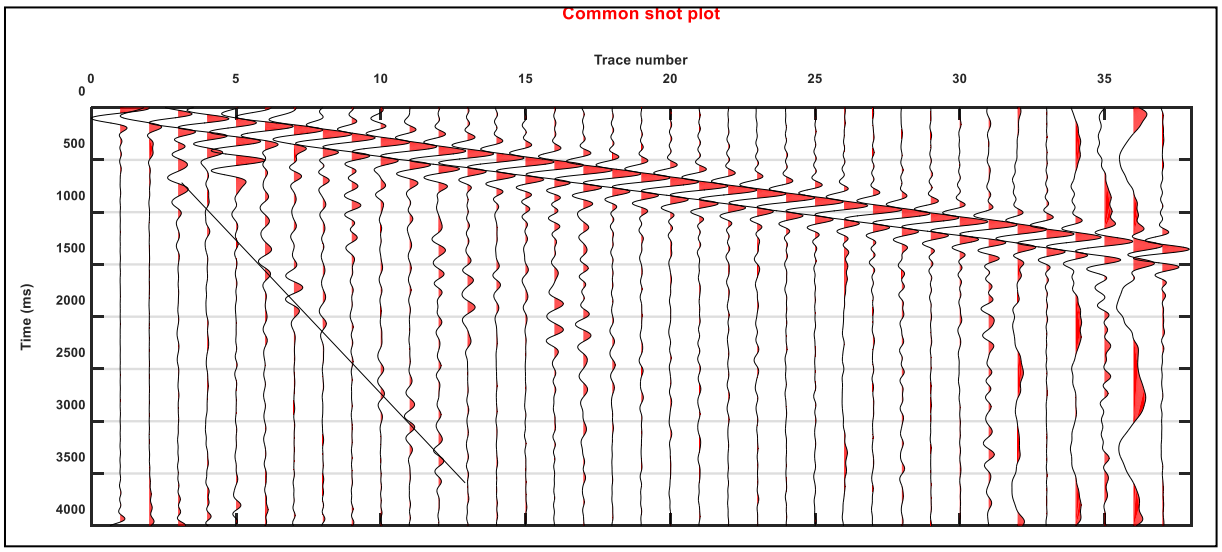

Figure 23: Common shot plot for detonating cord shot 1. The shot was fired on top of the ice, in front of node 1. The plot is heavy low-pass Ormsby-filtered (0-1-5-8 Hz). Note the long time axis. The gently sloped event is the air wave. The Scholte wave is marked with a line. The low frequency components of the flexural ice wave are visible as oscillations between the two previous events. When comparing single traces from different receivers, the Scholte wave is stronger the deeper the receivers are, and the flexural ice wave is stronger the shallower the receivers are.

The amplitudes of the Scholte wave are not very high compared to the surrounding events in Figure 23, thus the exact characteristics of the wave are difficult to determine. It is, however, easy to spot the presence of the Scholte wave. Some oscillations at earlier arrival times and higher velocities are also seen in the low-pass filtered plot in Figure 23. These are probably low frequency components of the flexural ice wave. The Scholte wave has stronger amplitudes at the receivers that are deeper, which means that it is stronger on the traces where the flexural ice wave is weaker, and opposite. If we zoom into the Scholte wave as in Figure 24, and only look at traces 6 to 9, we see clear differences in amplitude strength. There, receiver 6 and 7 were at 5 m depth, receiver 8 was at 3 m depth, and receiver 9 was at 1 m depth.

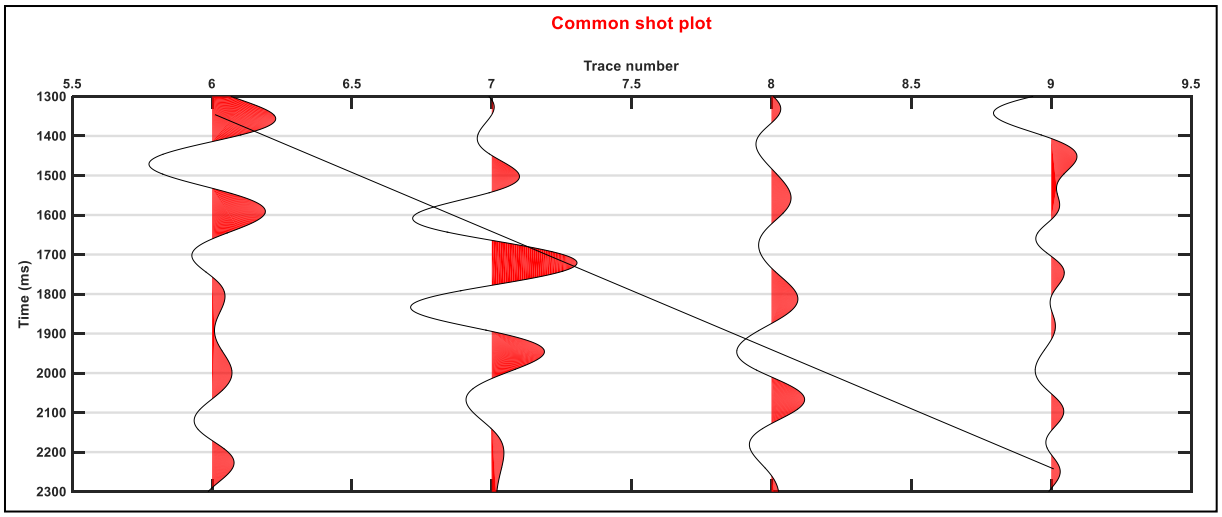

Figure 24: Parts of the common shot plot for detonating cord shot 1, from Figure 23. The shot was fired on top of the ice, in front of node 1. The plot is heavy low-pass Ormsby-filtered (0-1-5-8 Hz). Only traces 6, 7, 8 and 9 are displayed, i.e. the receiver responses at Unite 6 (receiver at 5 m depth), Unite 7 (receiver at 5 m depth), Unite 8 (receiver at 3 m depth) and Unite 9 (receiver at 1 m depth). The Scholte wave is stronger the deeper the receivers are.

We can see that Unite 6 and 7 record higher amplitudes that Unite 8, which again records higher amplitudes than Unite 9.

We can study the average frequency spectrum of a common shot gather for a detonating cord shot, to see how the frequencies are distributed. In such an average frequency spectrum, the spectral amplitude at each frequency is the average spectral amplitude for that frequency, computed from each of the traces in the gather. For all shots and all receivers, the frequency components recorded are found in the range 0 to 500 Hz, since the sampling rate was set to 1 ms, which means the Nyquist frequency was $\frac{1}{2\Delta t} = 500\ Hz$. Frequencies above this would not be visible in the frequency spectra, but the very low amount of frequencies above 450 Hz makes it natural to assume that a frequency spectrum of 0 to 500 Hz is appropriate. The frequency spectrum in Figure 25 is for the common shot gather for detonating cord shot 15.

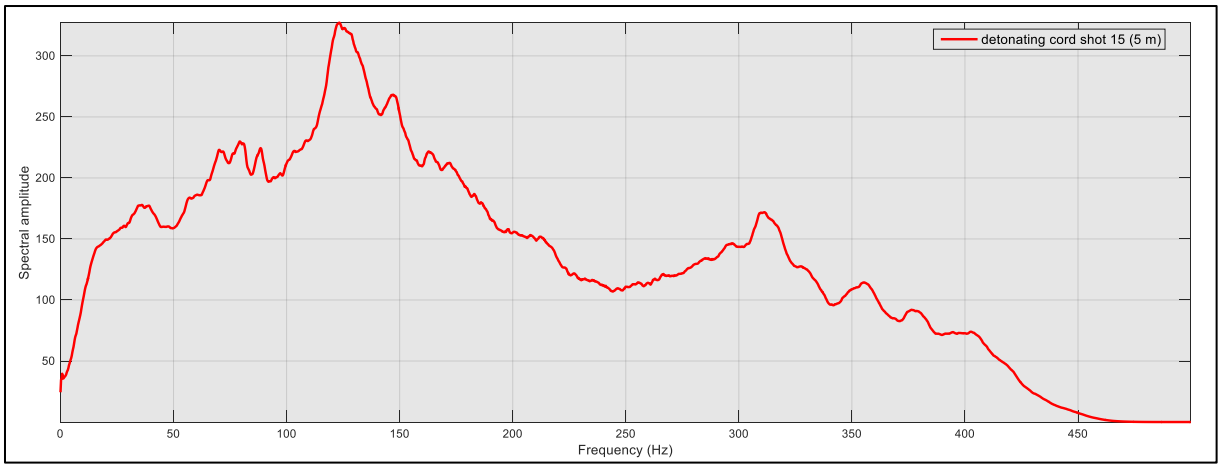

Figure 25: Average frequency spectrum for the common shot gather for detonating cord shot 15. The spectrum contains frequencies from 0 to 500 Hz, and most of the energy is contained at frequencies below 200 Hz.

Figure 25 shows that the frequencies in the detonating cord shot are mainly contained below 200 Hz. The highest peak is at approximately 140 Hz. A similar behaviour is seen in the frequency spectra for all detonating cord shots.

7.1.2. Common receiver plots

Plots displaying the response from all shots at one single receiver, were also made for each receiver. In a common receiver plot, each trace will represent one shot. Therefore, each common receiver plot from the detonating cord shots, contains 43 traces. Some of these will be presented in the current subsection. Note that also here the time axis is varying between the figures.

Figure 26 shows an example of a common receiver plot, where the Ormsby-filtered (0-5-80-90 Hz) receiver responses for all detonating cord shots at hydrophone receiver Unite 9 are displayed. Unite 9 is located at 1 m depth. Common receiver plots like this were made in addition to the common shot plots, to see if any other wave types could be identified in the data. They were also made to further study the apparent depth dependence of amplitudes, observed in the common shot plots in Figure 20 to 24.

Figure 26: Common receiver plot for the hydrophone receiver Unite 9. The receiver was located below node 9, at 1 m depth. The plot is Ormsby-filtered (0-5-80-90 Hz). Differences between the individual traces may be due to differences between the sources, or to the individual scaling that was applied to the plot. The shots were evenly spaced with shot interval 12.5 m, except from between trace 17 and 18 (shot interval was 25 m), between trace 36 and 41 (shot interval was 50 m), and between trace 41 and 43 (shot interval was 0 m). Refracted waves, reflected waves and air waves are visible.

Several events can be identified in Figure 26:

- A refracted wave can be seen arriving as the first arrival at some distance from the source. When the velocity is estimated from the receiver plots, it seems to be differing quite significantly between the different plots, but 3700 m/s to 4600 m/s seems to be a good approximation. This fits well with the expected velocity of a refracted wave, and the velocities of approximately 4000 m/s that were estimated from the common shot plot. Like in Figure 20, the event is marked with “A” in Figure 26.
- The thick package of events that in the common shot plot was identified as P-waves travelling in the water, can be observed here as well. The event is marked with “B” in Figure 26.
- The coupled air wave that was observed in the common shot plot, can be observed here as well. The velocity is computed from the slope of the wave, and is varying between the different receiver plots, but around 320 m/s to 330 m/s seems to be common. The event is marked with “C” in Figure 26, like in Figure 20. The dispersive nature of the air wave can be seen clearly in the receiver responses from the shallow receivers. Figure 27 shows this.

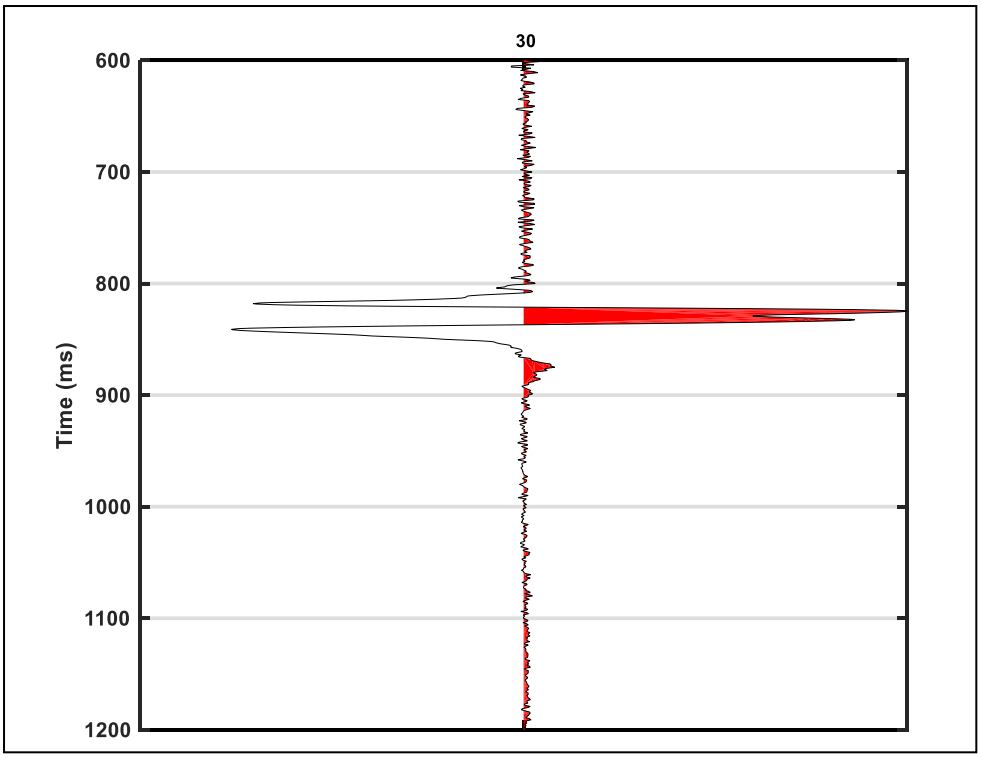

Figure 27: The receiver response at hydrophone receiver Unite 9 for detonating cord shot 30. The shot was fired on top of the ice, in front of node 31. The receiver was located at 1 m depth, below node 9. We can see that higher frequency components with low amplitudes arrive before high amplitude lower frequency components. This is probably due to velocity dispersion. Detonating cord shot 30 recorded at Unite 9 (1 m depth).

In Figure 27, high frequencies are arriving first, before some low frequency components of the air wave arrive with very high amplitudes at around 800 ms.

- Flexural ice waves can be seen as oscillations before and after the air wave in the common receiver plots as well. Compared to the air wave, they have low amplitudes, and are thus not that easily visible in many common receiver plots, like in Figure 26. However, they are easier to spot in the common receiver plots from shallow receivers, like in Figure 26, than in common receiver plots from deeper receivers. The oscillations are also easier to spot in low-pass Ormsby-filtered plots, as was shown in Figure 23.
- We do not see any events that could be the direct wave, just like in the common shot plot in Figure 20.

7.1.2.1. Changing receiver depths

Comparisons between common receiver plots from different receiver depths were done to further study the apparent depth dependence of amplitude strength. An example of this is shown in Figure 28.

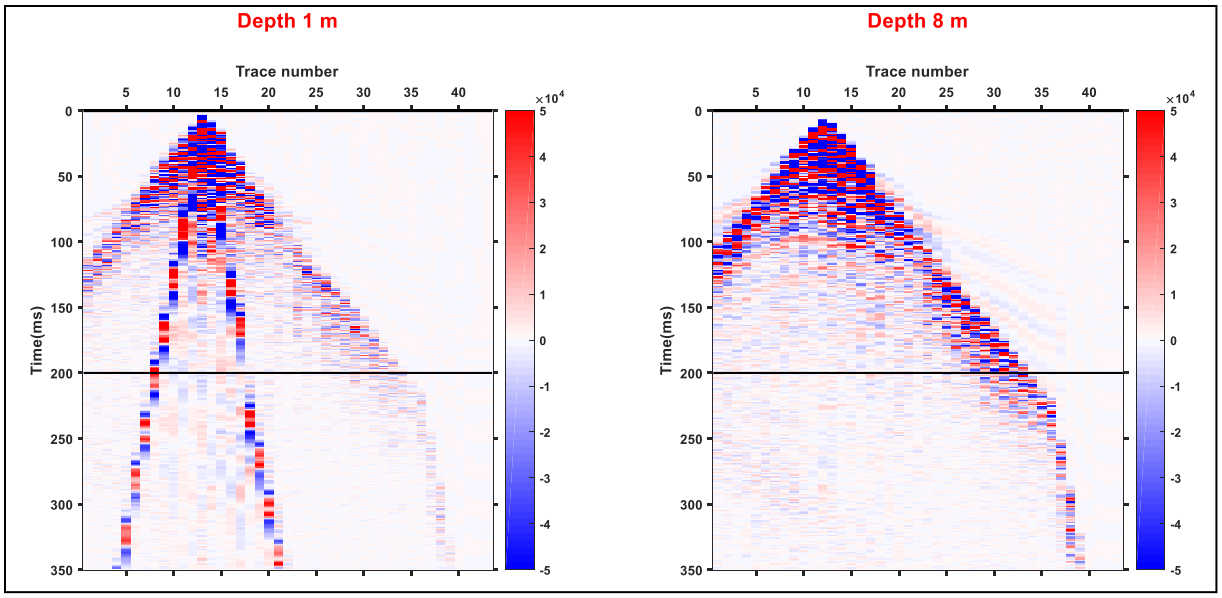

Figure 28: Two common receiver plots for all detonating cord shots. The same colour scale is used for both plots. The common receiver plot to the left is for the hydrophone receiver Unite 13. The receiver was then located at 1 m depth below node 13. The common receiver plot to the left is for the hydrophone receiver Unite 12. The receiver was then located at 8 m depth below node 12. The reflection amplitudes are stronger for deeper hydrophones. This applies to both the P-waves travelling in the water column, and reflections from deeper layers. Refractions are also stronger, while the opposite is seen for the air wave.

The two common receiver plots show the same detonating cord shots, and have the same scale, but are from receivers at different depths in the water. The figure to the left is from Unite 13, which is a receiver at 1 m depth. Here, the P-waves in the water are visible, but the amplitudes are not very high, especially at a distance away from the source. The air wave is, however, very easy to identify. The figure to the right is from Unite 12, which is a receiver at 8 m depth. Here, the amplitudes of the P-waves travelling in the water are much higher, but air wave is not possible to identify with this scaling. The refracted waves are also stronger in the right figure.

The same behaviour is seen when comparing other common receiver plots from receivers at different depths. It is clear is that the shallower the receiver is, the weaker are the reflections recorded. The air wave appears as a high amplitude wave in the common receiver plots from hydrophones at 1 m depth, and can be identified in the 3 m depth plots as well. It is, however, not nearly as clear as in the 1 m depth plots, and in the data from receivers at 5 m depth and deeper, the air wave is only visible when the plots are very closely investigated.

The average frequency spectra for all detonating cord shots from the two receivers at 1 and 8 m depth in Figure 28, can also be compared. This is shown in Figure 29.

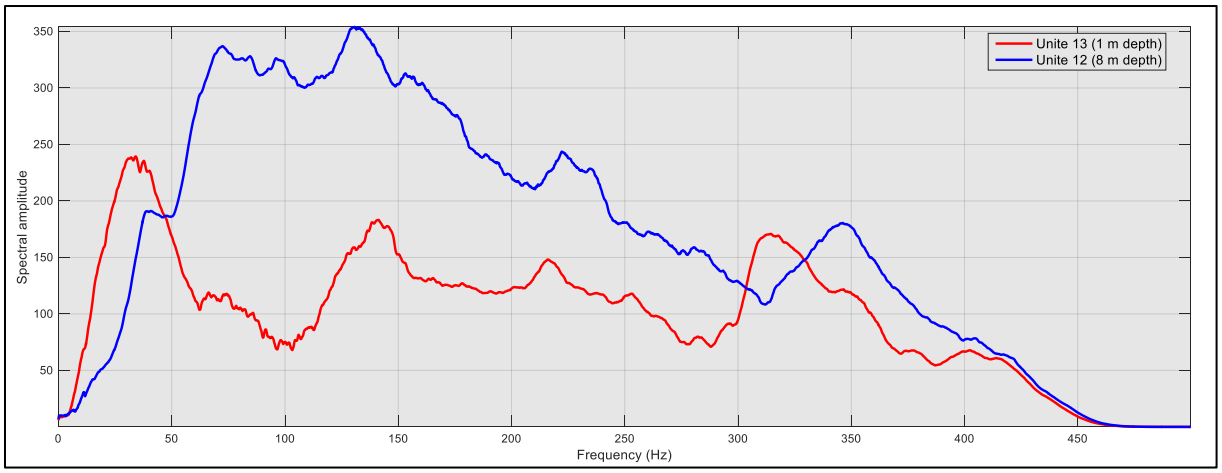

Figure 29: The two average frequency spectra for the common receiver gathers displayed in Figure 28. The red curve shows the average frequency spectrum for the common receiver gather at the receiver that was located at 1 m depth, below node 13. The blue curve shows the average frequency spectrum for the common receiver gather at the receiver that was located at 8 m depth, below node 12. The shallow receiver has most of its energy contained in peaks, while the energy is more evenly distributed between approximately 50 and 250 Hz for the deep receiver. The peak at approximately 30 Hz for the shallow receiver, is probably the air wave and the flexural ice wave.

The two spectra are quite different. The deep receiver generally gives higher spectral amplitudes than the shallow receiver. A peak at approximately 30 Hz is clear in the frequency spectrum from the shallow receiver, but not in the spectrum from the deeper receiver. 30 Hz is in the middle of the frequency band where the flexural ice wave and air wave is usually found, and thus this peak is assumed to be caused by that (Rovetta et al., 2009b). For the shallow receiver, peaks are also found at approximately 140 Hz and 210 Hz. For the deep receiver, the peaks are not as prominent, and most of the energy seems to be found around 70 to 140 Hz.

7.2. Air gun shots

During the 2016 Svea survey, several shots were also fired with air guns at 1.5 m, 3 m, and 5 m depth. The shots were recorded at the same receivers as the detonating cord shots.

7.2.1. Common shot plots

While the detonating cord shots were fired at 41 different locations, the shots using an air gun were only fired from two different locations; first the air gun was located below node 17, and later the air gun was located below node 1 – 50 m. The air gun was, however, placed at two different depths at each location. Common shot plots were made for the air gun shots, and Figure 30 shows one common shot plot from each of the two locations.

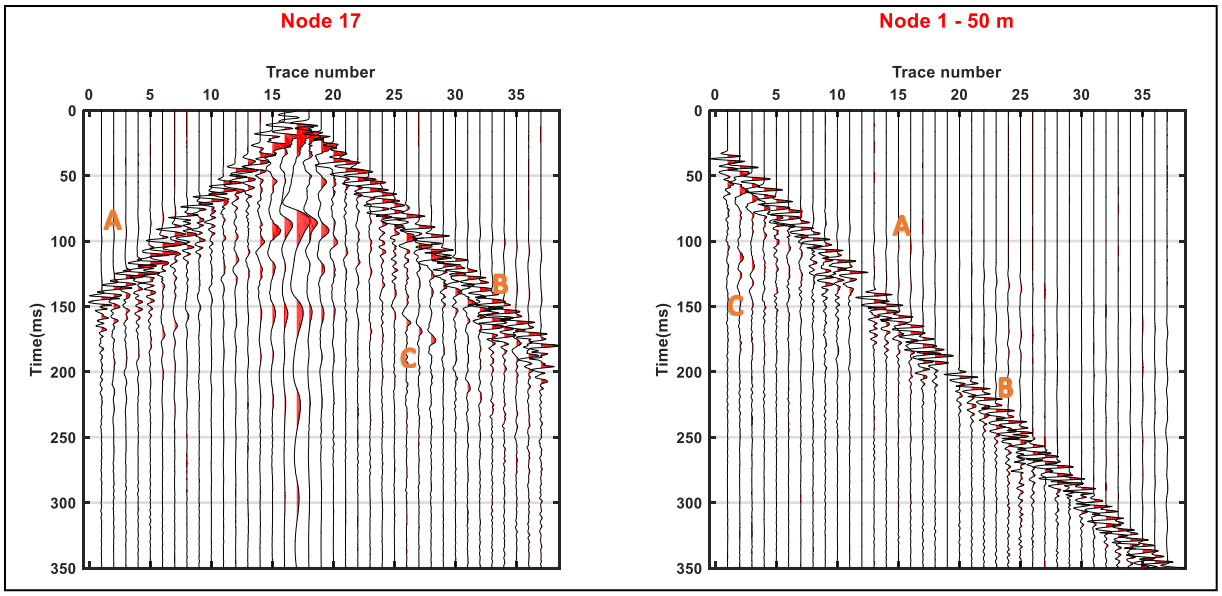

Figure 30: Two common shot plots for two air gun shots fired at the same depth at two different locations. The common shot plot to the left is for air gun shot 7. The shot was fired at 3 m depth below node 17. The common shot plot to the right is for air gun shot 38. The shot was fired at 3 m depth below node 1 – 50 m. The events are stronger in the record from the shot at node 17, probably since then the source was located in the middle of the spread.

Figure 30 shows the common shot plots for air gun shot 7 and 34. Shot 7 was fired at 3 m depth below node 17, and shot 38 was fired at 3 m depth below node 1 – 50 m. The two shot plots are obviously quite different due to different source locations, since node 17 is in the middle of the spread, and node 1 – 50 m is outside the spread. In some of the following figures, only parts of the shot gathers are studied, for easier comparisons between the two source locations. Several of the same events can, however, be observed in the two figures:

- The first arrival at a certain distance away from the source in Figure 30, is a wave travelling with a velocity of approximately 3750 m/s. This wave has a similar velocity and nature to the wave that was identified as a refracted wave in the detonating cord plots. It is therefore assumed to be a refracted wave from some shallow boundary. The event is weak in the unfiltered figure, but is marked with "A" in Figure 30.
- A thick "package" of events, travelling with a velocity of approximately 1500 m/s, is seen here as well. This is therefore assumed to be the guided P-waves travelling in the water, that were identified in the detonating cord plots. The event is marked with "B" in Figure 30. When we zoom into only some of the traces in Figure 30, we see that the reflected P-waves are stronger at the deeper receivers, just like what was seen in the detonating cord records. This is done in Figure 31.

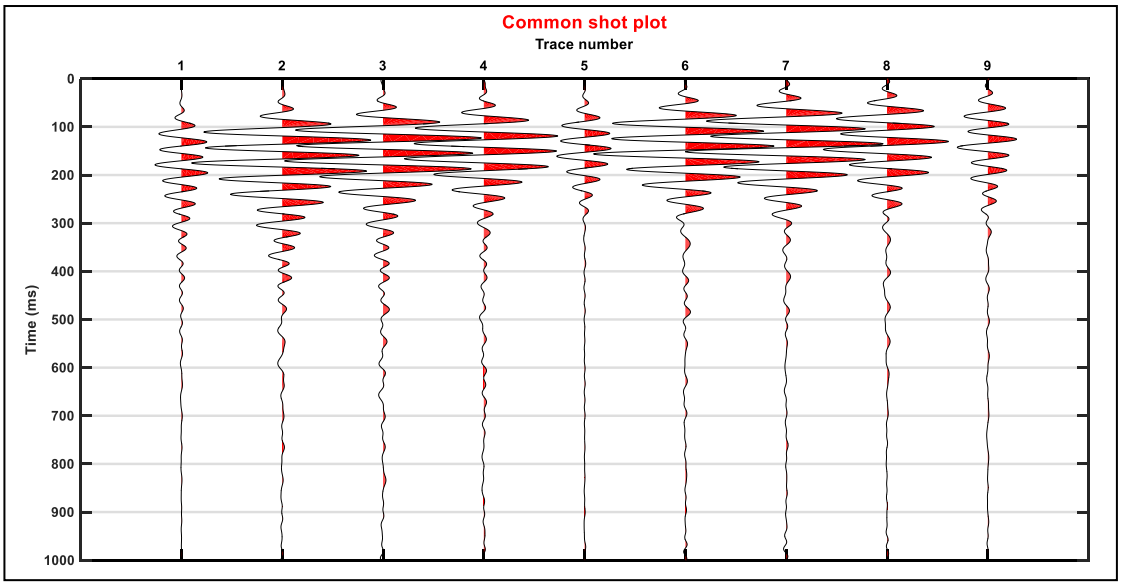

Figure 31: Common shot plot for air gun shot 7. The shot was fired at 3 m depth, below node 17. Ormsby-filtered (0-5-30-40 Hz), traces not individually scaled. Only traces from receivers Unite 1 to 9 are displayed. The reflected wave is recorded stronger at the deeper receivers. Receivers Unite 1, 5 and 9 are at 1 m depth, Unite 4 and 8 are at 3 m depth, and Unite 2, 3, 6 and 7 are at 5 m depth.

- An event that was not seen in the detonating cord records is identified below the guided P-waves. The event is almost parallel to the P-waves travelling in water, and based on this, combined with the fact that the shot was fired with an air gun, I assume that this is a bubble pulse caused by the air gun. We see that this event is stronger closer to the source. The event is marked with "C" in Figure 30.
- At later travel times, some curved events can be seen in Figure 30. Exactly what these events are is not clear, but based on their curved shape, I assume that they can possibly be reflections or multiples. Figure 32 below shows only parts of the two common shot plots that were displayed in Figure 30, and the mentioned bubble pulse and curved events can be seen in both plots. They are both easier to see in the common shot plot from the shot at node 17 (Figure 32, left), since the amplitudes are higher there.

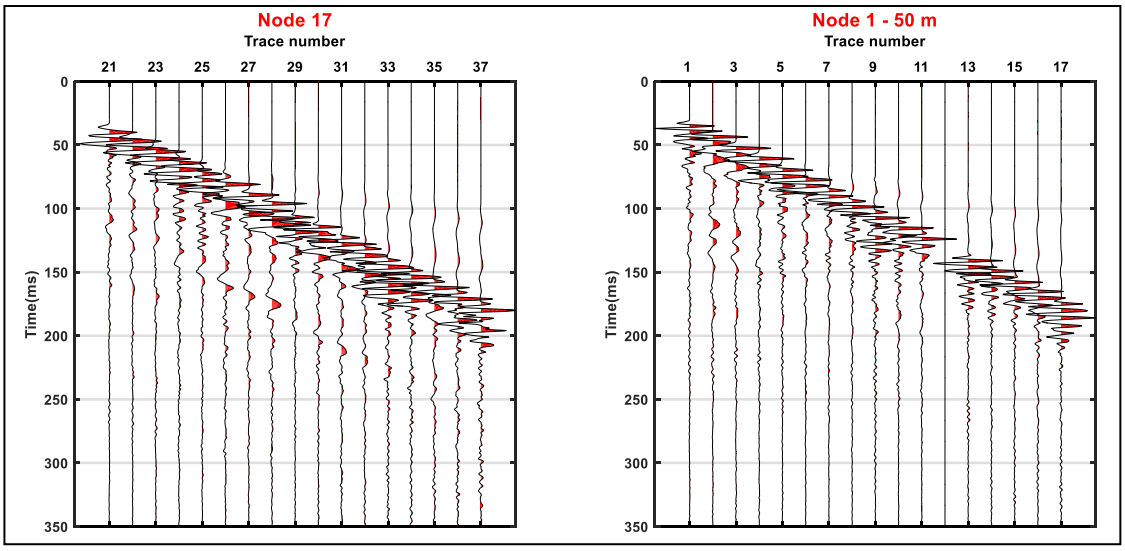

Figure 32: Parts of the common shot plot from air gun shot 7 and 38, from Figure 30. The plots are unfiltered. Only traces from receivers Unite 21 to 37 are displayed for shot 7, and from receivers Unite 1 to 17 are displayed for shot 38. Some weak, slightly curved events that might be reflections or multiples can be seen below the P-wave reflected from the sea bottom and the bubble pulse.

- We do *not* see the air wave, that was prominent in the seismic data from the detonating cord shots (e.g. Figure 20).
- Since both source and receiver are located in the water when using an air gun, we would expect a direct wave to travel at approximately 1500 m/s, since that is the P-wave velocity in water. I assume that a direct wave is present here, opposite to in the seismic data from the detonating cord shots. 1500 m/s is, however, the same velocity as the reflected P-waves travelling in the water travel with, therefore it is hard to discriminate the direct wave from the reflections in these records. The direct wave is probably a straight event, starting in t=0.

Differences seen between the different traces in Figure 30 and 32 are probably caused by the individual scaling of traces that was applied.

If the same heavy low-pass filter (Ormsby-filter 0-1-5-8 Hz) as we applied on the detonating cord data is applied on the air gun data in Figure 23 and 24, we see that the event that was identified as the Scholte wave is found in the air gun data as well. Figure 33 shows this.

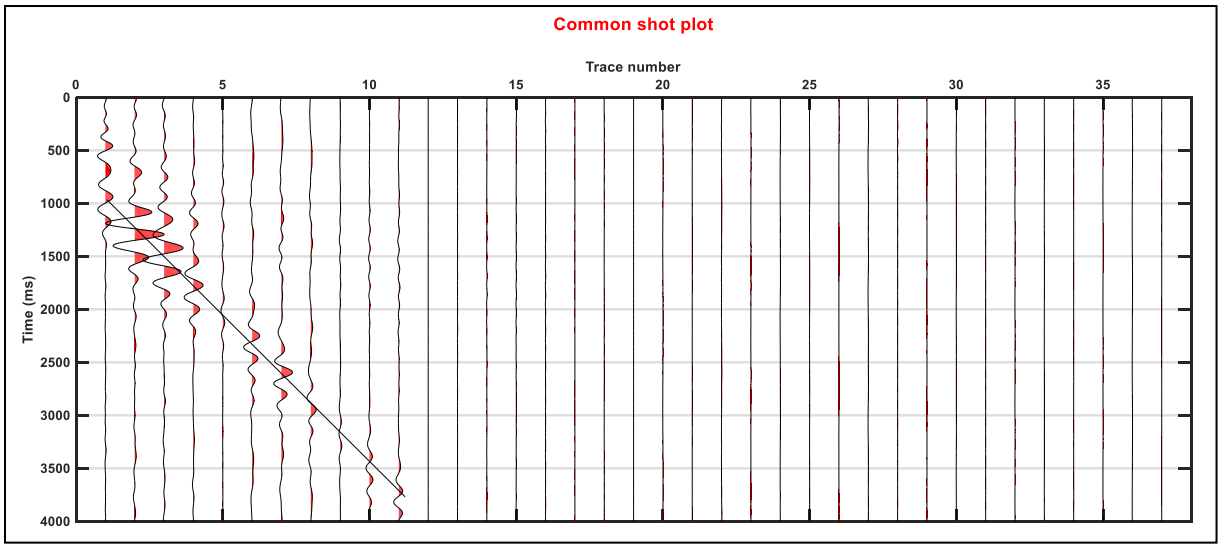

Figure 33: Common shot plot for air gun shot 38. The shot was fired at 3 m depth, below node 1 -50 m. The plot is heavy low-pass Ormsby-filtered (0-1-5-8 Hz). Note the long time axis. In the similar figure for detonating cord shot 1 (Figure 23), both air wave, Scholte wave and flexural ice wave were present. Here only the Scholte wave is clearly visible (marked with a line). Some oscillations that can be low frequency components of the flexural ice wave are weakly present. The Scholte wave is stronger the deeper the receivers are.

The Scholte wave is easier to spot in Figure 33 than it was in Figure 23. The amplitudes of the Scholte wave are much higher than the amplitudes of the surrounding waves in Figure 33, contrary to what was seen in Figure 23. A similarity between the figures is, however, that the amplitudes are recorded higher at the deeper receivers than at the shallow receivers (e.g. Unite 1, 5 and 9). The low frequency components of the flexural ice wave, that were identified in Figure 23, are not seen here.

7.2.1.1. Changing source depths

The shots were, as previously mentioned, fired with sources at different depths. To study if this had any effect on the data, we can compare common shot plots from shots fired at different depths. The following Figure 34 and 35 show how the seismic data is affected by changing the source depth, while keeping the location and pressure of the air gun constant.

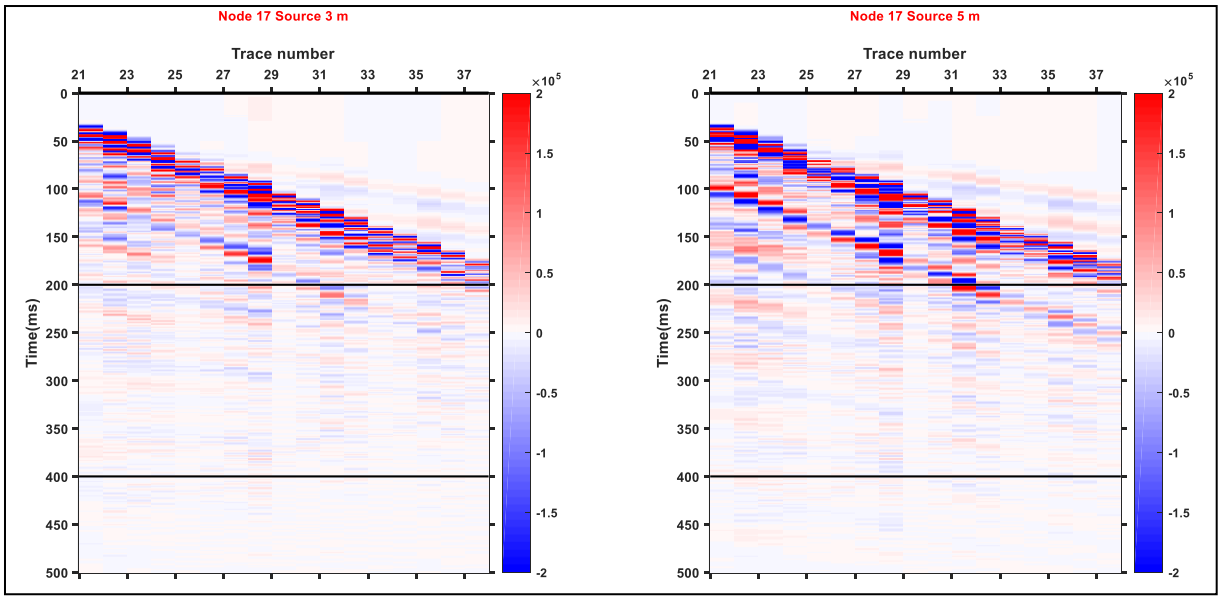

Figure 34: Two common shot plots for two air gun shots fired at different depths below node 17, with the same pressure (150 bar). The common shot plot to the left is for air gun shot 11. The shot was fired at 3 m depth below node 17. The common shot plot to the right is for air gun shot 17. The shot was fired at 5 m depth below node 17. The same colour scale is used for both plots. Both the reflected and the refracted waves are stronger in the figure to the right, where the source is deeper.

In Figure 34, the shots were fired below node 17 at 3 m and 5 m depth, respectively. The amplitudes are generally higher in the record from the deepest source (5 m), even though both shots were fired using the same air gun pressure (150 bar).

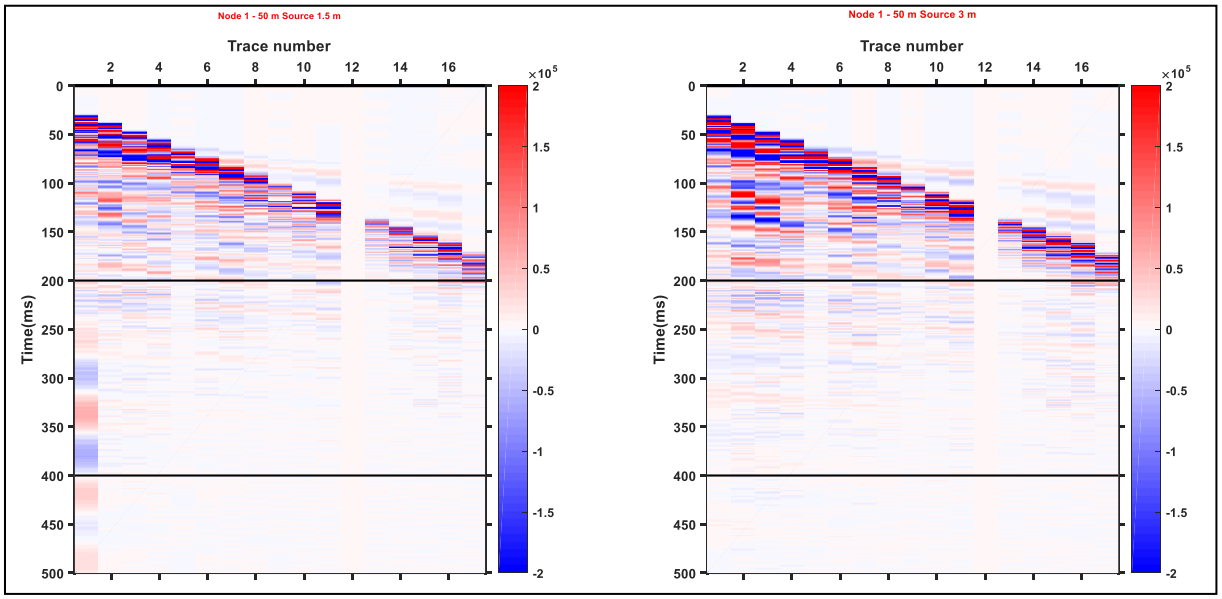

Figure 35: Two common shot plots for two air gun shots fired at different depths below node 1 - 50 m, with the same pressure (150 bar). The common shot plot to the left is for air gun shot 27. The shot was fired at 1.5 m depth below node 1 - 50 m. The common shot plot to the right is for air gun shot 26. The shot was fired at 3 m depth below node 1 – 50 m. The same colour scale is used for both plots. Both the reflected and the refracted waves are stronger in the figure to the right, where the source is deeper.

In Figure 35, the shots were fired below node 1 – 50 m, at 1.5 and 3 m depth, respectively. Also here the same air gun pressure was used (150 bar), and yet the amplitudes are different between the two shots. The record from the deepest source (3 m) generally has higher amplitudes than the record from the shallowest source (1.5 m).

We see that the bubble pulse is stronger when the air guns are deeper. However, the reflected P-waves and the refracted waves are also stronger, which is good in a survey where we want to study the subsurface.

The frequency spectra can also be studied, to look for any differences in frequency content from shots at different depths. The frequency spectra for shots close to node 17 are shown in Figure 36. The figure shows how the frequency spectra recorded at Unite 16 vary for a single shot with an air gun at 3 m depth (red), an air gun at 5 m depth (blue), and a detonating cord laid out on top of the ice (green).

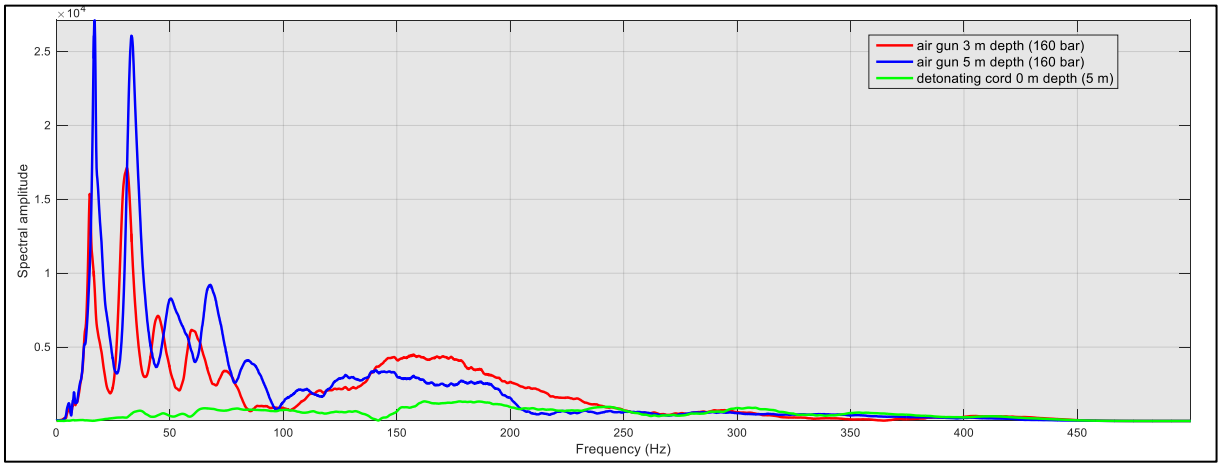

Figure 36: Three frequency spectra for the air gun shot 11 (fired at 3 m depth below node 17), air gun shot 17 (fired at 5 m depth below node 17), and detonating cord shot 17 (fired on top of the ice, in front of node 17). All frequency spectra are at the receiver Unite 16. The receiver was located at 8 m depth, below node 16. The blue curve shows the frequency spectrum for the deep air gun. There is quite a lot of the low frequencies, and little of the high frequencies. The red curve shows the frequency spectrum for the shallow air gun, and shows that the signal contains less of the low frequencies, and more of the high frequencies. The green curve shows the frequency spectrum for the detonating cord shot. This signal contains a lot less of all frequencies, especially the low frequencies.

What can be seen when comparing the two air gun shots in Figure 36, is that the shapes of the frequency spectra are similar, but that the shallow air gun gives less of the low frequencies, and more of the high frequencies than the deep air gun. The first peak is found at a lower frequency when the source is shallower, as well as the first notch. The distance between the peaks is also shorter when the source is shallower. From the first peak, the bubble period can be found from the formula T=1/f. The bubble period is approximately 34 ms for the shallow air gun, and 29 ms for the deep air gun. The frequency spectra from the detonating cord shot in Figure 36 is

quite different from the other two. It has lower spectral amplitudes in general, and especially at the low frequencies.

7.2.1.2. Changing air gun pressures

Finally, in addition to changing source position laterally and vertically, the air gun pressure was also varied between the shots. Figure 37 to 39 compare the effect of using an air gun with a high pressure (>150 bar), with using an air gun with a lower pressure (<110 bar). One figure is made for each source depth, to avoid this affecting the results when comparing the shot plots.

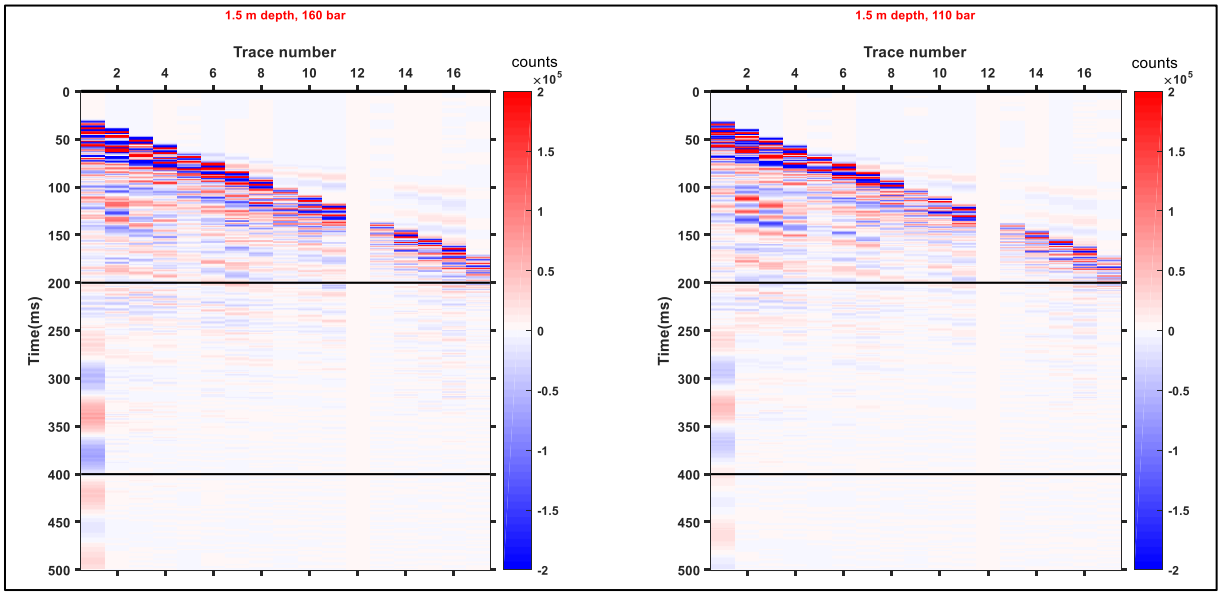

Figure 37: Two common shot plots for two air gun shots fired at the same depth below node 1 - 50 m, but with different pressures. The common shot plot to the left is for air gun shot 58. The common shot plot to the right is for air gun shot 53. Both shots were fired at 1.5 m depth below node 1 – 50 m. Shot 58 was fired with a 160 bar air gun pressure, while shot 58 was fired with a 110 bar air gun pressure. The same colour scale is used for both plots. Both the reflected and the refracted waves are stronger in the figure to the left, where the air gun pressure is higher.

Figure 37 shows two shots at 1.5 m depth below node 1 – 50 m. The seismic to the left was, however, acquired with a higher air gun pressure (160 bar) than the seismic to the right (110 bar). We see that the water bottom reflections and the refracted waves are strongest in the figure from the shot with the highest pressure, as well as most of the other amplitudes. There are, however, a few amplitudes around the bubble pulse that are stronger in the figure from the shot with the lower air gun pressure.

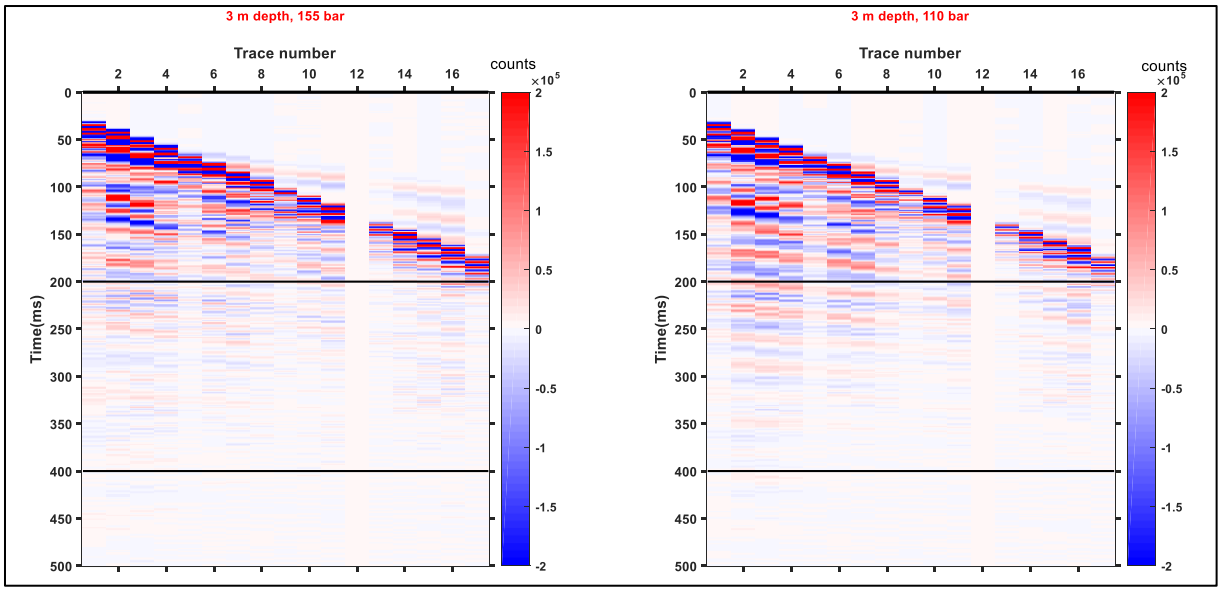

Figure 38: Two common shot plots for two air gun shots fired at the same depth below node 1 - 50 m, but with different pressures. The common shot plot to the left is for air gun shot 38. The common shot plot to the right is for air gun shot 37. Both shots were fired at 3 m depth below node 1 – 50 m. Shot 38 was fired with a 155 bar air gun pressure, while shot 37 was fired with a 110 bar air gun pressure. The same colour scale is used for both plots. Both the reflected and the refracted waves are stronger in the figure to the left, where the air gun pressure is higher.

Figure 38 shows two shots at 3 m depth below node 1 – 50 m, but like in Figure 37, the seismic to the left was acquired with a higher air gun pressure (155 bar) than the seismic to the right (110 bar). The water bottom reflections and the refracted waves are a bit stronger in the figure from the shot with the highest pressure, but right below approximately 200 ms, there are some higher amplitudes in the figure from the shot with the lower pressure.

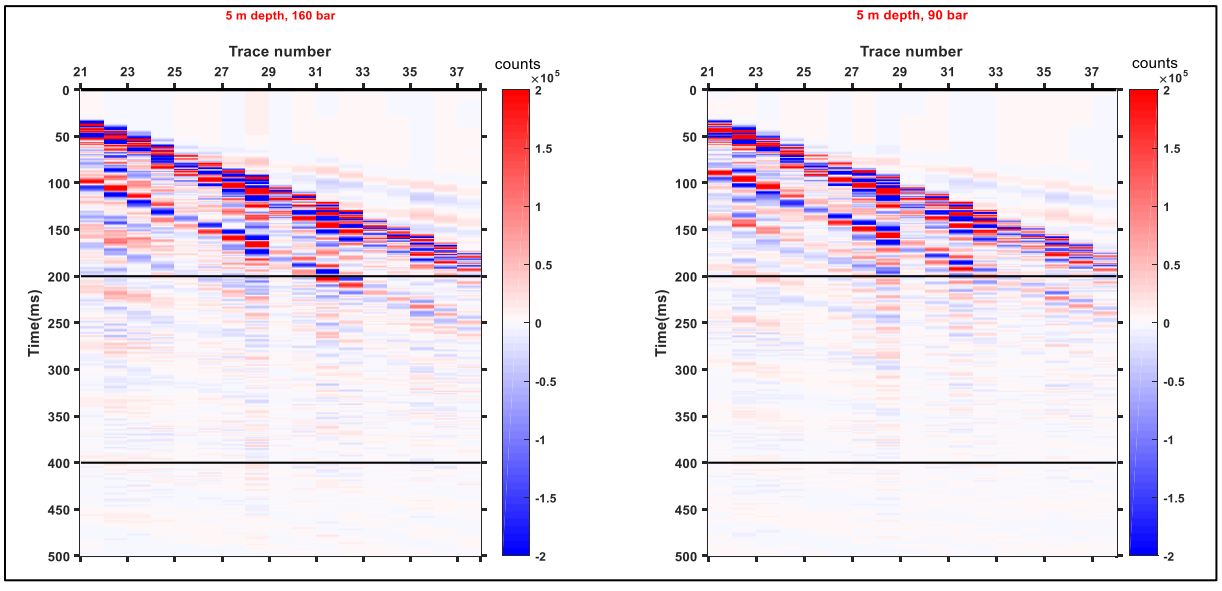

Figure 39: Two common shot plots for two air gun shots fired at the same depth below node 17, but with different pressures. The common shot plot to the left is for air gun shot 5. The common shot plot to the right is for air gun shot 23. Both shots were fired at 5 m depth below node 17. Shot 5 was fired with a 160 bar air gun pressure, while shot 23 was fired with a 90 bar air gun pressure. The same colour scale is used for both plots. Both the reflected and the refracted waves are stronger in the figure to the left, where the air gun pressure is higher.

Figure 39 shows two shots at 5 m depth below node 17, but like in the two previous figures, the seismic data to the left was acquired with a higher air gun pressure (160 bar) than the seismic to the right (90 bar). The amplitudes are higher at later arrival times in the figure from the shot with the highest pressure, but some amplitudes are stronger in the figure from the shot with the lowest pressure.

To sum up Figure 37 to 39, what we can see is that when using a higher pressure in the air gun, the amplitudes are generally higher, but there are some exceptions, especially close to the bubble pulse. From theory, we would expect higher amplitudes from higher pressures. The exceptions are therefore assumed to either have been caused by the shallow water, or by some mistake when recording the data. This will be briefly discussed in the next chapter. By comparing the three figures with each other, the amplitude strength can also be seen to increase with increasing source depth, as was seen in the previous subsections (e.g. Figure 34 and 35).

We can also study the effect of using different air gun pressures on the bubble period. In Figure 40, the receiver responses at Unite 22 (receiver at 3 m depth) for two single shots, fired at 5 m depth with different pressures below node 17, are shown. The traces are from the same two shots displayed in Figure 39, and have different scaling.

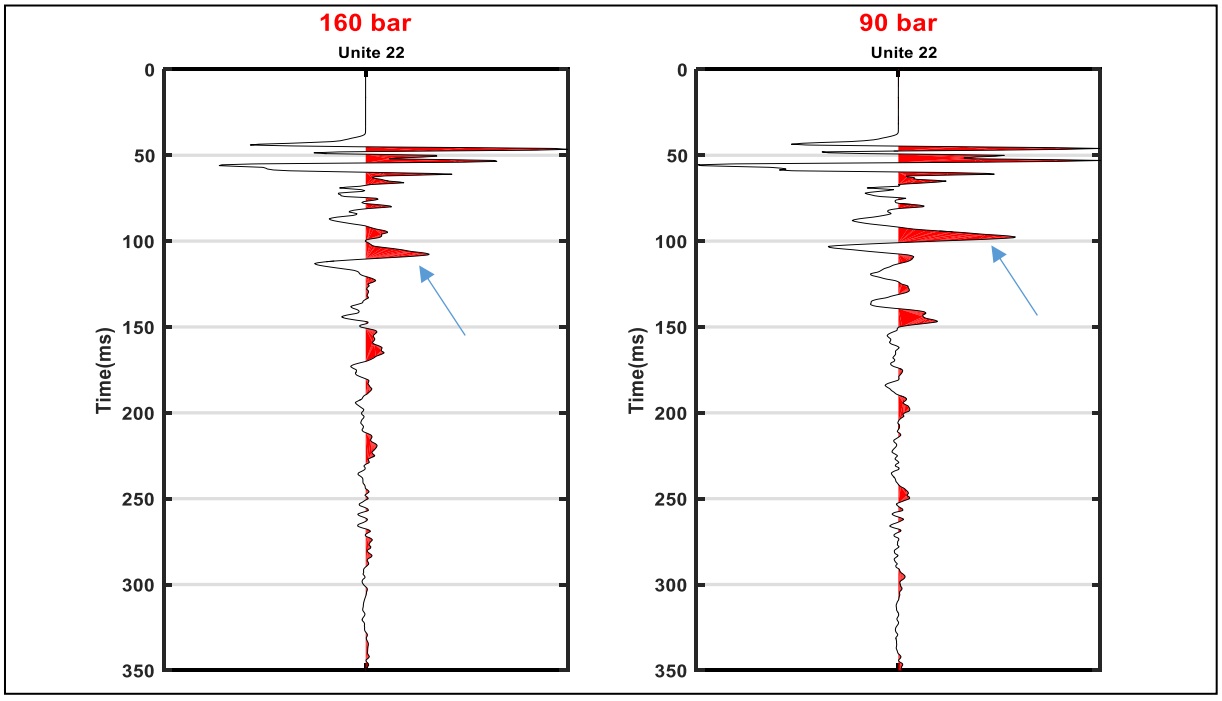

Figure 40: Receiver response at Unite 22 for air gun shot 5 and shot 23. The hydrophone receiver was located at 3 m depth below node 22. The two shots were both fired at 5 m depth below node 17, but shot 5 was fired with a higher air gun pressure (160 bar) than shot 23 (90 bar). The traces do not have the same scaling, so amplitudes should not be compared. The bubble periods are however clearly different. The blue arrows point at the first bubble pulse for each trace.

The amplitudes in the two traces can therefore not be compared. However, we see that the time between the primary pulse and the bubble pulse is longer when using a higher air gun pressure. In other words, the bubble pulse frequency decreases with increasing pressure. This is due to the larger maximum bubble size that occurs when using a higher air gun pressure, which means that the bubble will use a longer time to build up to its maximum size before it collapses.

The frequency spectra of the common shot gathers that were displayed in Figure 37 to 39 are shown below. Note that the amplitude axis values are different for the three spectra, and that the spectral amplitudes in Figure 43 are much higher than in Figure 41 and 42. This is probably partly because the shots in Figure 43 were fired in the middle of the spread, opposite to the shots in the other two figures.

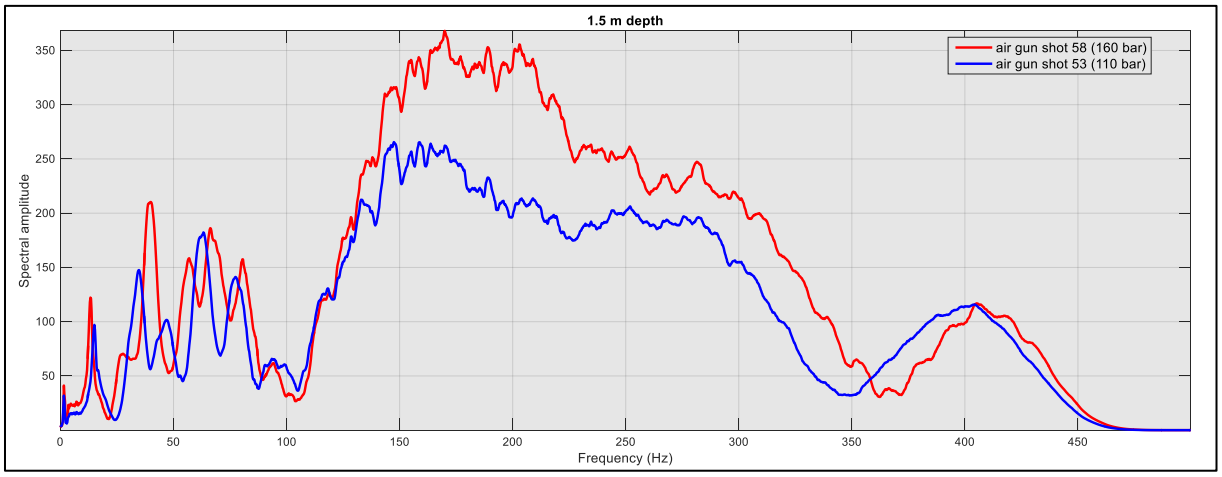

Figure 41: The two average frequency spectra for the common shot gathers displayed in Figure 37. The red curve shows the average frequency spectrum for the common shot gather for air gun shot 58 that was located at 1.5 m depth, below node 1 – 50 m, with an air gun pressure of 160 bar. The blue curve shows the average frequency spectrum for the common shot gather for air gun shot 53, located at 1.5 m depth below node 1 – 50 m, with an air gun pressure of 110 bar. We see that the high pressure shot gives higher spectral amplitudes than the low pressure shot, except from at a few low and high frequencies.

Figure 41 shows the average frequency spectra from the two common shot gathers that were displayed in Figure 37. The shots were fired at the same location and depth (1.5 m below node 1 – 50 m), but the red spectrum represents a shot with a higher pressure than the blue spectrum. The frequency spectra confirm what was seen in Figure 37; the amplitudes are generally higher when a higher air gun pressure is used, but with a few exceptions.

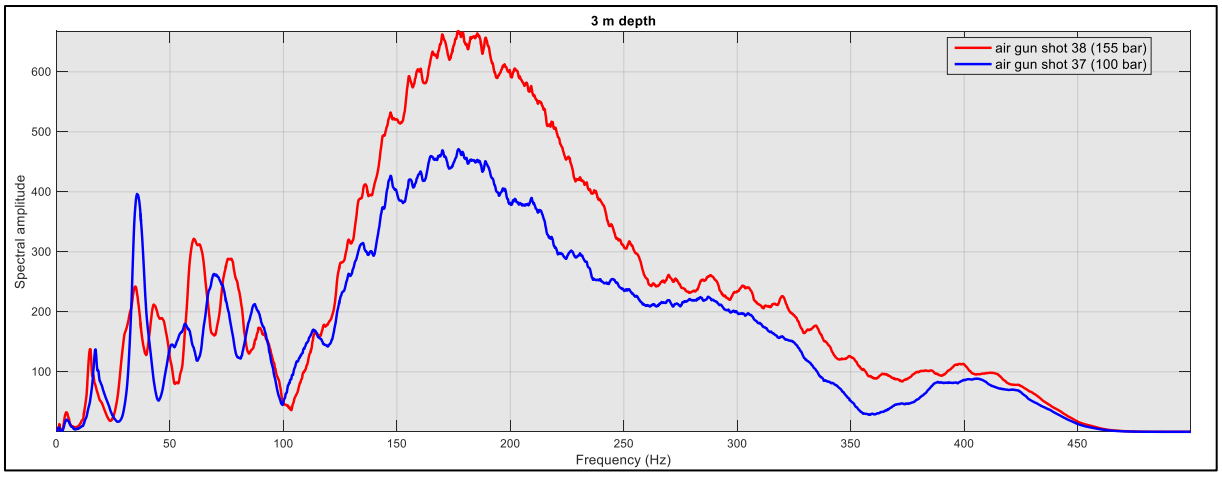

Figure 42: The two average frequency spectra for the common shot gathers displayed in Figure 38. The red curve shows the average frequency spectrum for the common shot gather for air gun shot 38 that was located at 3 m depth, below node 1 – 50 m, with an air gun pressure of 155 bar. The blue curve shows the average frequency spectrum for the common shot gather for air gun shot 37 that was located at 3 m depth, below node 1 – 50 m, with an air gun pressure of 100 bar. We see that the high pressure shot gives higher spectral amplitudes than the low pressure shot, with an exception at approximately 40 Hz.

Figure 42 shows the average frequency spectra from the two common shot gathers that were displayed in Figure 38. The shots were fired at the same location and depth (3 m below node 1 – 50 m), but the red spectrum represents a shot with a higher pressure than the blue spectrum. Like in Figure 41, the frequency spectra confirm what was seen in Figure 38; the amplitudes are generally higher when a higher air gun pressure is used, but there are some exceptions.

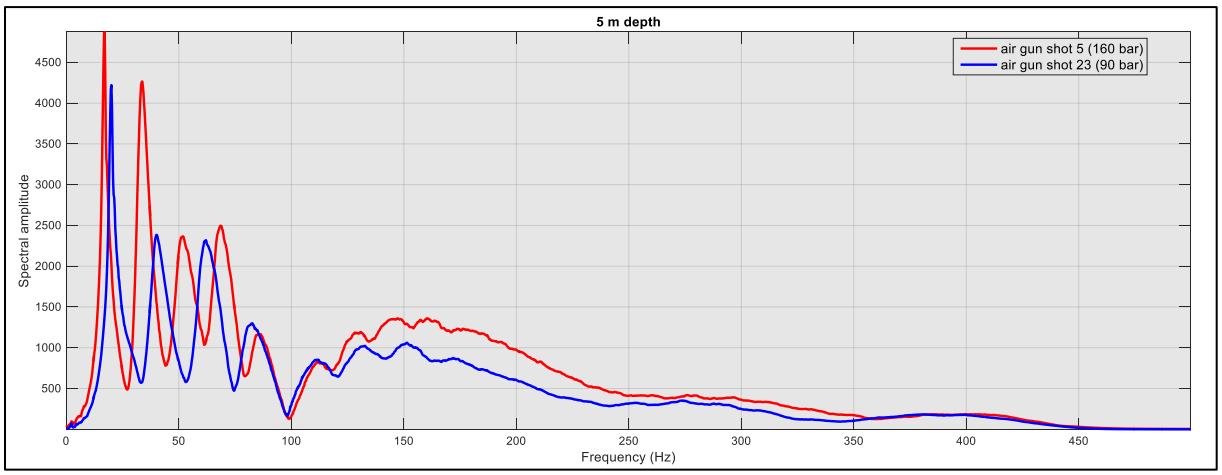

Figure 43: The two average frequency spectra for the common shot gathers displayed in Figure 39. The red curve shows the average frequency spectrum for the common shot gather for air gun shot 5 that was located at 5 m depth, below node 17, with an air gun pressure of 160 bar. The blue curve shows the average frequency spectrum for the common shot gather for air gun shot 23 that was located at 5 m depth, below node 17, with an air gun pressure of 90 bar. We see that the highest pressure generally gives higher amplitudes. The low frequency amplitudes are much higher than in the two previous figures.

Figure 43 shows the average frequency spectra from the two common shot gathers that were displayed in Figure 39. The shots were fired at the same location and depth (5 m below node 17), but the red spectrum represents a shot with a higher pressure than the blue spectrum. Also, here, the frequency spectra show that the amplitudes are generally higher when using a higher

air gun pressure, but there are a few exceptions. This is consistent with what was seen in Figure 39.

To sum up the last three figures, a shot with a higher air gun pressure will generally consist of frequencies with higher spectral amplitudes than a shot with a lower air gun pressure. Some exceptions are seen, mainly for some low frequencies (<100 Hz), for example at approximately 40 Hz in Figure 42. What can also be seen if comparing the spectra in Figure 41, 42 and 43 with each other, is that a deeper source seems to give a record that have much higher spectral amplitudes than a shallower source, especially at low frequencies. This is what was seen in subsection 7.2.1.1. as well. In a survey where we want the seismic waves to penetrate deep into the subsurface, having more of the low frequencies is desirable (Ten Kroode et al., 2013). It is, however, important to note that differences between Figure 43 and the previous two figures may also have been caused by the different air gun locations. This is because Figure 43 shows spectra from shots below node 17, while Figure 41 and 42 show spectra from shots below node 1 – 50 m.

7.2.2. Common receiver plots

A common receiver plot for all air gun shots includes 61 traces, where each trace is the receiver response at that receiver from one shot. The first 23 traces in each plot shows shots fired below node 17, and the last 38 traces shows shots fired below node 1 – 50 m. Thus, there is one receiver plot for each Unite hydrophone. Such a common receiver plot is shown in Figure 44.

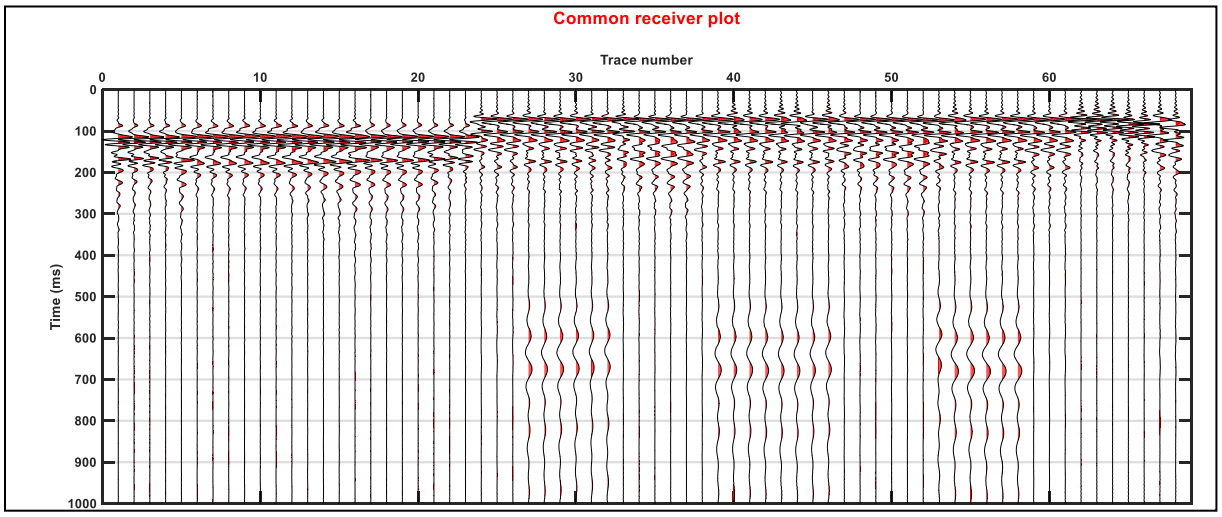

Figure 44: Common receiver plot for the hydrophone receiver Unite 5. The receiver was located below node 5, at 1 m depth. The plot is Ormsby-filtered (1-5-100-110 Hz). Differences between the individual traces may be due to differences between the sources, or to the individual scaling that was applied to the plot. The first 23 shots were fired below node 17, and the last 38 shots were fired below node 1 – 50 m. Refracted waves, reflected waves and bubble pulses are visible. The event starting at approximately 600 ms is only seen in some of the traces, and only in the common receiver plots from Unite 1, 5 and 9.

From Figure 44, we see that higher amplitudes are registered at the receivers when the air gun is below node 17 than when the air gun is below node 1 – 50 m. When the air gun is located below node 17, there is a shorter distance between source and receiver than when the air gun is located below node 1 – 50 m. This is because then the source is located in the middle of the spread, instead of outside the spread. Figure 45 shows that in addition to arriving with higher amplitudes, the events also arrive earlier when the distance between source and receiver is shorter. From Figure 46 we can see that events are recorded at the earliest arrival times when the Unite number is close to 17 for the air gun shots below node 17. For the air gun shots below node 1 – 50 m, a higher Unite number for the receiver, means increasing distance from the source, and thus the waves are arriving later when the Unite number increases.

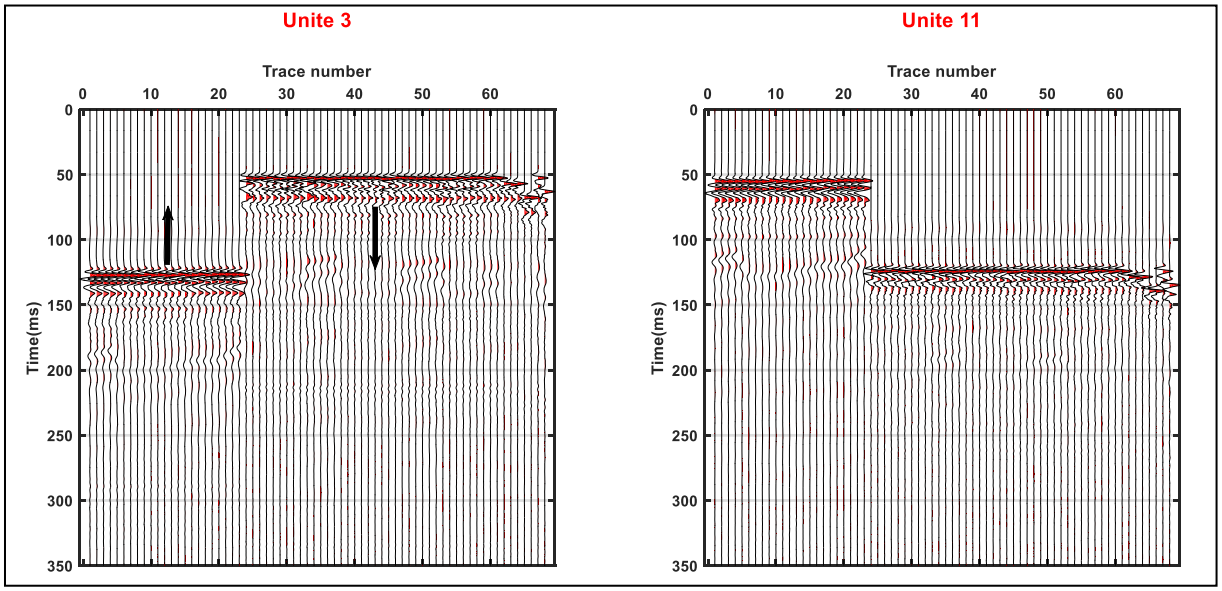

Figure 45: Common receiver plots for the hydrophone receivers Unite 3 and Unite 11. The shots at node 17 (the first 23 traces) will have arrival times closer to zero when the receiver is close to node 17. The shots at node 1 – 50 m (the last 38 traces) will have arrival times closer to zero the closer to the start of the spread the receiver is. Hence, the main "package" of wave events in the left part of the figure will move upwards when moving from Unite 1 towards Unite 17, and then the package will move downwards. In the right part of the figure, the main package of wave events will move down when moving from Unite 1 towards Unite 37.

Just like for the detonating cord records, common receiver plots from different receiver depths can be compared, to study the effect on amplitude strength of having the receivers at different depths. This is shown in Figure 46.

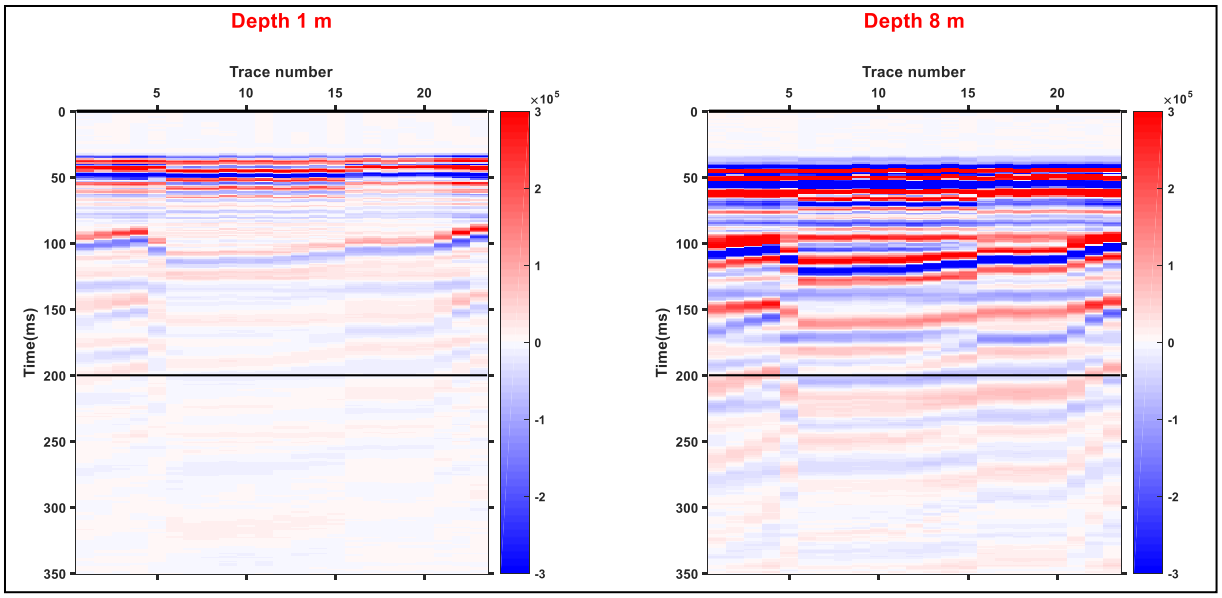

Figure 46: Two common receiver plots for the node 17 air gun shots. The same colour scale is used for both plots. The common receiver plot to the left is for the hydrophone receiver Unite 13. The receiver was then located at 1 m depth below node 13. The common receiver plot to the left is for the hydrophone receiver Unite 12. The receiver was then located at 8 m depth below node 12. The reflection and bubble pulse amplitudes and are stronger for deeper hydrophones. This applies to both the P-waves travelling in the water column, and reflections from deeper layers.

Figure 46 shows the common receiver plots from Unite 13 (1 m depth) and Unite 12 (8 m depth). The reflections are clearly stronger at the deeper receiver than at the shallower receiver. The same is also the case for the bubble pulse.

The frequency spectra from the two common receiver plots in Figure 46 can be compared, to study the effect of having the receivers at different depths.

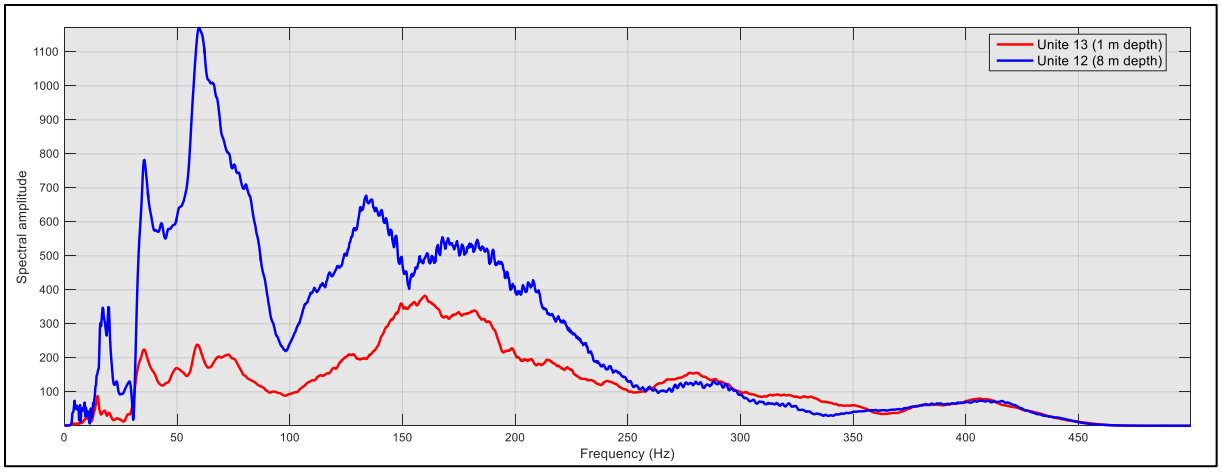

Figure 47: The two average frequency spectra for the common receiver gathers displayed in Figure 46. The red curve shows the average frequency spectrum for the common receiver gather at the receiver that was located at 1 m depth, below node 13. The blue curve shows the average frequency spectrum for the common receiver gather at the receiver that was located at 8 m depth, below node 12. The shallow receiver has most of its energy contained at high frequencies above 100 Hz, while the deep receiver has most of its energy contained at low frequencies below 100 Hz.

What we can see from Figure 47, is that just like for the detonating cord shots, the average frequency spectra for all the air gun shots from the two receivers are quite different. The deepest receiver generally has higher spectral amplitudes than the shallower receiver. The peak that was seen at the shallow receiver at approximately 30 Hz in the frequency spectrum for detonating cord shots (Figure 29), is not seen in the frequency spectrum from any of the receivers for the air gun shots. This fits well with what we know about the flexural ice wave and air wave being more present for sources above water than for sources in water. The air gun shots have a larger concentration of low frequencies (around 60 Hz) than the detonating line shots had (Figure 29), and the deeper receiver has most of its energy at these low frequencies.

In addition to the common shot plots, the common receiver plots can be used to study how having an air gun at either 1.5 m, 3 m or 5 m depth will affect the seismic data. In Figure 48, differences can be observed that correspond with the changing source depths. The coloured lines show which traces represent shots at which source depths.

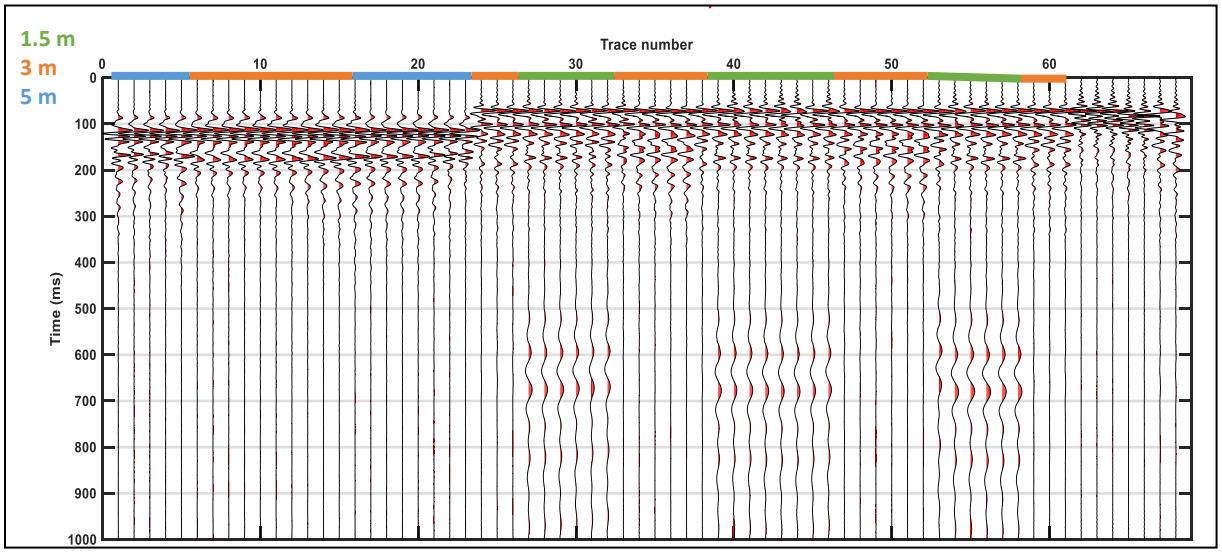

Figure 48: Common receiver plot for the hydrophone receiver Unite 5 that was displayed in Figure 44. The receiver was located below node 5, at 1 m depth. The plot is Ormsby-filtered (1-5-100-110 Hz). Shots were fired at different positions both laterally and vertically. The traces marked with blue were fired at 5 m depth, the traces marked with orange were fired at 3 m depth, and the traces marked with green were fired at 1.5 m depth.

Just like in the common shot plots, we can also in Figure 48 see that the bubble pulse is stronger at the deeper air guns than at the shallower air guns, except when the source and receiver are very close to each other (e.g. at Unite 17 when the shot is below node 17). We also see an event arriving at around 600 ms, but this event is only seen in the traces from 1.5 m shot depth. This event is also only visible in the common receiver plots from receivers at 1 m depth (i.e. Unite 1, 5 and 9). When comparing those receiver plots, we see that the wave travels with a velocity of approximately 170 m/s, and this makes me assume that this might be some components of

the flexural ice wave. If we zoom into only a few of the traces, differences can be studied in further detail. This is done in Figure 49 and 50 below.

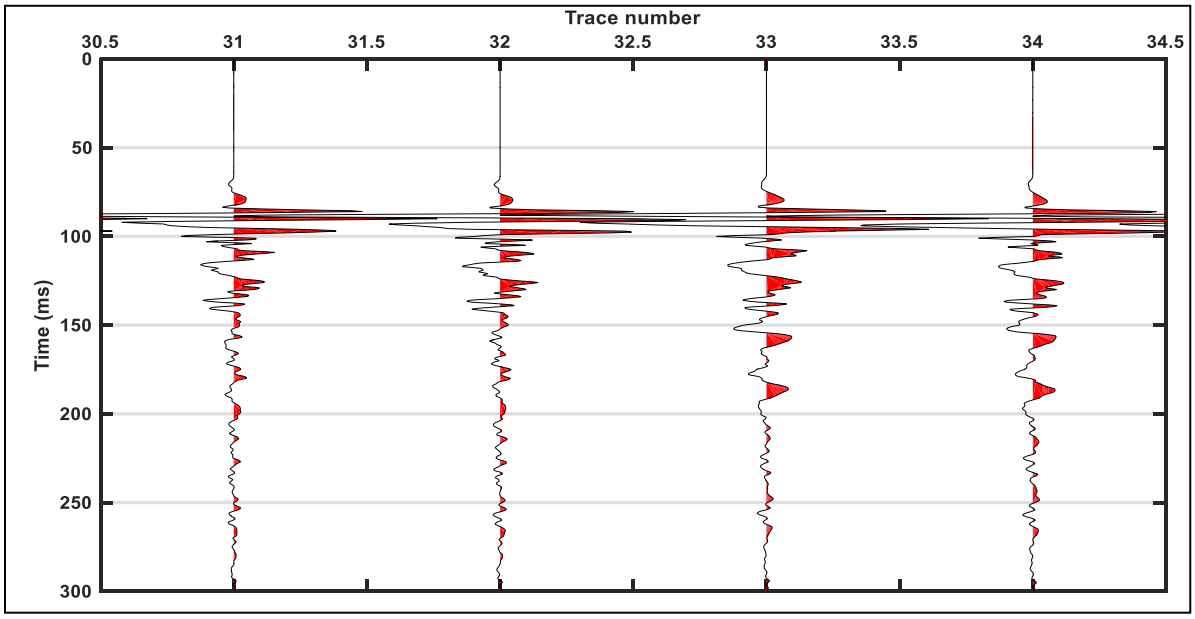

Figure 49: Parts of the common receiver plot for the air gun shots at hydrophone receiver 7. The receiver was located at 5 m depth, below node 7. Only traces 31, 32, 33 and 34 are displayed, i.e. the receiver responses from air gun shots 31, 32, 33 and 34. Air gun shots 31 and 32 were fired at 1.5 m depth below node 1 – 50 m, and air gun shots 33 and 34 were fired at 3 m depth below node 1 – 50 m. It seems like the shallower the source is, the more high frequencies the recorded signal contains.

In Figure 49, the two traces to the left are from shots where the source is at 1.5 m depth, and the two traces to the right are from shots where the source is at 3 m depth.

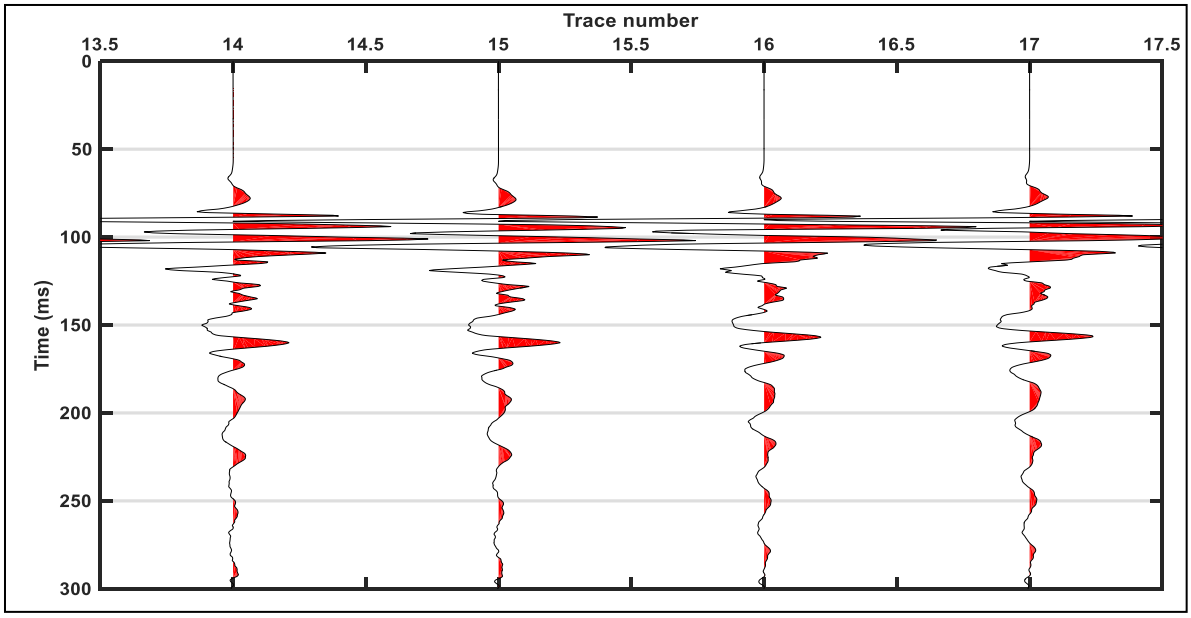

Figure 50: Parts of the common receiver plot for the air gun shots at hydrophone receiver 7. The receiver was located at 5 m depth, below node 7. Only traces 14, 15, 16 and 17 are displayed, i.e. the receiver responses from air gun shots 14, 15, 16 and 17. Air gun shots 14 and 15 were fired at 3 m depth below node 17, and air gun shots 16 and 17 were fired at 5 m depth below node 17. It seems like the shallower the source is, the more high frequencies the recorded signal contains.

In Figure 50, the two traces to the left are from shots where the source is at 1.5 m depth, and the two traces to the right are from shots where the source is at 3 m depth.

In both Figure 49 and 50, the first event that is seen is the refracted wave. This is recorded at the same time in all traces, independent of source depth, and the amplitude seems to be a bit stronger when the source is deeper. Then, the events that were identified as P-waves reflected from the water bottom are seen. What can be seen is that the shallower the source is, the more high frequencies the recorded signal contains. There are more oscillations in the traces from shots at 1.5 m depth than in the traces from shots at 3 m depth in Figure 49, and more oscillations in the traces from shots at 3 m depth than in the traces from shots at 5 m depth in Figure 50. The third event that is seen, is what was identified as the bubble pulses. We see that this is stronger on the traces from shots from deeper sources. As was seen in the frequency spectra of shots from different depths in the previous subsection (e.g. Figure 36, 41, 42 and 43), the shots from deeper sources generally have a higher amount of low frequencies, and a lower amount of high frequencies than the shots from the shallower sources. The traces in Figure 49 and 50 in this subsection show the same.

7.3. Pressure

7.3.1. Pressure variation with time

The amplitude values can be converted to pressure values (mBar), as described in subsection 6.2.1. By computing the pressure values from each shot at each receiver, we can be study the pressure variation of each shot with increasing time.

Figure 51 shows the pressure receiver responses for detonating cord shots 5 to 13 recorded at receiver Unite 9.

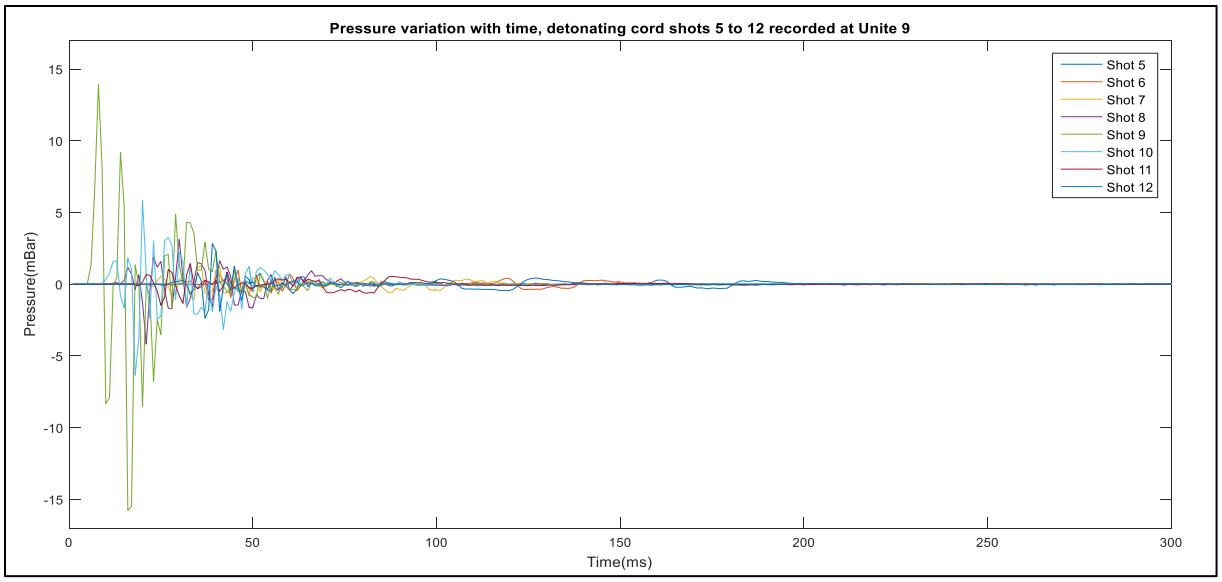

Figure 51: The pressure receiver response for detonating cord shots 5 to 13, recorded at Unite 9. The receiver was located at 1 m depth below node 9. The shots were all fired on top of the ice, in front of node 5 to 13. Since detonating cord shot 9 was fired closest to the receiver, the receiver response from that shot gave the highest pressure. The oscillations are probably due to reflections, refractions, air waves, surface waves and noise. No direct wave is seen.

For each shot, we see from Figure 51 that the signal is quite complex. No wave travelling directly from the source to the receiver was observed for the detonating cord shot in Figure 20, and is not observed in this figure either. The signal from each shot consists of several oscillations that are probably due to reflections, refractions, air waves, surface waves and noise. Each pulse is relatively long, as we would expect from a detonating cord (see subsection 3.1.2). We see that the strongest pressure value at Unite 9 in Figure 51 comes from detonating cord shot 9. The maximum pressure of a shot is expected to occur quite shortly after t=0, and thus the highest pressure from a shot is expected to be recorded at a receiver close to the shot point. Since the receiver interval (>12.5 m) is always higher than the receiver depth (<10 m), the shortest distance between source and receiver will always be when the source is right above or below the receiver.

How each shot is recorded at different receivers, can also be studied by comparing the same shot at different receivers. Figure 52 shows how an air gun shot at 3 m depth below node 17 is recorded at three different receivers.

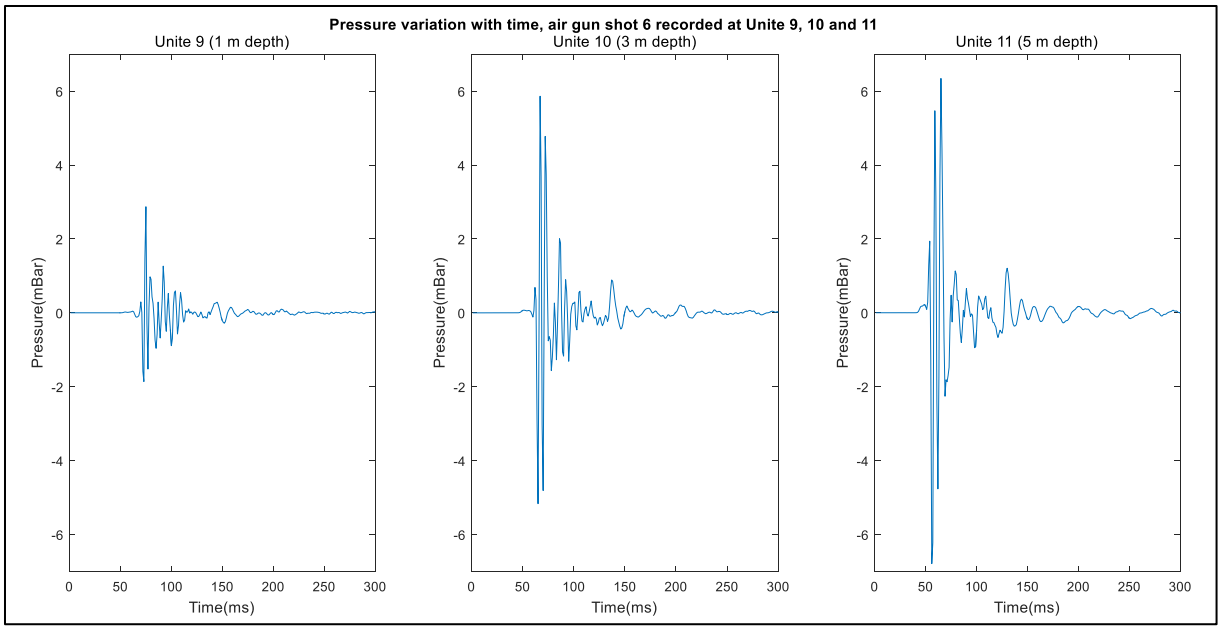

Figure 52: The pressure receiver response for air gun shot 6, recorded at the three different receivers Unite 9, Unite 10 and Unite 11. Unite 9 located at 1 m depth below node 9, Unite 10 was located at 3 m depth below node 10, and Unite 11 was located at 5 m depth below node 11. The shot was fired at 3 m depth below node 17. The maximum and minimum pressure values increase both with shorter distance between source and receiver, and with receiver depth. Therefore, the highest and lowest pressure values from air gun shot 6 were recorded at Unite 11.

First of all, it can be seen that the signals from the air gun shots in Figure 52 are quite different from the signals from the detonating cord shots in Figure 51. In Figure 52, we can see that the signal from each shot consists of several peaks and troughs. The first peak is probably the primary wave, that was travelling directly through the water from the source to the receiver, and the first trough is probably the ghost of the primary wave. The following oscillations are probably due to the oscillating air gun bubble, as well as reflections, refractions, surface waves and noise. The duration of the pulses is shorter than in Figure 51. The pressure values are higher when the receiver is close to the source position (node 17), just like for the detonating cord shots. However, the pressure values also seem to vary strongly with receiver depth. Shallower receivers show smaller absolute maximum and minimum pressure values than deeper receivers.

Based on both Figure 51 and 52, as well as the other seismic records, it looks like the pressure signature from one shot at a receiver, is quite complex. Therefore, the maximum and minimum pressure values were used to further investigate this.

7.3.2. Sound pressure level (SPL)

If we only extract the maximum and minimum pressure value from each shot at each receiver and use these to compute the peak-to-peak pressure, the highest SPL recorded at each receiver for each shot can be computed, using the *SPL.m* and *SPLairgun.m* MATLAB scripts. Each

figure is a schematic figure that shows how one single shot is recorded at all hydrophones, hence one figure is created for each shot. The following figures can be compared with Figure 18, that illustrated the receiver geometry during the survey. Each circle represents the location of a hydrophone, and the colour of the circle represents the strength of the SPL at that hydrophone. Some of the figures that were output by running the scripts are shown below. The upper figure (Figure 53) shows a detonating cord shot, and the two lower figures (Figure 54 and Figure 53) show one air gun shot at node 17, and one air gun shot at node 1 – 50 m, respectively. It is important to highlight that pressure values at receivers within 10 m from the source may be clipped, thus SPLs computed from those values should not be trusted.

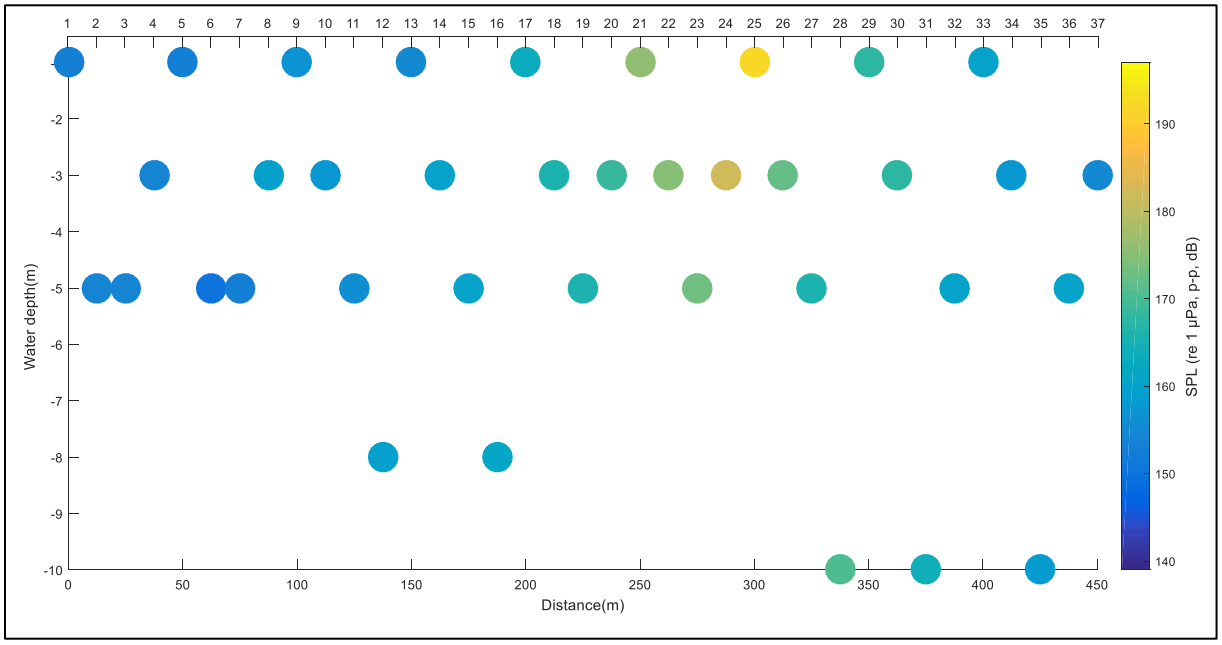

Figure 53: SPLs at each hydrophone receiver for detonating cord shot 24. The shot was fired on top of the ice, in front of node 25. Each circle represents a hydrophone, and the colours indicate decibel level. Yellow is high decibel level, and dark blue is low decibel level. The SPL decreases with increasing distance away from the source, but the decrease per unit distance is not constant. The SPL at the receiver closest to the shot position should not be trusted.

In Figure 53 for detonating cord shot 24, the detonating cord was laid out so that one end was at node 25, and the other end was 5 m away, towards node 24. Thus, it can be seen that the highest recorded SPL was at Unite 25 (receiver at 1 m depth). However, even though Unite 24 and Unite 26 are both at 3 m depth at the same distance away from node 25, Unite 24 will record a higher SPL than Unite 26, since the distance from the cord to Unite 24 is shorter. The highest SPL recorded outside 10 m distance from the source during the detonating cord shots, was 191.2 dB re 1 µPa, p-p, from shot 13 at Unite 12. 196.1 dB re 1 µPa, p-p, was the highest SPL recorded at all, but this was at a receiver at approximately 1 m distance from the source, therefore this

value may be clipped. SPLs are generally decreasing away from the source, but some exceptions are present. At e.g. receiver Unite 8, the SPL is higher than at receivers closer to the source.

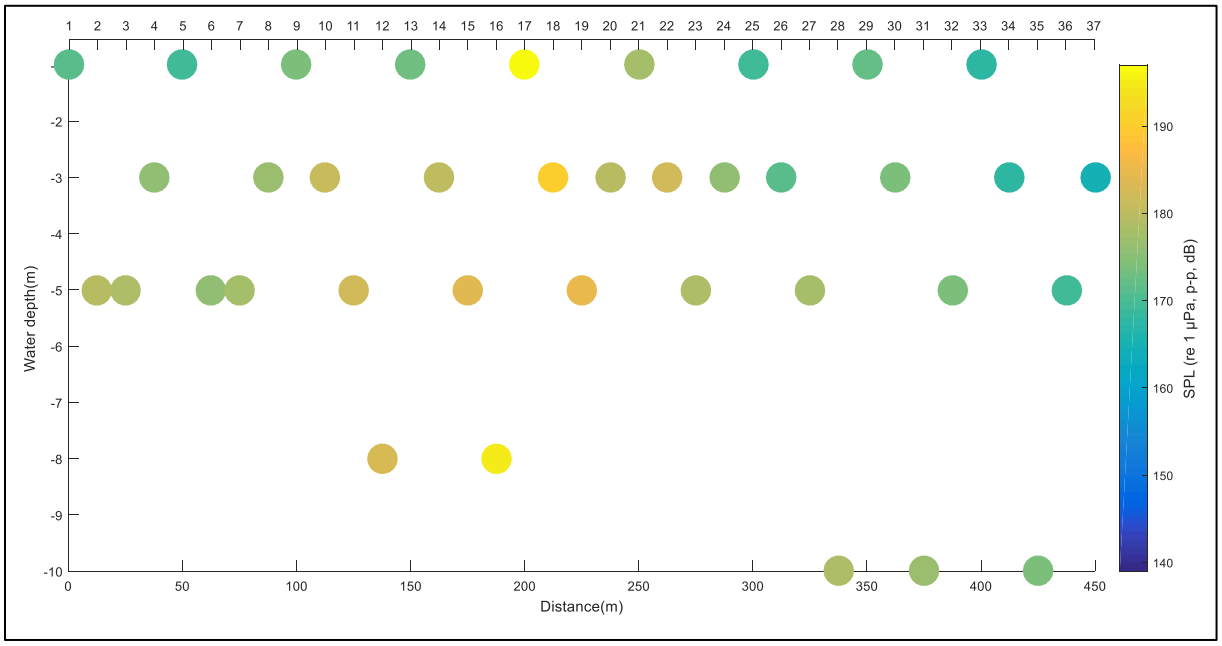

Figure 54: SPLs at each hydrophone receiver for air gun shot 6. The shot was fired at 3 m depth, below node 17. Each circle represents a hydrophone, and the colours indicate decibel level. Yellow is high decibel level, and dark blue is low decibel level. The SPL decreases with increasing distance away from the source, but the decrease per unit distance is not constant. The SPL at the receiver closest to the shot position should not be trusted.

In Figure 54 from air gun shot 6, the shot was fired at 3 m depth below node 17, with an air gun pressure of 160 bar. The figure shows that the recorded SPLs are generally higher than the SPLs recorded from the detonating cord shots. The highest SPL recorded outside 10 m distance from the source during the node 17 air gun shots, was 196.4 dB re 1 µPa, p-p, from shot 5. 198.1 dB re 1 µPa, p-p, was the highest SPL recorded at all, but this was at a receiver at approximately 2 m distance from the source, therefore this value may be clipped. If we compare using a source at 3 m depth with using a source at 5 m depth, we see that the recorded SPLs are higher when the source is at 5 m depth, which supports the higher amplitudes that were seen in the common shot plots when the source was deeper. Like in Figure 53, SPLs seem to decrease away from a source, but some exceptions are seen, e.g. at Unite 30, where the SPL is higher than at Unite 26, which was at the same depth, but closer to the source.

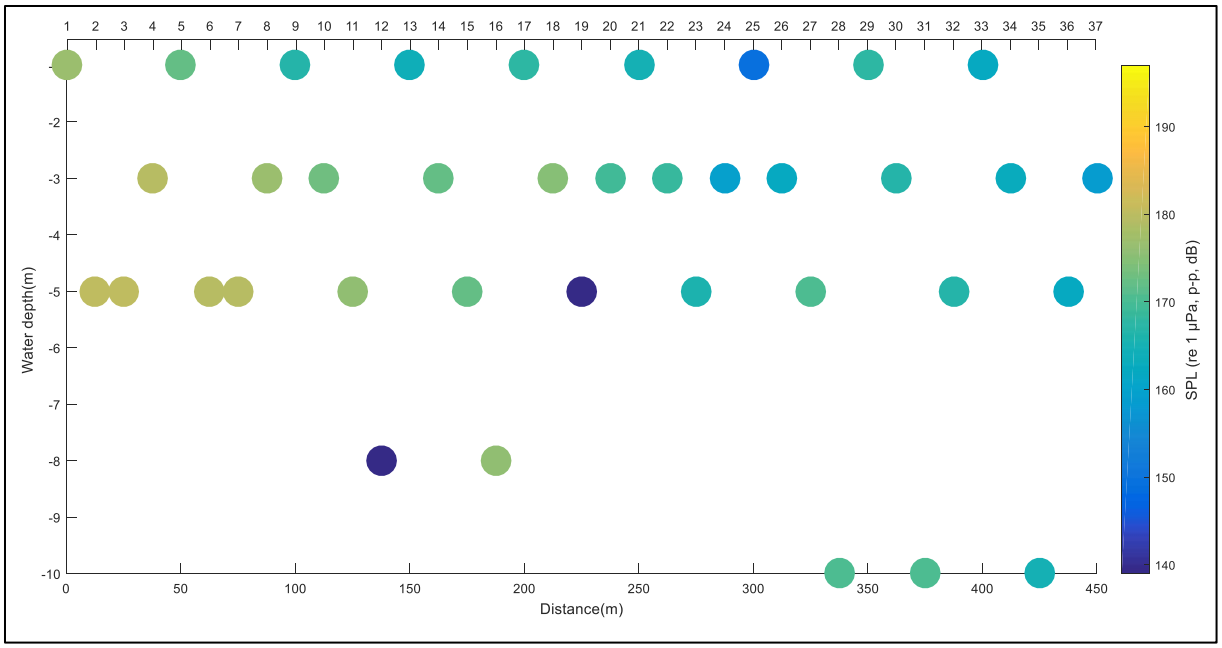

Figure 55: SPLs at each hydrophone receiver for air gun shot 38. The shot was fired at 3 m depth, below node 1 – 50 m. Each circle represents a hydrophone, and the colours indicate decibel level. Yellow is high decibel level, and dark blue is low decibel level. The SPL decreases with increasing distance away from the source, but the decrease per unit distance is not constant.

In Figure 55 from air gun shot 38, the shot was fired at 3 m depth below node 1 – 50 m, with an air gun pressure of 155 bar. As we might expect, the SPLs recorded are lower when the air gun is located at node 1 – 50 m instead of at node 17, since the air gun is located outside the spread, instead of in the middle of it. The highest SPL recorded during the air gun shots at node 1 – 50 m, was 183.0 dB re 1 µPa, p-p, at Unite 7 from shot 38. At Unite 12 and Unite 19, the recorded SPLs seem to be a lot lower than on the surrounding receivers. This behaviour is consistent for all shots from node 1 – 50 m. The very low values at these receivers make me assume that there might have been something wrong with the recordings at these receivers.

To sum up, Figure 53 to 55 show that for one single shot, the maximum SPL recorded at a receiver generally decreases with increasing offset between source and receiver, but in some instances, higher SPLs are seen further away the shot point than lower SPLs.

7.3.3. Sound exposure level (SEL)

Two MATLAB scripts for computing the SEL at each receiver were also written, as described in subsection 6.2.1. One SEL was computed using the rms pressure from all detonating cord shots, and one SEL was computed using the rms pressure from all the air gun shots. The pressure recorded at the hydrophone within 10 meters from each detonating cord shot was excluded from the computations, to make sure that no clipped pressure values were used in the computations. To account for this, only 42 detonating cord shots were assumed to be summed in each SEL

computation for the detonating cord shots. For the air gun shots, only Unite 17 was located within 10 meters from the shots, thus the SEL at Unite 17 should not be trusted. The duration was assumed to be 500 ms. Figures 56 and 57 below show the SELs computed at each receiver, where the colour bar is the same in both figures and goes from 166 to 186 dB re 1 µPa^{2}s, rms.

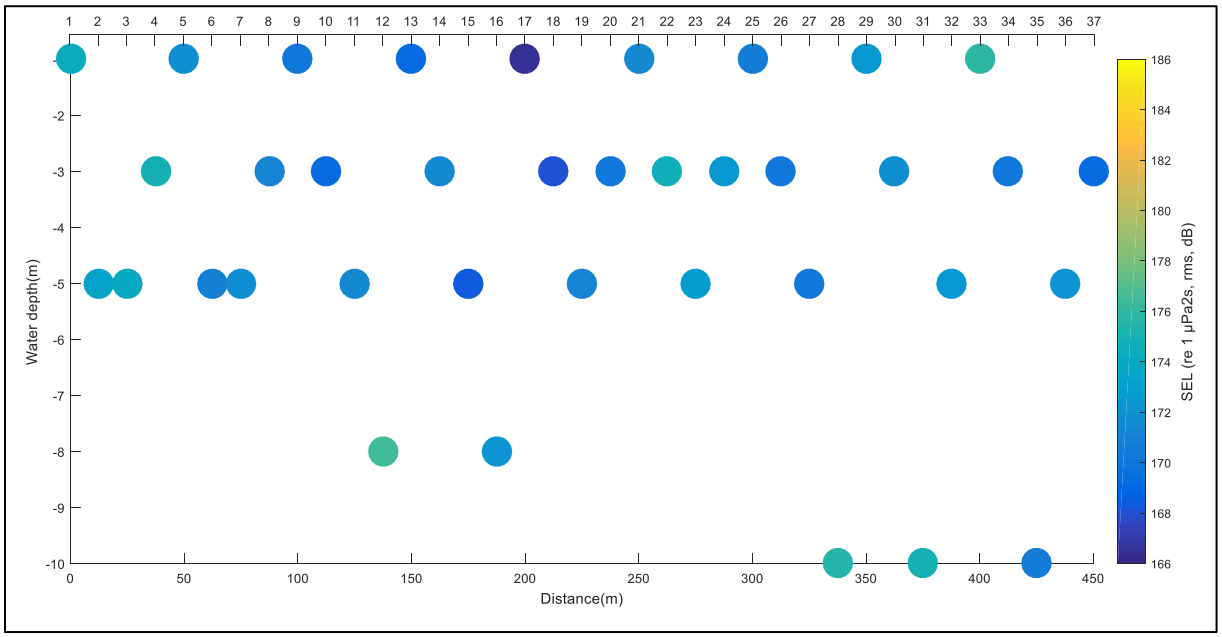

Figure 56: SELs at each hydrophone receiver for all detonating cord shots. Each circle represents a hydrophone, and the colours indicate decibel level. Yellow is high decibel level, and dark blue is low decibel level. The SEL is relative low, and the SEL is not varying a lot between the receivers. The SEL at the deeper hydrophones are higher than at the shallower hydrophones.

As can be seen in Figure 56, the SEL was varying between 166.6 and 176.3 dB re 1 µPa^{2}s, rms, for the detonating cord shots. The SEL is lower at the receivers close to the middle of the spread, which can be explained by the shot distance of 25 m between node 16 and node 18. Besides from that, the SELs are not varying a lot between the receivers. This is probably because shots were shot at different positions along the spread, which means that the distance between source and receiver was changing between each shot.

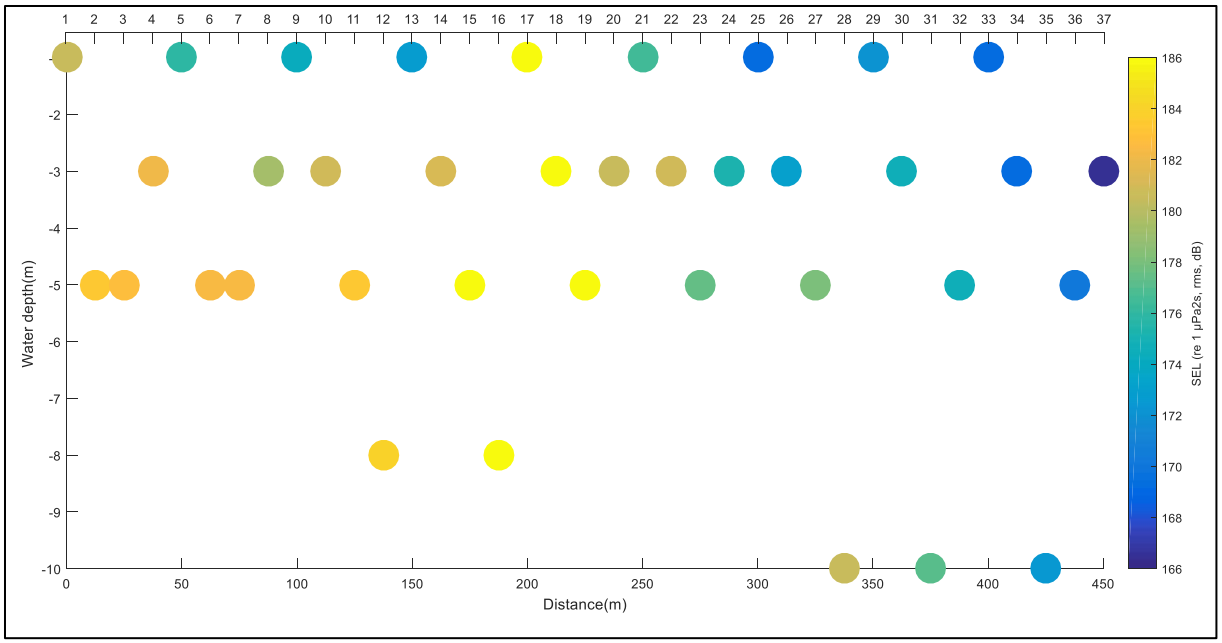

Figure 57: SELs at each hydrophone receiver for all air gun shots. Each circle represents a hydrophone, and the colours indicate decibel level. Yellow is high decibel level, and dark blue is low decibel level. The SEL is varying quite a lot between the receivers. The SEL is highest at the hydrophones closest to node 17, and it is also high close to node 1 – 50 m. The lowest SEL are found at the receivers with the highest Unite number.

As can be seen from Figure 57, the SEL was varying between 166.5 and 196.8 dB re 1 µPa^{2}s, rms, for the air gun shots, when ignoring the SEL of 203 dB re 1 µPa^{2}s, rms, at Unite 17.

The SELs are varying much more between the different receivers for the air gun shots in Figure 57 than for the detonating cord shots in Figure 56. The SELs are highest close to node 17, which is natural since 23 of the air gun shots were shot below node 17. The SELs are also higher closer to node 1, which makes sense since 38 of the air gun shots were shot below node 1 – 50 m. Unite 7 is in the middle between node 1 – 50 m and node 17, and thus is makes sense that the value at Unite 7 is higher than at the surrounding receivers. The lowest SEL is found at Unite 37, which was furthest away from the source for all air gun shots. The SELs are generally higher when the receivers are deeper in the water.

7.4. Wave propagation underwater

The A-values can be computed using both detonating cord data and air gun data. However, detailed inspection of the SPLs from both data sets show that the SPLs are varying a lot in the detonating cord data. A clear directionality is present, which is not seen when studying the air gun data. Therefore, the focus here is on computing A-values from the node 17 air gun data.

An air gun is a point source, which means that the distance measurements from the source to the receiver will be more accurate when using the air gun data than when using the detonating

cord data. To calculate the A-values, the procedure described in chapter 6 was followed. Since the formula P(r)=P(s)-Alog(r) has two unknowns, P(s) and A, linear regression is used to determine the P(s) and A for each node 17 air gun shot. The computed source levels gave an average P(s)=201.81 dB re 1 µPa, p-p, with a standard deviation of 1.20, and the computed A-values gave an average A=12.92, with a standard deviation of 0.55.

The computed P(s) and A are inserted into P(r)=P(s)-Alog(r) to make best fitted curves. These are displayed in Figure 58 below. The curves are not linear, due to the logarithmic distance term in the formula. In the figure, the experimental P(r) are also inserted, to be able to compare the computed curves with the actual values.

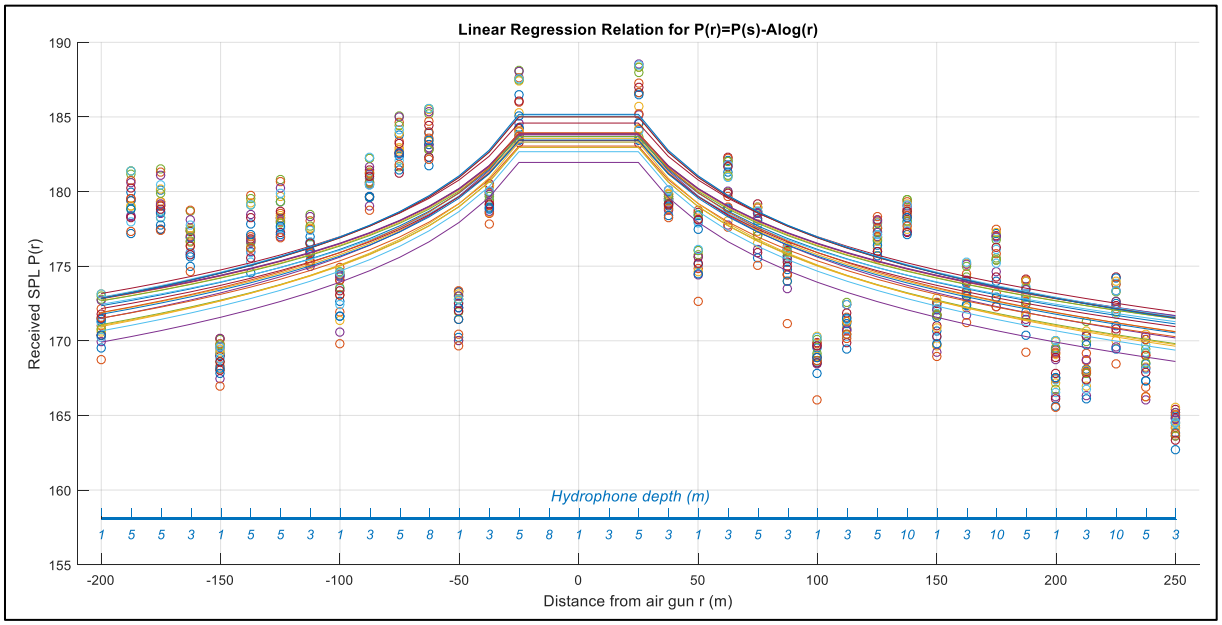

Figure 58: Best fitted A- and P(s)-values were computed using linear regression. Due to the logarithmic distance term in the formula P(r)=P(s)-Alog(r), the fitted curve is not linear in this figure where P(r) is plotted against distance from air gun.

From Figure 58 we see that the fitted curves match better with the experimental values at the deeper receivers than at the shallower receivers. It can also be seen that the values are generally a bit higher in the left part of the figure. This is a further indication that water depth may impact on the propagation, since the water depth was smaller under the left part of the spread (Figure 18).

During the computations, only SPLs >25 m away from the source were used, to be sure not to use any clipped SPLs. This is the reason why the curve is flat between 0 and ±25 m from the source in Figure 58.

Computation of A using the SPLs from the node 17 air gun shots gives values varying between 12.0330 and 13.6858. This means that the values are similar, but not entirely consistent. It seems

like differences coincide with differences in hydrophone depth. The recorded P(r) is lower at the distances that correspond to shallow hydrophones, and opposite. The P(r) at shallow hydrophones seem to differ more from the fitted curve than P(r) at deeper hydrophones. The coefficient of determination is a value R^2 that can show whether there is a good fit between the model and the data. R^2 is calculated using the formula

$$R^2 = 1 - \frac{\sum_{i=1}^{n}(y_i - \hat{y}_i)^2}{\sum_{i=1}^{n}(y_i - \bar{y}_i)^2}. \quad (32)$$

R^2 will be between 0 and 1, and a value close to 1 means that there is a good fit between the model and the values and opposite. The computed R^2-values are the following

R^2 = 0.3259, 0.3481, 0.3990, 0.4225, 0.1282, 0.2754, 0.2127, 0.2313, 0.2107, 0.2386, 0.2789, 0.3053, 0.3382, 0.3703, 0.4016, 0.2049, 0.1482, 0.1359, 0.1493, 0.1403, 0.3102, 0.3973, 0.4409.

This shows that the computed A- and P(s)-values are not very certain, and these differences between the different shots can be seen clearly in Figure 58 as well.

The fitted A-values of 12.0330 to 13.6858, combined with the relatively low R^2-values, indicate that a simple formula such as P(r)=P(s)-Alog(r), with A being a constant, is not sufficient in this shallow water sea ice covered area. The best fit indicates that the attenuation is lower than spherical spreading, and higher than cylindrical spreading.

8. Discussion

In this discussion, the results that were presented in the previous chapter will be discussed in light of theory. The chapter will start with a discussion of the advantages and disadvantages involved with using detonating cords or air guns as seismic sources. A review will then be made of the characteristics of the waves, and how they change when source type, air gun pressure and equipment depths are changed. Then a discussion will follow about how the seismic data in this study compares to theory about hearing and hearing damages in pinnipeds, and the last section will finally discuss the usefulness of this work.

8.1. Detonating cords versus air guns as seismic sources

This section discusses the differences between using a detonating cord or an air gun as a seismic source, and how this affects the quality of the seismic data. It was stated in chapter 3 that an appropriate source should give a signal that is broadband, resembles a pulse, is repeatable, and is safe to use (Kearey et al., 2002). It is therefore desirable with a source that fulfils these requirements. As was highlighted by e.g. Hegna and Parkes (2011), when changing survey geometry to improve the quality of seismic data, we want to make the reflections stronger, but also the level of noise lower. In other words, the goal is to enhance the signal-to-noise ratio.

In marine seismic surveys, air guns are the preferred seismic source today (Landrø and Amundsen, 2010). Detonating cords are often used in land seismic surveys, but several other seismic sources are also common in land seismic surveys (Kearey et al., 2002, Eisen et al., 2015). The presence of sea ice makes it possible to use both these types of seismic sources in an Arctic environment. This is because the floating ice can work as ground for a land seismic source, but holes can also be drilled through the ice so that a marine seismic source can be lowered into the water (Del Molino et al., 2008). A disadvantage of land seismic, compared to traditional marine streamer seismic, is that usually land seismic is more time consuming than marine seismic, since moving the equipment around is more difficult (Kearey et al., 2002).

In Arctic environments, the opposite is often seen. While detonating cords can be laid out on top of the ice quite effectively, holes need to be drilled through ice, sometimes meters thick, to be able to use air guns (Del Molino et al., 2008, Johansen et al., 2011). Using air guns also require that the water has a certain depth to avoid mud entering the air gun, while detonating cords can be used independently of water depth. Therefore, when conducting seismic surveys in the Arctic, marine surveys might be more time consuming than land surveys.

However, even though placing equipment in the water below the ice can be more time consuming during the acquisition process than placing equipment on top of the ice, the needed processing effort may be reduced (Del Molino et al., 2008). Less processing effort will be needed to remove the flexural ice wave, the air wave, and noise caused by harsh weather conditions, which can save time in later stages. A goal should be to find an acquisition geometry that balances time spent acquiring the data, with improved quality of the data due to that acquisition geometry. That is, the reduced processing time needed due to improved quality of the seismic data needs to be higher than the extra time it takes to perform the acquisition. Additionally, an air gun is cheaper to use than a detonating cord, since the fuel is pressured air, which is cheaper than the expensive dynamite used in detonating cords (Sercel, 2016).

The different sources also give signals with different characteristics. The signal created by both an air gun and a detonating cord will be a pulse, but the pulses will have some clear differences. This was seen in Figure 51 and 52, showing the pressure signatures from seismic shots. The duration of the source pulse is longer when using a detonating cord than when using an air gun source. However, the rise time for detonating cords is shorter than the rise time for air guns (Gordon et al., 2003). Air guns are commonly "ramped up" when used in a seismic survey, by gradually increasing the intensity of the sound from the air gun. This is, however, not common practice when using dynamite. It should be possible to ramp up when using detonating cords as well, by using detonating cords of different lengths, but this would probably be more time consuming and expensive than ramping up air guns. When this technique is used, sounds that are uncomfortable, but not harmful to marine mammals, will hopefully scare animals away from the acquisition area before they get physically harmed (Marine Mammal Commission, 1972, Dragoset, 2000, Gausland, 2000, Tolstoy et al., 2004, Dunlop et al., 2016). Kvadsheim et al. (2017) refer to some recent studies that show that marine mammals may be able to downscale their hearing sensitivity if they know that a loud sound is coming. This is also an interesting argument for further studies about the use of ramp up procedures to avoid hearing damages in pinnipeds.

Due to the characteristics of the pulses, dynamite is generally considered more harmful to animal life than air guns, and due to environmental and biological considerations, the use of dynamite under the ice layer has been prohibited in Arctic areas (Del Molino et al., 2008). However, measures can be taken to make sure seismic data acquired with both types of sources have as little impact on the environment as possible. " Leaving no mark behind" is a very important aspect of Arctic seismic exploration (Trupp et al., 2009).

One measure that can be taken is to lay out the detonating cord as a line when it is used. In this way, the energy is spread out over a larger area, and the impact on the ground is less. Another reason why a detonating cord is usually laid out as a line is because this will create a directionality. This is favourable if we want to focus the energy towards the receivers (Johansen et al., 2011). Therefore, a detonating cord can be regarded as a line source, while an air gun can be regarded as a point source.

It is easier to repeat the same signal several times when using an air gun rather than a detonating cord (Sharpe, 1942, Dragoset, 2000). See e.g. the similarities between the traces from the same air gun depth and pressure in Figure 49 or 50. We have no figures in this thesis where the repeatability of the detonating cord can be shown in the same matter. Nevertheless, since we saw that a detonating cord generates more high frequency energy than low frequency energy (Figure 36), these waves are probably more prone to changes during the shooting than waves from air guns. Thus, they are probably less repeatable.

Differences in the seismic wavefield will also occur when using the different sources. Direct waves, reflected waves, and refracted waves will usually be created by both source types, but different source-induced waves are often present. In this survey, the air wave that was very prominent in the detonating cord records could not easily be identified in the air gun records (e.g. Figure 20 versus 30). This was probably the case because the air gun was fired underwater and not in the air, as was explained by Press and Ewing (1951b). A strong air wave means that quite a lot of the source energy has leaked into the air, which can partly explain why higher amplitudes were registered in our data when using an air gun rather than a detonating cord (Johansen et al., 2011). On the other hand, the bubble pulse that was seen in the air gun records is a wave that is created when using an air gun, and not when using detonating cords (e.g. Figure 20 versus 30) (Dragoset, 2000). Mini GI air guns were used in Svea in 2016 to minimize the bubble pulse, but a bubble pulse was still clearly seen in all air gun records. Bubble pulses from GI air guns have been reported to appear stronger than usual in seismic records when the water surface is covered by ice, since the bubble will be trapped in the water below the ice (Betterly et al., 2007).

Surface waves were seen in seismic records from shots with both source types. Flexural ice waves seemed to be more common in the detonating cord records than in the air gun records (e.g. Figure 23 versus 33). In Figure 44, an event travelling with a velocity of approximately 170 m/s was observed in traces from receivers at 1 m depth and air guns at 1.5 m depth, but not in any of the traces from deeper hydrophones and air guns. This might be components of the

flexural ice wave from an air gun shot. Betterly et al. (2007) also observed flexural ice waves in their records when they were using a GI air gun just below the sea ice, but in most studies, the flexural ice wave appears clearest when the source is placed on top of the ice (Rendleman and Levin, 1990, Henley, 2007). It was not easy to determine the exact characteristics of the flexural ice wave from these data, and this is often the case in seismic surveys. The ice properties often change from place to place and season to season, and people and snowmobiles moving on the ice might cause cracks in the ice that make the ice more inhomogeneous. This, in addition to ice thickness and temperature, may affect the nature of the flexural ice waves (Proubasta, 1985, Jensen, 2016).

Scholte waves were found in records from shots with both source types, but were seen clearer in the air gun records (e.g. Figure 23 versus Figure 33). This can be explained by the fact that shots from air guns tend to contain more low frequencies than shots from detonating cords (e.g. Figure 36). Since a Scholte wave is travelling with very low velocities and frequencies, this means that it should be stronger when it is created by a source with a high low frequency content. The low frequencies and velocities means that it should not be as difficult to distinguish Scholte waves from reflections as flexural ice waves during processing. Therefore, the presence of these are not believed to affect the data quality in as large a degree as the flexural ice waves.

It was claimed in subsection 4.2.2. that a Scholte wave becomes dispersive due to different velocities in different sediment layers in the water bottom, as well as limited water depth. The dispersive nature of the Scholte wave that was observed during this survey (Figure 23, 24 and 33) fits well with reported observations from the area. The water bottom has been reported to consist of glacial and sedimentary deposits from when the Paula glacier was moving forward, and later retreated around 600 years ago (Cöster, 1925, Larsen and Lyså, 2015). The water depth was also reported to be varying from 7.05 m to 13.15 m, over a distance of 450 m (Figure 19). For determining the dispersion characteristics of the Scholte wave (e.g. for determining the shear wave velocity profile of the shallow subsurface), it should be easier to use the air gun records, since the Scholte wave was easier to discriminate from other events in those records. This was not the purpose of this survey, but is still an interesting observation.

A short discussion about the direct wave is also necessary, since this is a wave that is usually present in all seismic records, but that was not visible at all in the detonating cord data from the 2016 Svea survey (e.g. Figure 20). A direct wave is a wave travelling from a source to a receiver without being reflected on the way. In the case of a source on ice and receiver in water, this would mean a wave travelling partly as an extensional wave in the ice, and partly as a P-wave

in the water. Since no direct wave was seen in the detonating cord records, it could be tempting to assume that there was no direct wave travelling in the ice in 2016. However, we could observe reflected and refracted waves, therefore we assume that the source generated waves travelling in all directions, including directly towards the receiver. We can instead assume that the direct wave did not reach the hydrophone.

An explanation for the non-existent direct wave in the seismic records can be that the ice had a Poisson's ratio close to zero. This suggestion is built on reports about the ice being "slushy" during the survey in 2016, not on any specific measurements of Poisson's ratio. Poisson's ratio says something about how much a contraction or elongation of a material in one direction will lead to elongation or contraction in the direction perpendicular to that (i.e. the ratio of transverse strain to axial strain), and is usually between -0.5 and 0.5 (Gelius, 2012a). Figure 59 shows the principles of Poisson's ratio, in the case of an elongated cylinder.

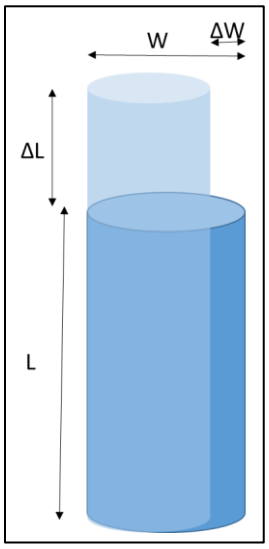

Figure 59: The principles of Poisson's ratio visualized. The filled blue cylinder is the shape of the cylinder before deformation happens, and the transparent blue cylinder is after deformation happens. $|\varepsilon_{zz}|=\frac{\Delta L}{L}$ *is the strain in the axial direction.* $|\varepsilon_{rr}|=\frac{\Delta W}{W}$ *is the strain in the transverse direction. Then Poisson's ratio is given by* $v=\frac{|\varepsilon rr|}{|\varepsilon zz|}$. *v=0 means that a contraction or elongation in one direction will not lead to deformation in the direction perpendicular to that. The cylinder in the figure has a positive Poisson's ratio.*

If Poisson's ratio is zero, it means that a contraction or elongation in one direction will not lead to deformation in the direction perpendicular to that. Therefore, a compressional wave travelling horizontally within the ice will not lead to vertical movement, and thus no compressional wave will be transferred to the water. This explanation is supported by the fact that no direct wave was observed in the vertical component of the geophone data either, but an event that can be the direct wave was observed in the horizontal component of the geophone data (Senior Engineer Bent Ole Ruud 2016, personal communication).

To sum up, the amount of noise that can mask reflections seems to be higher in the seismic records from detonating cord shots rather than from air gun shots. This is confirmed by Figure 60, displaying the variable density of the unprocessed common shot plots for detonating cord shot 3 to the left, and air gun shot 32 to the right.

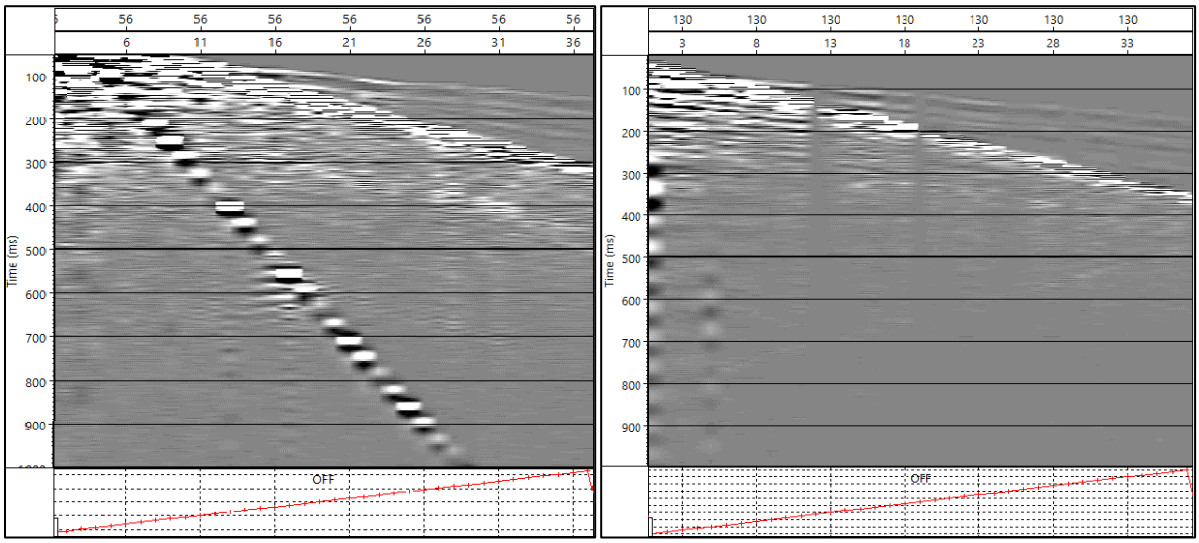

Figure 60: Unfiltered common shot plots for detonating cord shot 3 (left) and air gun shot 32 (right). Detonating cord shot 3 was fired on top of the ice, in front of node 3. Air gun shot 32 was fired at 1.5 m depth below node 1 – 50 m. Variable density is displayed. There is a higher amount of noise in the common shot plots for the detonating cord shot than for the air gun shot. Figure made using Vista.

In the seismic records, the P-waves reflected from the water bottom were the only reflections clearly visible (e.g. Figure 20 versus Figure 30). Identifying other reflections was difficult since the offset between source and receiver was maximum 500 m, which is too short to clearly see the typical curvature of a reflection in a seismogram. While there was nothing that resembled reflections in the detonating cord records, there were some events that could be reflections (or multiples) in the air gun records. The frequency spectra from air gun shots and detonating cord shots were also quite different, and this will be further discussed in subsection 8.3.4. In general, there seems to be more of the high frequencies in the detonating cord shots, and more of the low frequencies in the air gun shots.

8.2. The significance of survey geometry

As was shown in the results chapter, the quality of the seismic data can be affected by several factors related to acquisition geometry. The depth of both source and receiver can have an impact on how the seismic data is recorded, as well as the pressure of the air gun.

8.2.1. Receiver depth

It is assumed that differences that were seen between records from seismic receivers located at different depths in the water (e.g. Figure 28 and 46) may have been caused by a few different factors. One is that the waves were travelling different distances to reach the different receivers. Differences caused by this are consistent with the theory of geometrical spreading, which says that energy per unit area will decrease with increasing distance away from a source (Kearey et al., 2002). Absorption will also lead to a decrease in energy level with increasing travel distance. The second is that a surface ghost may have had a larger impact on the shallower receivers than on the deeper receivers. This was for example reported by Tolstoy et al. (2004). Each of the events that were seen in the seismic records will in the next paragraphs be discussed relative to these arguments.

When alternating between having the hydrophone receivers at different depths in the water, the reflections were stronger when the hydrophones were deeper in the water (e.g. Figure 21 and 31, and Figure 28 and 47). The clearest example, in the seismic records from both source types, was the thick package of parallel events that were identified as P-waves travelling in the water. The waves were identified as P-waves reflected from the water bottom both because they were relatively strong (i.e. they probably had not travelled very far since little attenuation had happened, and had probably been reflected from a high contrast boundary), and because they were travelling with the P-wave velocity of water (approximately 1500 m/s). Increasing amplitude with increasing receiver depth is believed to be valid for all reflections from the subsurface.

This is because an increasing amplitude with increasing receiver depth can be explained by the fact that a wave will be attenuated relatively rapidly in water (University of Rhode Island and Marine Acoustics inc., 2013). Thus, when a receiver is located deeper in the water, the reflections need to travel a shorter distance in the water to reach the receiver than when the receiver is located higher up in the water column. It will therefore experience less attenuation. This effect is illustrated in Figure 61.

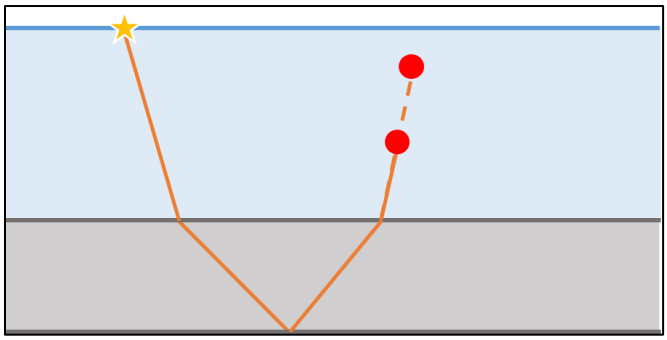

Figure 61: A reflected wave has to travel a shorter distance in the water to reach a deep receiver than to reach a shallow receiver. Since attenuation due to geometrical spreading and absorption increases with increasing distance, the amplitude at the deep receiver will be higher than at the shallow receiver.

However, interference between a wave travelling directly towards the receiver, and a wave reflected from the water surface, may have an even larger impact on the reflection amplitude. As was explained in subsection 3.1.1., the reflection coefficient at the water surface is close to -1. Thus, a wave that hits the water surface from below will be almost completely reflected from the surface, changing polarity in the process. This effect is illustrated in Figure 62.

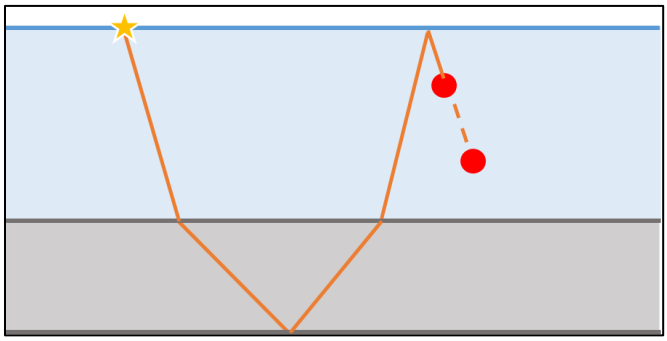

Figure 62: A receiver ghost will arrive sooner at a shallow receiver than at a deep receiver. This will lead to more destructive interference at the shallow receiver than at the deep receiver. Therefore, the reflection amplitude at the shallow receiver will be weaker than at the deep receiver.

This can happen both on the receiver side, and on the source side. Just like the reflection is stronger when the travel distance is shorter, the receiver ghost will also be stronger if the distance the wave must travel to the receiver after being reflected is shorter. This is when the distance from the surface to the receiver is shorter. The most important thing is, however, that since the ghost will have the opposite polarity of the primary wave, destructive interference between the two waves is likely to occur at the receiver if the primary wave and the ghost arrive very close to each other (Landrø and Amundsen, 2010).

Refracted waves appeared both in the detonating cord data, and the air gun data. The velocities were varying between each shot, between approximately 3700 m/s and 4600 m/s (e.g. Figure 20 and 30). This coincides with common P-wave velocities in sediments (Gelius, 2012a). The

varying velocities were probably due to the waves being refracted from different boundaries during the different shots. The refracted waves showed a similar behaviour as the reflected waves regarding depth dependence (e.g. Figure 28 and 46).

For the coupled air wave, the opposite behaviour as for the reflected and refracted waves was observed. The air wave was recorded stronger at the shallower receivers, and weaker at the deeper receivers (e.g. Figure 22). As previously explained, an air wave is a compressional wave travelling in air, due to a source being fired above the water surface. The air wave leads to a coupled wave travelling in the water, which is why the air wave can be seen on records from receivers in water. In the records from this survey, the air wave was most visible in the detonating cord records. The detonating cords were placed above the water surface when they were fired, while the air guns were located under the water surface. The distance to the air was shorter when the receivers were placed closer to the water surface, and therefore the air wave was recorded stronger on the shallow receivers. A few interesting features with the air wave were observed in the seismic data, and deserve some attention.

First, from e.g. Figure 20, the velocity of the air wave was computed to be around 320 to 330 m/s. The P-wave velocity in air is known to be 330 m/s, which means that the air wave in this study was travelling slower than expected. This lower air wave velocity can be explained by the low temperatures during the survey, since P-wave velocity has a slight temperature dependence (Kohnen, 1974).

Another interesting feature of the air wave was that it seemed to be dispersive. This was highlighted in Figure 27. An air wave is always created when a seismic source is used in air, but it is usually not dispersive. The velocity dispersion seen in these data was probably caused by the presence of ice, that lead to air-coupled flexural ice waves in the water. This was shown by Press and Ewing (1951b), and discussed in subsection 4.2.1. Press and Ewing (1951b) also showed that for a source in water instead of in air, the air-coupled flexural waves will have negligible amplitudes for the frequencies that give air-coupled flexural waves in air (Press and Ewing, 1951b). This is consistent with what we saw in our data.

Third, a slightly curved event with approximately the same slope as the air wave was seen arriving around a second after the air wave in some of the detonating cord records (e.g. Figure 20). This made me assume that this event was somehow related to the air wave, and that we probably observed a coupling of a refracted air wave. Since an air wave is a compressional wave travelling above water, it is natural to assume that just like when a wave is travelling into

the subsurface, parts of the wave will be reflected if the wave hits a surface. Most people have experienced that if they stand close to a mountainside and scream, parts of the sound will be reflected as echoes from the mountainside. The survey area in the Van Mijen fjord was located between several high mountains, and the fjord itself was relatively narrow. Only records from shots located outside the end of the spread contained this event. For detonating cord shot 37 (Figure 20), the event arrived approximately 1050 milliseconds after the air wave. This corresponds to a distance of 346.6 m, if we assume that the wave was travelling at 330 m/s. We therefore assume that the refracted air wave came from headland going out into the fjord. Just like the air wave, the refracted air wave was more visible in the records from the shallower receivers, which further supports that this wave was somehow related to the air wave.

A receiver depth dependence was also observed for the surface waves. The flexural ice wave was not easy to distinguish from other events in the seismic data from this survey, but was for example seen in the low-pass filtered shot plot in Figure 23. The flexural ice wave appeared very dispersive, and a reduction in strength with increased receiver depth was observed. This was reported by Rendleman and Levin (1990) as well, who compared signal-to-noise ratios for receivers at different depths. They concluded that a better signal-to-noise ratio was obtained when the receiver depth was increased.

Increasing amplitude loss with increasing distance due to geometrical spreading and absorption, can probably partly explain why the flexural ice waves were recorded stronger at the shallower receivers than at the deeper receivers. The flexural ice wave itself will travel within an ice layer floating on top of the water surface, but will give rise to a coupled wave travelling in the water layer. Since this coupled flexural ice wave originates in the ice, the distance the wave must travel to the receiver is shorter when the receiver is close to the ice. The reduced amplitude strength can be explained theoretically by using the derivation by Press and Ewing (1951a), partly presented in section 4.2. In that derivation, the solutions of the wave equations in an air-ice-sea environment were presented. The waves travelling in the water layer were assumed to follow the wave equation in Equation 19: $\nabla^2\varphi_2 = \frac{1}{v_{p2}^2}\frac{\delta^2\varphi_2}{\delta t^2}$. Then the solution is given in Equation 22: $\varphi_2 = Ee^{-\varsigma z}e^{i(kx-\omega t)}$.

Equation 22 gives the elastic P-wave potential in the water. The potential is proportional to the pressure in the water, which again is proportional to the amplitude (Equation 26). Thus, it can be seen from Equation 22 that the amplitude of the flexural ice wave will decrease exponentially with increasing depth z in water.

If the argument about geometrical spreading and absorption is assumed to hold for the Scholte wave as well, the coupled Scholte wave travelling in the water should be stronger when the receiver is located deeper in the water. This is because a deeper receiver would mean a receiver closer to the interface where the Scholte wave travels. A stronger Scholte wave at the deeper receivers is what was shown in Figure 24, and the argument from before therefore holds. The derivation by Press and Ewing (1951a) can, however, also be used to explain the depth dependence of the Scholte wave.

The model by Press and Ewing (1951a) assumed that the water depth was unlimited. It can be shown that if a water bottom layer is added as well, a coupled Scholte wave will occur in the water layer. It can, however, be argued that the amplitude of this wave will increase exponentially with increasing depth z in water, instead of decreasing. In Equation 22, the depth was included in the term $e^{-\varsigma z}$, which contained the constant ς, given by Equation 25: $\varsigma^2 = k(1-\frac{c^2}{v_{p2}^2})$. This equation shows that the constant only depends on frequency, phase velocity, and the P-wave velocity in water (1500 m/s). For the Scholte wave, ς will be negative instead of positive due to the added water bottom, thus the amplitude will be proportional to $e^{+\varsigma z}$, instead of to $e^{-\varsigma z}$ (Senior Engineer Bent Ole Ruud 2017, personal communication, 02.05.17).

Since both the flexural ice wave, and the Scholte wave are considered noise, opposite conclusions about where it would be best to locate the receivers can be drawn, based on the results. The fact that the flexural ice wave is stronger at the shallow receivers would be an argument for locating the receivers deep in the water. The fact that the Scholte wave is stronger at the deep receivers would on the other hand be an argument for locating the receivers shallow in the water. However, as pointed out in section 8.1, since a Scholte wave is travelling with very low frequencies and velocities, removing the Scholte wave during processing is probably easier than removing the flexural ice wave. Therefore, it is probably better to have a stronger Scholte wave than a stronger flexural ice wave, i.e. locating the receivers deeper in the water. This is the best conclusion based on the receiver depth dependence of the reflected, refracted and air waves as well. We can also assume that the impact of noise from weather and ocean waves will be less when the receivers are deeper.

8.2.2. Air gun depth and pressure

Differences were also seen when the air gun source was located at different depths in the water. The air gun was located at 1.5 m, 3 m and 5 m depth, but direct comparisons between 1.5 m

and 5 m source depths are not possible. This is because the shots at those depths were fired at two locations with different water depths. However, in general, both the bubble pulse, the reflections, and the refracted waves appeared to be stronger when the air gun was deeper in the water.

There are two competing factors that determine how a signal is affected by a changed source depth. These are the response of the air gun, and the source ghost (Landrø and Amundsen, 2010, Hegna and Parkes, 2011, Haavik and Landrø, 2015). Hegna and Parkes (2011) claim that the response of an air gun will be affected by depth in a larger degree than a receiver.

The Rayleigh-Willis formula that was presented as Equation 15: $T = k\frac{P^{1/3}V^{1/3}}{(P_{atm}+\rho gD)^{5/6}}$, shows that the bubble period T decreases with increasing source depth D. Since f=1/T, the frequency will increase when the period decreases, i.e. signals from a smaller and deeper air gun should contain more high frequencies than signals from a bigger and shallower air gun. Based on only this, it sounds reasonable that placing the source as shallow as possible would be best in a seismic survey where the goal is to penetrate deep into the subsurface.

However, when an air gun is located under water, a ghost may occur on the source side, as well as on the receiver side (Figure 62). A source ghost is the part of the primary wave that was first travelling towards the water surface, and was then reflected to join the primary wave travelling towards the subsurface (Landrø and Amundsen, 2010). The ghost will travel closer to the primary wave if the distance the wave must travel before it is reflected from the surface is shorter, i.e. when the source is shallower. When a marine seismic source, such as an air gun, is placed close to the water surface like in this survey, the source ghost can therefore have a large impact on the wave signature (Richardson et al., 1995, Landrø and Amundsen, 2010, Hegna and Parkes, 2011). The source ghost will thus attenuate the low frequencies due to destructive interference, and this effect can be decreased by increasing the source depth (Hegna and Parkes, 2011). Based on this, it can be concluded that it would be better to have the source deeper in the water, opposite to the conclusion in the previous paragraph.

We also saw differences in the amplitude of the bubble pulse when we were changing the depth of the source (Figure 34 and 35). The bubble pulse was stronger when the source was deeper, but it arrived closer to the primary pulse (Figure 49 and 50). When the bubble period was computed from Figure 36, the deep air gun had a period approximately 5 ms shorter than the shallow air gun. This behaviour was reported by Haavik and Landrø (2015) as well.

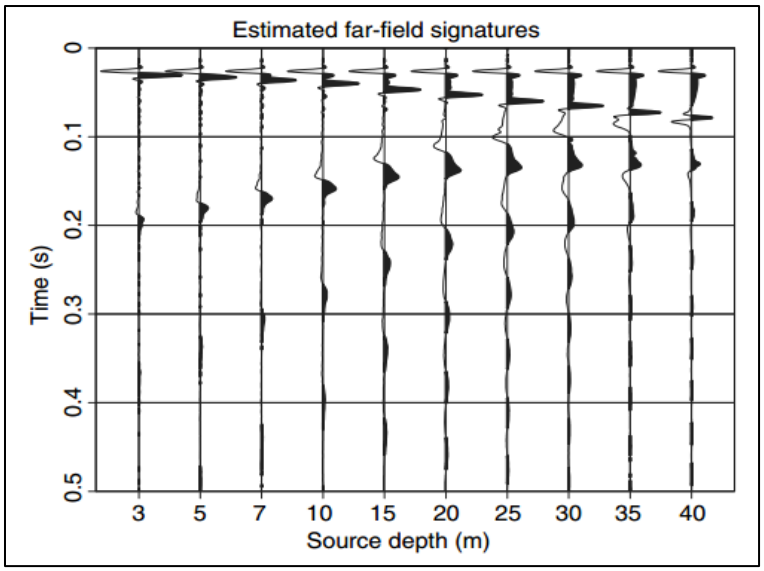

Figure 63: Figure from Haavik and Landrø (2015). The figure shows the estimated far-field signatures that would be recorded at a receiver vertically below a 600 in^3 air gun. The different traces represent the signatures from shots from sources at depths varying from 3 to 40 m. The bubble pulse period is decreasing when the source depth increases. Also, the source ghost is delayed when the source depth increases. This is explained by the increasing travel distance from the source to the surface when the source is deeper.

In Figure 63 from Haavik and Landrø (2015), we see that the bubble period decreases with increasing source depth, as was explained by the Rayleigh-Willis formula. We can, however, also see that the amplitude of the bubble pulse increases. Both the decreased bubble period, and the increased bubble amplitude with increased source depth, can be explained by the fact that the hydrostatic pressure increases with increasing water depth. As explained in subsection 3.1.1., the reason why the air gun bubble will oscillate is due to different pressures inside and outside the bubble. When the hydrostatic pressure increases, the point when the hydrostatic pressure is larger than the internal pressure of the bubble will be reached earlier, and the hydrostatic pressure will push more on the bubble (Haavik and Landrø, 2015). This is when the air gun is located deeper in the water.

The effect of changing source depth was also briefly studied for the surface waves. The flexural ice waves appeared stronger when the source was shallower, and the Scholte wave appeared stronger when the source was deeper in the water. The same arguments as was used to explain the effect of changing receiver depth, based on geometrical spreading, absorption, and the derivation by Press and Ewing (1951a), can be used to explain this.

Based on the Rayleigh-Willis formula, we see that if everything except from the air gun pressure is kept constant, T should increase, and the amplitude should be stronger. This behaviour was, however, not seen in all seismic records in this study. Using an air gun with a higher pressure did give an increased T, but did not necessarily give higher amplitudes for all events (Figure

37, 38, 39 and 40). A possible explanation for this can be the very limited water depth in the area, and the short distance between source and receiver. Since the distances were short, it might be that the higher pressure air guns were not able to reach their maximum size before they reached the receiver, or that the differences were so small that they were difficult to observe.

8.3. Pinnipeds and seismic surveys

The SPLs, SELs, frequency spectra and wave propagation constants that were computed will be discussed in the next few subsections. After that, the effect seismic surveys may have on pinnipeds will be discussed in subsection 8.3.6, by comparing the computed properties with theory about hearing in pinnipeds.

8.3.1. Pressure

When studying the pressure versus time records, we could see that the recorded signals were quite complex (Figure 51 and 52). This was especially the case for the air gun signals in Figure 52. Figures showing the signals a conventional air gun and a mini GI air gun are supposed to generate were provided by the manufacturer (Sercel, 2016). As can be seen in Figure 64, those signals have a very simple far field signature.

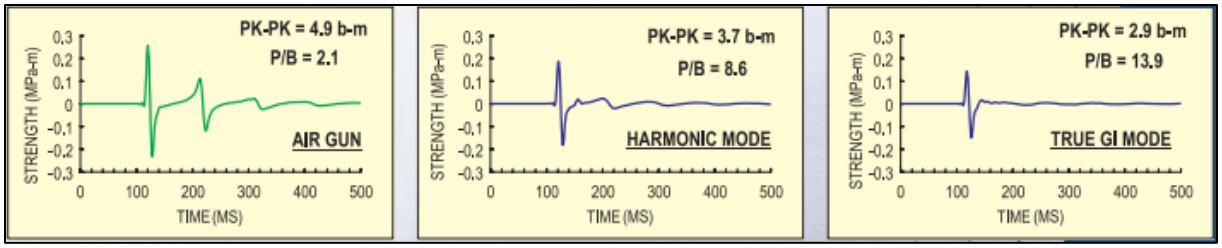

Figure 64: Figure from Sercel (2016). Far field signature for a conventional air gun (left), a GI air gun with delayed injection (middle), and a GI air gun with perfectly timed injection (right), as given by the manufacturer of the air guns. Same pressure (138 bar), volume (150 in^3) and depth (6 m) was used in all three figures.

The reason why our signals looked so complex compared to signals provided the manufacturer, might be that the manufacturer recorded the pressure signatures at large depths right below the air gun, while in this study, due to limited water depth, the hydrophones were located at an angle relative to the air gun (Sercel, 2016). This is important to consider when studying the differences seen between the pressure signatures at different receivers for a single air gun shot at node 17 (Figure 52). The angle between source and receiver varied between the receivers, and may have affected the pressure signature.

When the distance between a source and a receiver increases, it is likely that the seismic waves will be reflected at the water bottom several times, creating several multiples. This will spread

the energy out over a larger time in the records than if the hydrophones are located straight below the air gun. This can explain why we saw lower pressures spread out over a larger time, than what we would expect from Figure 64. In Figure 52, it was seen that the p-p pressure was higher when the receiver was located closer to node 17, but also when the receiver was located deeper in the water. This depth dependence may be an effect of the receiver ghost.

8.3.2. Sound pressure level (SPL)

Air guns usually have an output of approximately 210 to 250 dB re 1 µPa, p-p, at 1 m distance from the source (Gausland, 2000). This is the so-called source level, which can be back-calculated as explained in subsection 6.2.1. In this study, the highest SPLs were 196.1 dB re 1 µPa, p-p, at approximately 1 m distance for the dynamite shots (Figure 53), and 198.4 dB re 1 µPa, p-p, at approximately 1 m distance for the air gun shots (Figure 54 and 55). Since these SPLs were computed from peak-to-peak pressures at hydrophones very close to the sources, these values may have been clipped and should not be trusted. Using linear regression, the maximum back-calculated source level was 204.3 dB re 1 µPa, p-p, for the node 17 air gun shots, when excluding the hydrophones within 25 m distance from the source. This shows that the source levels in this survey probably were a bit lower than in a typical seismic survey. The results also showed that the SPLs were generally higher when using an air gun source than when using a detonating cord source.

In Figure 53, 54 and 55, lower SPLs were recorded further away from a seismic source rather than lower SPLs at some receivers. If these values were the true SPLs at that location, this means that some kind of mechanism or propagation pattern led to higher decibel levels occurring after lower ones. This possibility will be discussed further in subsection 8.3.5. However, it may also be that the SPLs were not actually higher at those receivers, but that there was a problem with the computation of the decibel levels. The SPLs were computed from the pressures, that in turn were computed from the amplitudes. The counts were converted to mBar using the sensitivity that was supplied by the manufacturer of the hydrophones, and was assumed to be the same for all hydrophones. If there were individual differences in the sensitivities between the hydrophones, this might have contributed to incorrect SPLs.

8.3.3. Sound exposure level (SEL)

The SELs were computed using Equation 30. The formula requires the instantaneous pressure and duration of this at all times, and thus the peak-to-peak pressure is complicated to use when

computing SEL. Therefore, the rms pressure was computed instead. The duration was set to the length of the time window, i.e. 500 ms.

A few uncertainties are related to the computed SELs. First of all, the SELs were computed separately for the detonating cord shots and all the air gun shots, while actually there was no 12 hour break between the shots with the two source types. There was, however, a 20 hour break between the air gun shots at the two locations. Since the main point of this study was not to determine where this specific survey would affect pinnipeds, but rather to study more generally how a seismic survey in an area like this can affect pinnipeds, this was not accounted for. The pressure values at receivers from shots within 10 m distance of the receiver were also taken out from the computations, thus not all shots were used to compute the SELs.

The SELs were computed to be less than 176.3 dB re 1 μPa^2s, rms, for the detonating cord shots (Figure 56), and less than 196.8 dB re 1 μPa^2s, rms, for the air gun shots (Figure 57). It is important to note that since the SPLs were computed from peak-to-peak pressure, and the SELs were computed from rms pressure, the numbers are not directly comparable. It can, however, be seen that the SELs were quite a bit lower than the SPLs, and that there was quite some variation between the SELs at the different receivers. The variation between the receivers was much larger for the air gun shots than for the detonating cord shots. This can be explained by the fact that when using detonating cords, the shots were fired at varying locations along the whole spread, while when using air guns, the shots were only fired at two locations. Therefore, the distance between source and receiver was varying more during the detonating cord shots, meaning that the SEL at each receiver was computed from pressures varying more than when using the air gun shots.

8.3.4. Frequency spectra

As mentioned in the background theory of this thesis, previous studies on hearing in marine mammals have revealed that they cannot hear very low frequencies well. Pinnipeds have been reported to hear frequencies down to 50 Hz, but with a much higher sensitivity for higher frequencies (Southall et al., 2007, Kastelein et al., 2009, National Marine Fisheries Service, 2016). In the 2016 Svea survey, the hydrophones recorded frequencies from 0 to 500 Hz, and most of the energy was found at frequencies below 450 Hz, with the main part found at frequencies lower than 200 Hz (e.g. Figure 29, 36 and 47). This is what is common to observe in seismic surveys. Based on this, pinnipeds should not be able to hear many of the frequencies present in a typical seismic survey.

Both the flexural ice wave and the Scholte wave are dispersive. Therefore, they consist of several frequency components, but have most of their energy centred around some main frequencies. The air gun shots generally had higher spectral amplitudes than the detonating cord shots in the frequency spectra, both for low and high frequencies (Figure 36). However, the detonating cords gave high amplitudes at frequencies around 30 Hz at the shallow receivers, which is a frequency that cannot be heard by pinnipeds (Figure 29). The exact characteristics of the flexural ice wave were difficult to determine in this survey, but in a previous study, it was reported to contain frequencies between 6 and 87 Hz (Rovetta et al., 2009a). Therefore, the peak at 30 Hz probably comes from air waves/flexural ice waves. The Scholte wave appeared to have very low main frequency components centred around 4-5 Hz (Figure 23 and 33), and can thus probably not be heard by pinnipeds at all.

When it comes to different receiver depths, Figure 29 showed that the peak at approximately 30 Hz was present in the frequency spectrum for detonating cord shots at a receiver at 1 m depth, but not in the frequency spectrum from the deeper receiver. Except from that peak, the frequency spectra from both source types consisted of more high frequencies when the receiver was shallow, and more low frequencies when the receiver was deep. Thus, based on the frequency spectra, it seems like it is better to have the receivers deeper in the water to enhance the low frequencies, supporting the conclusion in the section about receiver depths above.

As discussed in subsection 8.2.2., two competing factors determine how the signal from an air gun is affected by changing the source depth. These two factors are the bubble oscillations, and the ghost (Hegna and Parkes, 2011, Landrø and Amundsen, 2014). During a seismic survey, it is desirable to have a broad spectrum of frequencies, but low frequencies are especially important to be able to penetrate deep into the subsurface, while high frequencies can be more important for shallow seismic surveys (Ten Kroode et al., 2013). Figure 36 show that two air gun shots fired at different depths gave similarly shaped frequency spectra, but the deep air gun gave higher amplitudes at the low frequencies, and lower amplitudes at the high frequencies. The shallow air gun gave less of the low frequencies and more of the high frequencies, while the detonating cord gave a lot less of all frequencies, especially the low frequencies.

Some depressions in the frequency spectra were seen, and the location of these change with changing source depth (e.g. Figure 37). These frequencies, that have a clearly lower normalized amplitude than other frequencies, are identified as notches. It is the frequencies between the first and the second notch that are useful in low frequency seismic studies (Landrø and Amundsen, 2010).

The location of the notches can be explained by two formulas. The first one directly relates the notches in the frequency spectrum to the bubble period T:

$$f_{bn} = \frac{n+\frac{1}{2}}{T}, \qquad n=0, 1, 2, \ldots \tag{33}$$

(Haavik and Landrø, 2015). As we saw earlier, the bubble period T will decrease with increasing source depth (Landrø and Amundsen, 2014). Thus, the bubble notch frequency, f_{bn}, should increase with increasing source depth. The second formula shows that notches can also be caused by the interference of the primary downgoing wavefield and the wavefield from the source ghost:

$$f_{gn} = \frac{c}{2z} n, \qquad n=0, 1, 2, \ldots \tag{34}$$

(Haavik and Landrø, 2015). Based on this formula, the frequency where the ghost notch occurs, f_{gn}, should increase with decreasing source depth z. Thus, increasing the source depth should give bubble notches at higher frequencies, but ghost notches at lower frequencies (Figure 65).

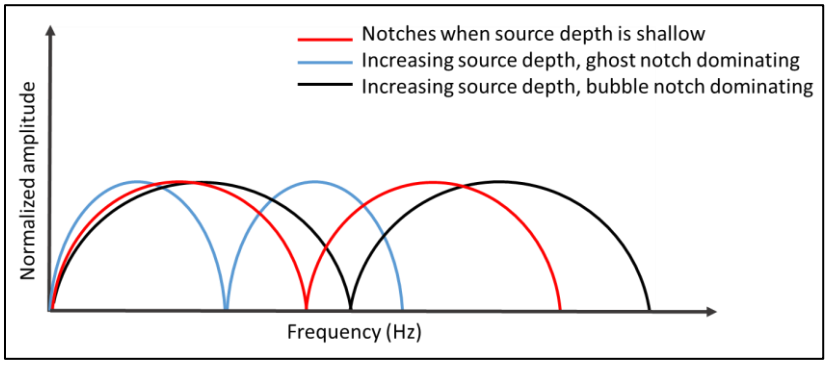

Figure 65: Interference due to a surface ghost give a low frequency first notch (blue spectrum), while bubble oscillations give a high frequency ghost notch (black spectrum). Therefore, increasing the source depth may move the notches of the original frequency spectrum (red spectrum) to a lower frequency, or to a higher frequency, depending on which factor is dominating.

Which of these two effects dominate, can vary. Haavik and Landrø (2015) claimed that when using an array, the bubble notches are often small compared to the ghost notches. Landrø and Amundsen (2014), on the other hand, claimed that "nasty notches" would occur in the low-frequency end of the spectrum when using a single air gun, due to bubble oscillations. In our case, we only used a single air gun, and we see that the first notch (around 100 Hz) occurs at higher frequencies when shots are from deeper sources (Figure 36). This indicates that the notch was mainly caused by the bubble oscillations, since this is consistent with the first formula. However, in Figure 36 it was also seen that there was a higher amount of low frequencies when the source was deeper, which according to the discussion in 8.2.2. should mean that the ghost effect was dominating. Landrø and Amundsen (2010) claim that due to ghost notches, a deeper

source should give a lower first ghost notch, and higher low frequencies than a shallower source, but only the latter is seen here. The reason for this behaviour might be that the receiver in Figure 37 was not located straight below the source, but at an angle away from the source. The receiver was also located very close to all three sources, and the shallow water depth might have affected the frequency spectra.

When Hermannsen et al. (2015) were studying the propagation of waves from an air gun survey for frequencies up to 125 kHz, they found that the shallow water had a significant effect on the spectral composition of an air gun pulse. They reported that the shallow water environment seemed to work as a high pass filter, where low frequencies were not propagating well, but very high frequencies could travel far. This behaviour in shallow waters was discussed by Farcas et al. (2016) as well.

Hermannsen et al. (2015) found very high frequencies in their air gun survey, even though they used an air gun centred around 50 Hz. They blame this behaviour on the poor propagation of low frequencies in shallow water transmission channels, due to interference with the water surface and the water bottom. What Hermannsen et al. (2015) and Farcas et al. (2016) claimed, can be explained in detail by using a paper by Jensen and Kuperman (1983), who later also wrote a book about this subject (Jensen et al., 2011). For compressional waves, the dominant sound attenuation tendency in the water column is an increasing loss of sound level with decreasing frequency, because the dominant effect is greater penetration into the bottom with decreasing frequency (Jensen and Kuperman, 1983). I.e., since low frequencies can penetrate more easily into the water bottom than high frequencies, there will be a loss of low frequencies for waves propagating in the water column. This is opposite to how it commonly is, with high frequencies being attenuated first.

8.3.5. Wave propagation underwater

The results showed that SPL generally decreased with increasing distance away from the source, but with several deviations (Figure 53, 54 and 55). The deviations may be explained by different sensitivities in the hydrophones, but may, however, also be explained by other factors. The medium may for example have been heterogenous, leading to more attenuation in some directions than in others.

It is interesting to study how the SPLs change with distance between the receivers, to see if a clear propagation pattern can be observed. The formula P(r)=P(s)-Alog(r)-Br-C was presented as Equation 13 in chapter 2. The formula was used by Gausland (2000), and a similar formula

is used in several other papers to explain wave propagation in water (Richardson et al., 1995, Hermannsen et al., 2015, Farcas et al., 2016). This discussion will use this formula as a basis for studying wave propagation.

The results in this thesis were obtained over a distance of less than 500 m, thus when using the formula P(r)=P(s)-Alog(r)-Br-C, B can as an approximation be assumed to be insignificant. Gausland (2000) assumes this value to be approximately 2-5 dB per kilometre in water, while Hermannsen et al. (2015) claim that for frequencies below 10 kHz, B will be even lower. Assuming C equal to zero may not be valid since the water was covered with ice, and the topography of the water bottom was quite varying (Richardson et al., 1995). However, if it is assumed to be open, the formula simplifies to P(r)=P(s)-Alog(r), which is of the same form as the formula 11 and 12 that were derived in subsection 2.5.1. C higher than zero would make P(r) lower, due to higher attenuation.

In subsection 2.5.1. it was shown that for spherical spreading, the A in this formula would be 20, and for cylindrical spreading, the A would be 10 (University of Rhode Island and Marine Acoustics inc., 2013). Gausland (2000) claims that during a seismic survey, the frequencies used are so low that they will penetrate the water bottom, thus leading to spherical spreading and making A=20 appropriate. It has, however, appeared from several studies that determining A in shallow water is not that easy (e.g. (Richardson et al., 1995, Hermannsen et al., 2015, Farcas et al., 2016)). To my knowledge, there are no studies that look at wave propagation in a shallow water environment with sea ice cover, in detail.

The best fitted A-values from this survey were found using linear regression, to see if any similar A-values could be found. It appears that the wave propagation during the 2016 Svea survey did not follow spherical nor cylindrical spreading. The decrease in sound level per unit length was not constant, which could be seen from the very low R^2. This indicates that it is not possible to determine a consistent constant A to use in the propagation loss formula (Figure 58).

Wave propagation not following spherical or cylindrical spreading in shallow water environments is reported by e.g. Richardson et al. (1995), Association of Oil and Gas Producers (2008), and Hermannsen et al. (2015). Richardson et al. (1995) discuss how different conditions can lead to many other types of spreading than spherical or cylindrical spreading, which would mean other values for A. In their book, they generally recommend using A=20 for deep water, and A=15 for shallow water, but emphasize that special conditions can change these values. Richardson et al. (1995) claim that interference effects due to surface reflections can increase

the spreading loss if both source and receiver are placed at less than 1/4λ depth, but they also claim that shallow water can decrease the propagation loss if waves are refracted upwards. In the present study, the results showed the latter tendency, and the computed A-values are generally lower than what would be the case if A=15.

Hermannsen et al. (2015) found a value of A=18 appropriate in the shallow waters where they performed their survey. They blamed this on the effect that was explained in the paper by Jensen and Kuperman (1983). Since low frequencies are relatively rapidly attenuated in water, it may be that at relatively large distances away from a seismic source, the compressional waves that have been reflected or refracted from a shallow boundary in the subsurface, are stronger than the waves that have been travelling directly through the water (Association of Oil and Gas Producers, 2008). Since the seismic velocities in sediments are often much higher than in water, these waves may also reach the receiver before a wave travelling directly towards the receiver, thus being confused with primary reflections (Gausland, 2000, Kearey et al., 2002). However, this would be a more likely explanation at relatively large offsets than at the low offsets used during this survey. This can explain why geometrical spreading models that describe wave propagation and sound levels at a distance away from a source often tend to fail in shallow water (Association of Oil and Gas Producers, 2008). Richardson et al. (1995) suggest that solving the parabolic wave equation is the best way to describe wave propagation in very shallow water environments. This is, however, very time consuming, which is why the approach suggested by e.g. Gausland (2000) is the focus of this thesis.

In this study, A-values were only computed using the node 17 air gun shots (Figure 58). When studying the detonating cord shots, a clear directionality was obvious. This was probably due to the previously discussed directionality, that focuses most of the energy in one direction (Johansen et al., 2011). This means that lower A-values would probably be computed in front of the source than after the source. Also, we registered that there was no direct wave recorded for the detonating cord shots, which means that the pressure values that would be used for computing A, would be from reflected or refracted waves.

From Figure 58, we saw that A did not vary a lot between the different shots, but did vary a lot between the different receivers. This suggests that the differences in A were not due to random noise. The small differences that were found between different shots may have been due to either the different air gun pressures used, the different depths the shots were fired at (3 m or 5 m node 17, and 1.5 m or 3 m at node 1 – 50 m), or due to the shots altering the ground conditions

before the next shot (e.g. creating cracks in the ice). What is more interesting to study is the large differences in A that were seen between different receivers.

The large variations in A between different receivers may have been caused by properties of the environment the seismic waves were travelling in. It was seen that many of the differences corresponded to different receiver depths, which suggests that a depth dependent A might be necessary to explain wave propagation (Figure 58). The computed A-values gave a better match with the actual SPLs at the deeper receivers than at the shallow receivers, suggesting that different A-values should be computed for propagation at different depths.

In Svea in 2016, the survey area had both shallow water depth, and sea ice cover. The differences in A may therefore have been caused by variations in ice, sediment, and water properties (Richardson et al., 1995, Farcas et al., 2016). For a wave travelling in shallow water, the main mechanism for sound propagation will be repeated reflection and scattering at the water bottom and water surface (Farcas et al., 2016). If the water surface is covered with sea ice, there will be a different contrast in acoustic impedance at the water surface than if there is air above the water surface. Since the reflection coefficient at a boundary depends on the acoustic impedances of the layers above and below the surface, this may affect the reflection. An ice sheet floating on water also tends to have an uneven bottom, thus diffractions may occur when the waves hit the ice from below (Richardson et al., 1995, Khaidukov et al., 2014, Farcas et al., 2016). The sea ice was also described as “slushy” during the 2016 Svea survey, which may have affected the ice properties.

The acoustic properties of the shallow sediment layers can also influence wave propagation, since these will have an impact on how the waves are reflected from the water bottom. A larger difference in acoustic properties between water and sediments will give a higher reflection coefficient at the water bottom, and opposite (Farcas et al., 2016). Previous studies have shown that the shallow subsurface in the study area mainly consists of glacial deposits and sediments (Cöster, 1925, Larsen and Lysså, 2015). Additionally, the topography of the water bottom can have a large impact on the spreading of the wave, since this partly determines the angle a wave will be reflected with (Richardson et al., 1995, Farcas et al., 2016). In the present study, there was quite a lot of variation in topography in the area (Figure 18).

Last, water properties can impact sound propagation in shallow water environments. Water temperature and salinity can affect the speed of sound in water, and variations in sound speed

can give refractions of a wave. Over short distances such as in this study, the variations in sound speed are assumed to be small (Richardson et al., 1995, Davis et al., 1998, Farcas et al., 2016).

8.3.6. Pinniped hearing

Everything that has been discussed up until now are factors that are important to consider when discussing the impacts of seismic surveys on pinnipeds. The 2016 Svea survey was a relatively small survey compared to what is common during a commercial survey, with relatively few shots fired over a short distance. This means that the results from this survey cannot necessary be transferred to a commercial survey. The results can, however, still give a good indication of whether a seismic survey in a shallow marine sea ice covered area can be harmful to pinnipeds.

When the results are discussed here, it is based on the computed decibel levels, frequency spectra, and shallow water wave propagation loss constants. The shots were also assumed to be repeated several times. This is what is common in a seismic survey, therefore this is the most relevant to focus on for the scope of this thesis. Both SPL and SEL were computed, to be able to study the difference between only shooting one seismic shot, with shooting several times in a row. A few uncertainties are related to using the computed numbers to determine whether any hearing damage can be expected from this seismic survey.

First of all, 180 dB re 1 µPa, rms, was presented as the lowest value often used to determine the extent of seismic shut down zones. This criterion is given from the rms pressure, which was used to compute the SEL, but not to compute the SPL. Corrections are needed to convert from rms pressure to p-p pressure, and 180 dB re 1 µPa, rms, would correspond to approximately 190 dB re 1 µPa, p-p (Gausland, 2000). Therefore, using the limit of 180 dB re 1µPa on the SPL data may be conservative, and 190 dB re 1µPa may be more accurate. The SELs were computed from rms pressure, thus a lower limit may be appropriate for the SELs.

Second, no M-weighting based on audiograms was performed on the SPLs and SELs. Most audiograms have a peak close to the centre of the frequency range that the animal can hear. Compared with Figure 16 from National Marine Fisheries Service (2016), most of the energy in the waves in the present study was probably found at frequencies that pinnipeds either cannot hear, or that they have a 20 to 45 dB lower hearing sensitivity for than the best heard frequencies. Thus, we can assume that the sound levels from air guns centred at low frequencies may need to have SPLs quite a lot higher than 190 dB re 1 µPa, p-p, to be harmful to pinnipeds.

The SPLs that were recorded at different receivers in this survey showed values that decayed quickly away from a receiver. Only at a distance lower than 50 m from the seismic source were decibel values above 190 dB re 1 µPa, p-p, recorded (Figure 53, 54 and 55). When computing the SELs, the values were lower, and no receivers experienced a SEL higher than 180 dB re 1 µPa, rms, from the detonating cords shots. From the air gun shots, most receivers located between node 1 – 50 m and node 17 experienced a SEL higher than 180 dB re 1 µPa, rms, but mostly just a few decibels above the limit (Figure 56 and 57). Based on this, we could conclude that a single exposure to an air gun or detonating cord shot would probably not be able to cause hearing damage in a pinniped located at any of the receiver positions. The same is believed to be the case for exposure to 43 detonating cord shots from varying locations. Exposure to 61 air gun shots might, however, be harmful to a pinniped, but it is not likely unless the pinniped stays very close to the source for a long time.

It can be discussed whether a pinniped would stay in an area where it is exposed to high sound levels for a long enough time to be exposed to that many seismic shots. Studies have indicated that pinnipeds tend to move away from an area when they are exposed to high sound levels, at least unless the area is very attractive for some reason (Harris et al., 2001, Gordon et al., 2003, Miller et al., 2005, Southall et al., 2007, Kvadsheim et al., 2017). This in itself can be a problem, since behaviour change can affect the animal's access to food, or ability to protect itself from dangers (Gordon et al., 2003). It is, however, not clear that seismic shots with a single air gun or detonating cords of 5 m length will be able to cause either behaviour change, TTS or PTS in pinnipeds (Harris et al., 2001). This is similar to the conclusion by Hermannsen et al. (2015). They calculated SELs of 192 dB re 1 μPa^2s, and concluded that the use of single air guns in a shallow water environment will probably not cause hearing damage in pinnipeds, but the presence of high frequencies makes behaviour changes likely.

When comparing the effect of changing source and receiver depth, we saw that the amplitudes of reflected waves seemed to be higher when the sources and receivers were deeper in the water. However, we also saw that when the sources where deeper in the water, there was a higher concentration of frequencies below approximately 75 Hz, and a lower concentration of frequencies above 75 Hz (Figure 36). This indicates that when the source is deeper in the water, a higher amount of the energy is contained at frequencies pinnipeds cannot hear. This is also supported by the computed A-values, that showed a higher mismatch with the experimental values at the shallower receivers.

It should be clear from the previous discussion that there are several uncertainties involved with determining how large seismic shut down zones should be. According to Hermannsen et al. (2015), the seismic shut down zones used today are commonly around 500 meters, but Harris et al. (2001) used a smaller zone of 150-250 meters, claiming that this would be the radii of 190 dB re 1 µPa, rms. Different propagation patterns can drastically change the size of the affected zones, since small changes in radii can lead to large changes in affected area. An example given by Gordon et al. (2003) is that for some likely propagation patterns, the size of the zone where SPL>140 dB re 1 µPa is found, can vary by 4000 times and 16 million individuals affected.

Based on this, it should be clear that there is a risk involved with using simple geometrical spreading relations to determine exposure zones. Tolstoy et al. (2004) found clear differences in recorded decibel levels at receivers in deep and shallow water (~30 m depth). In shallow water areas with highly acoustically reflective sediments in the subsurface, higher decibel levels than what sound propagation models could indicate were recorded, and Tolstoy et al. (2004) blamed this on bottom reverberations. Farcas et al. (2016) compared the sound levels predicted by a simple geometrical spreading model with A=15, with sound levels computed using the parabolic wave equation (which was the approach suggested by e.g. Richardson et al. (1995)). They found that the simple spreading model underestimated the sound levels close to the source, and substantially overestimated the sound levels further away from the source.

As was mentioned in subsection 8.3.1., the pressure signatures seem to be more complex when a receiver is not located straight below a source. This would probably be the case if the receiver was a marine mammal as well (Gordon et al., 2003). Madsen et al. (2006) connected multisensory acoustic recording tags to cetaceans during an air gun array survey in deep waters in the Gulf of Mexico, and found that sound levels were recorded higher when the whales were deeper in the water. They also found that the frequency content was varying when the receivers were at different depths in the water. This is consistent with what was seen when comparing different receiver depths in this study, and was by Madsen et al. (2006) blamed on complex wave propagation patterns. They claimed that the primary pulse was detected several times at each receiver due to reflections at the sea bottom, and thus their conclusion was also that exposure zones (i.e. seismic shut down zones) should not be based on simple geometrical spreading models.

Yet another argument for using conservative seismic shut down zones can be that the use of seismic shot down zones requires that someone observes the survey area constantly, looking for pinnipeds within the specified zone. This method is good in theory, but can have flaws in

practice, since it can be difficult to spot the pinnipeds when only looking for them visually. Pinnipeds spend quite a lot of time under water, and harsh weather conditions with rough water can make it difficult to spot them. In the Arctic, sea ice can cover the pinnipeds, and there are also periods when it is very dark (Harris et al., 2001). Therefore, it might be difficult to stop the seismic operations before the pinnipeds are too close to the source. If the seismic shut down zones are large, this gives more time for observers to look for the pinnipeds before they are actually too close to the source.

Other ways of monitoring pinnipeds are by passive acoustic measurements or telemetry, but both of these methods have limitations as well. Passive acoustic measurements require that the pinnipeds are vocal and that the amount of background noise is low, and telemetry requires that the pinnipeds are marked. Telemetry is a good way to get more knowledge about the behaviour of pinnipeds close to a seismic, but cannot be used to monitor all pinnipeds in the vicinity of a seismic survey (Gordon et al., 2003). Aerial photographs can be used to determine the abundance of seals in a survey area, but cannot be used to monitor pinnipeds constantly during a seismic survey (Krafft et al., 2006).

8.4. Usefulness of the work

This thesis has shown that the acquisition geometry can have a large impact on the quality of seismic data acquired in a shallow water sea ice covered environment. The thesis has for example shown that using an air gun seems to give higher quality seismic data, and the same is the case when placing the sources and receivers deeper in the water. This could be useful knowledge to have during the planning phase of future studies, where the goal is to map the subsurface in detail, for example for oil and gas exploration.

Not much is previously known about wave propagation in a shallow water environment with sea ice cover, and this thesis has shown that the propagation pattern in such an environment seems to differ from shallow water environments without sea ice cover. The thesis has therefore shown that this is a topic that needs further attention, and that more detailed studies are needed to understand the wave propagation in such an environment.

Due to the many factors that make it complicated to understand the wavefield in a shallow water sea ice covered environment, this work cannot give any direct recommendations for if and where a pinniped may be harmed by a seismic survey, but the results support previous reports that have suggested that the seismic shut down zones used today may be conservative.

9. Conclusions

9.1. Main conclusions

- To enhance the signal-to-noise ratio, and thus the quality of the seismic data, it seems to be better to use an air gun rather than a detonating cord when conducting seismic surveys in a shallow water sea ice covered environment. Also, when comparing with the criteria given by Kearey et al. (2002) that were listed on page 17 of this thesis, an air gun fulfils these criteria to a higher degree than detonating cords.
- To enhance the signal-to-noise ratio, it also seems better to locate both the seismic source and the seismic receiver deeper in the water column. This is because the strength of the reflections and refractions increases with depth, and the strength of the air wave and the flexural ice wave decreases with depth. The strength of the bubble pulse and the Scholte wave increases with depth, but these are assumed to be less important for the quality of the seismic data than the reflections, refractions, air waves and flexural ice waves.
- Locating the air gun and hydrophones deep in the water also seems to increase the amount of low frequencies that are often useful for deep-penetrating seismic surveys.
- Based on SPLs and SELs, this seismic survey should most likely not be able to harm pinnipeds unless they stay very close to a seismic source for a long time. SPLs above 190 dB re 1 µPa, p-p, were only found within 50 m from a source, and SELs were mostly just a few decibels above 180 dB re 1 μPas^2, rms. No M-weighting was applied to the data, and since most of the energy was found at low frequencies (<200 Hz), SPLs and SELs could probably have been up to 20-45 dB higher than the limits above, without harming pinnipeds.
- Determining how, if, and where a seismic survey will affect a pinniped is difficult. There seems to be a complex wave propagation pattern in the area that cannot be described using simple geometric spreading laws.

9.2. Future work

- The results presented in this study showed that using an air gun as a source gave better results than using a detonating cord. It was also mentioned that using air guns may be more time consuming than using detonating cords in a sea ice covered environment. It was claimed that if we should change acquisition geometry to enhance the quality of the seismic, a goal should be to find an acquisition geometry that reduces the processing

time more than the time spent acquiring the data increases. No evaluation of time spent versus time saved was done in the current thesis, but should be done in the future.

- The apparent impact of water depth when studying the acquisition geometry was only briefly mentioned in this thesis (e.g. in Figure 58), but should be further studied.
- The data should be properly processed to be able to interpret the subsurface based on the seismic data. This could help us identify the events in the records with a higher certainty, as well as get a better idea of the properties of the subsurface. This could make it easier to determine the causes for the wave propagation observed, as well as determining the dispersion characteristics of the Scholte- and flexural ice waves.
- A denser network of hydrophones should be set up to study wave propagation in more detail. Hydrophones should also be placed denser to study the effect of depth in even more detail, and to avoid spatial aliasing. The survey should also be 3D to be able to study the wave propagation in several directions. When the hydrophone data was acquired in Svea in 2016, geophone and OBS data were acquired simultaneously with the hydrophone data. Further discussion about the effect of survey geometry on seismic data quality should include these data as well. Similarities and differences between these data can for example reveal surface waves that only appear in some of the data.
- Receivers that can pick up high frequencies should also be used more often. Several authors have claimed that shallow water can work as a high-pass filter, and this would be interesting to study in a shallow water sea ice covered environment. In Figure 36, the first notch did not appear where we from theory would expect it to when varying the source depth. How shallow water will affect the frequency content of a signal is a complex subject that should be further studied. One broadband hydrophone was used in the 2016 Svea survey, but those results were not included in this thesis. Further work on the data presented in this thesis should include that data as well.
- More work on the impact of sound from seismic surveys on pinnipeds should be done, preferably by collaboration between geophysicists and biologists. M-weighting should be applied to the data, for example using the approach described in the Technical Guidance by National Marine Fisheries Service (2016).
- Further studies about the propagation of waves in a shallow water sea ice covered environment must be done. The propagation pattern in such an environment seems to be quite complex, and to be able to assess the impact of seismic surveys on pinnipeds in such areas, the propagation pattern needs to be better understood.

References

AANES, R., AARS, J., ANDERSEN, M., FUGLEI, E., GABRIELSEN, G. W., LYDERSEN, C., KOVACS, K., STEEN, H. & STRØM, H. (eds.) 2011. *Ferdsel og dyreliv på Svalbard - en veileder i møte med Svalbards natur,* Norwegian polar institute.

ASSOCIATION OF OIL AND GAS PRODUCERS 2008. Fundamentals of Underwater Sound. International Association Of Oil & Gas Producers.

ASSOCIATION OF OIL AND GAS PRODUCERS 2011. An overview of marine seismic operations. International Association Of Oil & Gas Producers.

BETTERLY, S., SPEECE, M., LEVY, R., HARWOOD, D. & HENRYS, S. 2007. A novel over-sea-ice seismic reflection survey in McMurdo Sound, Antarctica. *Terra Antartica,* 14**,** 97.

BLACKWELL, S. B., LAWSON, J. W. & WILLIAMS, M. T. 2004. Tolerance by ringed seals (Phoca hispida) to impact pipe-driving and construction sounds at an oil production island. *The Journal of the Acoustical Society of America,* 115**,** 2346-2357.

BOHLEN, T., KUGLER, S., KLEIN, G. & THEILEN, F. 2004. 1.5 D inversion of lateral variation of Scholte-wave dispersion. *Geophysics,* 69**,** 330-344.

BOIERO, D., WIARDA, E. & VERMEER, P. 2013. Surface-and guided-wave inversion for near-surface modeling in land and shallow marine seismic data. *The Leading Edge,* 32**,** 638-646.

BOIERO, D., WIARDA, E., WEST, L. & VERMEER, P. Near-surface modelling in shallow marine environments using surface and guided waves. 76th EAGE Conference and Exhibition 2014, 2014. European Association of Geoscientists and Engineers.

BOUSKA, J. 2008. Advantages of wide-patch, wide-azimuth ocean-bottom seismic reservoir surveillance. *The Leading Edge,* 27**,** 1662-1681.

BUREK, K. A., GULLAND, F. & O'HARA, T. M. 2008. Effects of climate change on Arctic marine mammal health. *Ecological Applications,* 18**,** 126-134.

CHAPMAN, C. 2004. *Fundamentals of seismic wave propagation*, Cambridge university press.

CORMIER, V. F. 1982. The effect of attenuation on seismic body waves. *Bulletin of the Seismological Society of America,* 72**,** S169-S200.

CRUM, L. A. & MAO, Y. 1996. Acoustically enhanced bubble growth at low frequencies and its implications for human diver and marine mammal safety. *The Journal of the Acoustical Society of America,* 99**,** 2898-2907.

CÖSTER, F. 1925. Results of the Swedish Expedition to Spitzbergen in 1924. Quarternary Geology of the Region around the Kjellström Valley. *Geografiska Annaler,* 7**,** 104-121.

DAVIS, R. A., THOMSON, D. H. & MALME, C. 1998. Environmental assessment of seismic exploration on the Scotian Shelf. LGL Limited.

DEL MOLINO, G., ROVETTA, D., MAZZUCCHELLI, P., RIZZO, F., ANDREOLETTI, C. & SANDRONI, S. Seismic exploration on ice: the flexural wave noise challenge. 2008 SEG Annual Meeting, 2008. Society of Exploration Geophysicists.

DOSSO, S. & BROOKE, G. 1995. Measurement of seismo-acoustic ocean-bottom properties in the high Arctic. *The Journal of the Acoustical Society of America,* 98**,** 1657-1666.

DRAGOSET, B. 2000. Introduction to air guns and air-gun arrays. *The Leading Edge,* 19**,** 892-897.

DTCC n.d. DT-44-14A Pressure Sensitive Detector for Geophysical Exploration.

DUNLOP, R. A., NOAD, M. J., MCCAULEY, R. D., KNIEST, E., SLADE, R., PATON, D. & CATO, D. H. 2016. Response of humpback whales (Megaptera novaeangliae) to ramp-up of a small experimental air gun array. *Marine pollution bulletin,* 103**,** 72-83.

EISEN, O., HOFSTEDE, C., DIEZ, A., KRISTOFFERSEN, Y., LAMBRECHT, A., MAYER, C., BLENKNER, R. & HILMARSSON, S. 2015. On-ice vibroseis and snowstreamer systems for geoscientific research. *Polar Science,* 9**,** 51-65.

ENGER, P. S., ØRITSLAND, N. A. & LYDERSEN, C. 1987. Lydtrykksmålinger i forbindelse med seismiske undersøkelser på Svalbard våren 1986. *In:* PRESTRUD, P. & ØRITSLAND, N. A. (eds.)

Miljøundersøkelser i tilknytning til seismisk virksomhet på Svalbard 1986: et ledd i konsekvensutredning av petroleumsvirksomhet på Svalbard. Norsk Polarinstitutt.

ENGÅS, A., LØKKEBORG, S., ONA, E. & SOLDAL, A. V. 1996. Effects of seismic shooting on local abundance and catch rates of cod ((Gadus morhua) and haddock)(Melanogrammus aeglefinus). *Canadian Journal of Fisheries and Aquatic Sciences,* 53**,** 2238-2249.

FARCAS, A., THOMPSON, P. M. & MERCHANT, N. D. 2016. Underwater noise modelling for environmental impact assessment. *Environmental Impact Assessment Review,* 57**,** 114-122.

FINNERAN, J. J., DEAR, R., CARDER, D. A. & RIDGWAY, S. H. 2003. Auditory and behavioral responses of California sea lions (Zalophus californianus) to single underwater impulses from an arc-gap transducer. *The Journal of the Acoustical Society of America,* 114**,** 1667-1677.

GAUSLAND, I. 2000. Impact of seismic surveys on marine life. *The Leading Edge,* 19**,** 903-905.

GAUTIER, D. L., BIRD, K. J., CHARPENTIER, R. R., GRANTZ, A., HOUSEKNECHT, D. W., KLETT, T. R., MOORE, T. E., PITMAN, J. K., SCHENK, C. J. & SCHUENEMEYER, J. H. 2009. Assessment of undiscovered oil and gas in the Arctic. *Science,* 324**,** 1175-1179.

GELIUS, L.-J. 2012a. Elastic waves. *Petroleum geophysics.* Bergen: UniGEO as.

GELIUS, L.-J. 2012b. Seismic Signal Theory and Processing. *Petroleum geophysics.* Bergen: UniGEO as.

GJØYSTDAL, H., IVERSEN, E., LECOMTE, I., KASCHWICH, T., DROTTNING, Å. & MISPEL, J. 2007. Improved applicability of ray tracing in seismic acquisition, imaging, and interpretation. *Geophysics,* 72**,** 261-271.

GOOLD, J. C. & FISH, P. J. 1998. Broadband spectra of seismic survey air-gun emissions, with reference to dolphin auditory thresholds. *The Journal of the Acoustical Society of America,* 103**,** 2177-2184.

GORDON, J., GILLESPIE, D., POTTER, J., FRANTZIS, A., SIMMONDS, M. P., SWIFT, R. & THOMPSON, D. 2003. A review of the effects of seismic surveys on marine mammals. *Marine Technology Society Journal,* 37**,** 16-34.

HAAVIK, K. E. & LANDRØ, M. 2015. Variable source depth acquisition for improved marine broadband seismic data. *Geophysics,* 80**,** 69-73.

HAAVIK, K. E. & LANDRØ, M. 2016. Estimation of source signatures from air guns fired at various depths: A field test of the source scaling law. *Geophysics,* 81**,** 13-22.

HALL, K. W., NIETO, C. E., GALLANT, E. V. & STEWART, R. R. 2001. Multicomponent seismic survey over ground-fast and floating ice, MacKenzie Delta, NWT. *Consortium for Research in Elastic Wave Exploration Seismology (CREWES) Research Report,* 13**,** 29-45.

HARRIS, R. E., MILLER, G. W. & RICHARDSON, W. J. 2001. Seal responses to airgun sounds during summer seismic surveys in the Alaskan Beaufort Sea. *Marine Mammal Science,* 17**,** 795-812.

HARRISS, R. 2016. Arctic Offshore Oil: Great Risks in an Evolving Ocean. *Environment: Science and Policy for Sustainable Development,* 58**,** 18-29.

HARTMANN, D. L., KLEIN TANK, A. M. G., RUSTICUCCI, M., ALEXANDER, L. V., BRÖNNIMANN, S., CHARABI, Y., DENTENER, F. J., DLUGOKENCKY, E. J., EASTERLING, D. R., KAPLAN, A., SODEN, B. J., THORNE, P. W., WILD, M. & ZHA, P. M. 2013. Observations: Atmosphere and Surface. *In:* STOCKER, T. F., D. QIN, G.-K. PLATTNER, M. & TIGNOR, S. K. A., J. BOSCHUNG, A. NAUELS, Y. XIA, V. BEX AND P.M. MIDGLEY (eds.) *Climate Change 2013: The Physical Science Basis. Contribution of Working Group I to the Fifth Assessment Report of the Intergovernmental Panel on Climate Change.* Cambridge, United Kingdom and New York, NY, USA: Cambridge University Press.

HEGNA, S. & PARKES, G. 2011. The low frequency output of marine air-gun arrays. *SEG Technical Program Expanded Abstracts 2011.* Society of Exploration Geophysicists.

HENLEY, D. C. 2003. Coherent noise attenuation in the radial trace domain. *Geophysics,* 68**,** 1408-1416.

HENLEY, D. C. Attenuating the ice flexural wave on arctic seismic data. 69th EAGE Conference and Exhibition-Workshop Package, 2007.

HERMANNSEN, L., TOUGAARD, J., BEEDHOLM, K., NABE-NIELSEN, J. & MADSEN, P. T. 2015. Characteristics and propagation of airgun pulses in shallow water with implications for effects on small marine mammals. *PloS one,* 10**,** e0133436.

HOFFE, B. H., LINES, L. R. & CARY, P. W. 2000. Applications of OBC recording. *The Leading Edge,* 19**,** 382-391.

JAW, K.-S. & LEE, J.-S. 2008. Thermal behaviors of PETN base polymer bonded explosives. *Journal of thermal analysis and calorimetry,* 93**,** 953-957.

JENSEN, F. B. & KUPERMAN, W. A. 1983. Optimum frequency of propagation in shallow water environments. *The Journal of the Acoustical Society of America,* 73**,** 813-819.

JENSEN, F. B., KUPERMAN, W. A., PORTER, M. B. & SCHMIDT, H. 2011. *Computational ocean acoustics*, Springer Science & Business Media.

JENSEN, K. 2016. *Modelling and processing of flexural wave noise in sea ice.* Master thesis, The University of Bergen.

JOHANSEN, T. A., DIGRANES, P., VAN SCHAACK, M. & LØNNE, I. 2003. Seismic mapping and modeling of near-surface sediments in polar areas. *Geophysics,* 68**,** 566-573.

JOHANSEN, T. A., RUUD, B., BAKKE, N. E., RISTE, P., JOHANNESSEN, E. P. & HENNINGSEN, T. 2011. Seismic profiling on Arctic glaciers. *First Break,* 29**,** 65-71.

JOHNSTON, D. H., TOKSÖZ, M. & TIMUR, A. 1979. Attenuation of seismic waves in dry and saturated rocks: II. Mechanisms. *Geophysics,* 44**,** 691-711.

KASTAK, D. & SCHUSTERMAN, R. J. 1998. Low-frequency amphibious hearing in pinnipeds: Methods, measurements, noise, and ecology. *The Journal of the Acoustical Society of America,* 103**,** 2216-2228.

KASTELEIN, R., MOSTERD, P., VAN SANTEN, B., HAGEDOORN, M. & DE HAAN, D. 2002. Underwater audiogram of a Pacific walrus (Odobenus rosmarus divergens) measured with narrow-band frequency-modulated signals. *The Journal of the Acoustical Society of America,* 112**,** 2173-2182.

KASTELEIN, R. A., WENSVEEN, P. J., HOEK, L., VERBOOM, W. C. & TERHUNE, J. M. 2009. Underwater detection of tonal signals between 0.125 and 100kHz by harbor seals (Phoca vitulina). *The Journal of the Acoustical Society of America,* 125**,** 1222-1229.

KEAREY, P., BROOKS, M. & HILL, I. 2002. *An introduction to geophysical exploration*, John Wiley & Sons.

KHAIDUKOV, V. G., LISITSA, V. V., RESHETOVA, G. V. & TCHEVERDA, V. A. Numerical study of the seismic wave fields in the transition zone in winter. 2014 SEG Annual Meeting, 2014. Society of Exploration Geophysicists.

KOHNEN, H. 1974. The temperature dependence of seismic waves in ice. *J. Glaciol,* 13**,** 144-147.

KRAFFT, B. A., KOVACS, K. M., ANDERSEN, M., AARS, J., LYDERSEN, C., ERGON, T. & HAUG, T. 2006. Abundance of ringed seals (Pusa hispida) in the fjords of Spitsbergen, Svalbard, during the peak molting period. *Marine Mammal Science,* 22**,** 394-412.

KREBES, E. 2004. Seismic forward modeling. *CSEG Recorder,* 30**,** 28-39.

KUGLER, S., BOHLEN, T., BUSSAT, S. & KLEIN, G. 2005. Variability of Scholte-wave dispersion in shallow-water marine sediments. *Journal of Environmental & Engineering Geophysics,* 10**,** 203-218.

KVADSHEIM, P. H., SIVLE, L. D., HANSEN, R. R. & KARLSEN, H. E. 2017. Effekter av menneskeskapt støy på havmiljø: rapport til Miljødirektoratet om kunnskapsstatus. Oslo: Forsvarets forskningsinstitutt.

LAMB, H. 1904. On the propagation of tremors over the surface of an elastic solid. *Philosophical Transactions of the Royal Society of London. Series A, Containing Papers of a Mathematical or Physical Character,* 203**,** 1-42.

LANDRØ, M. & AMUNDSEN, L. 2010. Marine Seismic Sources Part I. *Geo ExPro,* 7**,** 32-34.

LANDRØ, M. & AMUNDSEN, L. 2014. Is it optimal to tow air guns shallow to enhance low frequencies? *Geophysics,* 79**,** 13-18.

LANDRØ, M., AMUNDSEN, L. & BARKER, D. 2011. High-frequency signals from air-gun arrays. *Geophysics,* 76**,** 19-27.

LARSEN, E. & LYSÅ, A. 2015. Da Paulabreen skapte Svalbards største innsjø. Available: http://forskning.no/geofag/2015/08/da-paulabreen-skapte-svalbards-storste-innsjo [Accessed 29.04.17].

LOVE, A. E. H. 1892. *A treatise on the mathematical theory of elasticity*, Cambridge University Press.

MADSEN, P. T., JOHNSON, M., MILLER, P., AGUILAR SOTO, N., LYNCH, J. & TYACK, P. 2006. Quantitative measures of air-gun pulses recorded on sperm whales (Physeter macrocephalus) using acoustic tags during controlled exposure experiments. *The Journal of the Acoustical Society of America,* 120**,** 2366-2379.

MALAKOFF, D. 2002. Suit ties whale deaths to research cruise. *Science,* 298**,** 722-723.

MARINE MAMMAL COMMISSION 1972. The marine mammal protection act of 1972.

MARSAN, D., WEISS, J., LAROSE, E. & MÉTAXIAN, J.-P. 2012. Sea-ice thickness measurement based on the dispersion of ice swell. *The Journal of the Acoustical Society of America,* 131**,** 80-91.

MILLER, G., MOULTON, V., DAVIS, R., HOLST, M., MILLMAN, P., MACGILLIVRAY, A. & HANNAY, D. 2005. Monitoring seismic effects on marine mammals—southeastern Beaufort Sea, 2001-2002. *Offshore oil and gas environmental effects monitoring/Approaches and technologies***,** 511-542.

NATIONAL MARINE FISHERIES SERVICE 2016. Technical Guidance for Assessing the Effects of Anthropogenic Sound on Marine Mammal Hearing: Underwater Acoustic Thresholds for Onset of Permanent and Temporary Threshold Shifts. U.S. Dept. of Commer., NOAA.

NATIONAL SNOW AND ICE DATA CENTER. n.d. *All About Arctic Climatology and Meteorology* [Online]. Available: https://nsidc.org/cryosphere/Arctic-meteorology [Accessed 30.09 2016].

OECD/IEA 2016. World Energy Outlook 2016 - Executive Summary. Paris.

PARKES, G. & HATTON, L. 1986. *The Marine Seismic Source*, Springer.

PASCOUET, A. 1991. Something new under the water: The bubbleless air gun. *The Leading Edge,* 10**,** 79-81.

PRESS, F. & EWING, M. 1951a. Propagation of elastic waves in a floating ice sheet. *Eos, Transactions American Geophysical Union,* 32**,** 673-678.

PRESS, F. & EWING, M. 1951b. Theory of Air-Coupled Flexural Waves. *Journal of Applied Physics,* 22**,** 892-899.

PROUBASTA, D. 1985. Ice saw-An incisive solution to seismic noise. *The Leading Edge,* 4**,** 18-23.

RAYLEIGH, L. 1885. On waves propagated along the plane surface of an elastic solid. *Proceedings of the London Mathematical Society,* 17**,** 4-11.

REICHMUTH, C., HOLT, M. M., MULSOW, J., SILLS, J. M. & SOUTHALL, B. L. 2013. Comparative assessment of amphibious hearing in pinnipeds. *Journal of Comparative Physiology A,* 199**,** 491-507.

RENDLEMAN, C. & LEVIN, F. K. 1990. Seismic exploration on a floating ice sheet. *Geophysics,* 55**,** 402-409.

RICE, S. L., DUDLEY, T., SCHNEIDER, C., PIERCE, R. J., HORN, B., CAMERON, S., BLOOR, R. & ZHOU, Z.-Z. 2013. Arctic seismic acquisition and processing. *The Leading Edge,* 32**,** 546-554.

RICHARDSON, W. J., GREENE JR, C. R., MALME, C. I. & THOMSON, D. H. 1995. *Marine mammals and noise*, Academic press.

ROVETTA, D., MAZZUCCHELLI, P., DEL MOLINO, G. & SANDRONI, S. Flexural Ice Wave: modelling by analytical approach. 2009 SEG Annual Meeting, 2009a. Society of Exploration Geophysicists.

ROVETTA, D., MAZZUCCHELLI, P., DEL MOLINO, G. & SANDRONI, S. Parsimonious Flexural Ice Wave Modelling in Complex Media. 71st EAGE Conference and Exhibition incorporating SPE EUROPEC 2009, 2009b. European Association of Geoscientists and Engineers.

RYPDAL, C., LIPPETT, D., HEDGELAND, D., BAKER, S. & LIE, F. Methods for Efficient and Safe 3D Seismic Acquisition in Arctic Conditions. OTC Arctic Technology Conference, 2012. Offshore Technology Conference.

SATO, R. 1967. Attenuation of seismic waves. *Journal of Physics of the Earth,* 15**,** 32-61.

SCHENK, C. J., BROWNFIELD, M., CHARPENTIER, R., COOK, T., GAUTIER, D., HIGLEY, D., KIRSCHBAUM, M., KLETT, T., PITMAN, J. & POLLASTRO, R. 2012. An estimate of undiscovered conventional oil and gas resources of the world, 2012. *USGS Fact Sheet,* 3028.

SCREEN, J. A. & SIMMONDS, I. 2010. The central role of diminishing sea ice in recent Arctic temperature amplification. *Nature,* 464**,** 1334-1337.

SEABED GEOSOLUTIONS. 2015. *Trilobit* [Online]. Available: http://www.seabed-geo.com/sites/default/files/downloads/Trilobit%20Spec%20Sheet%202014%20US%20LoRez.pdf [Accessed 23.05 2017].

SERCEL. 2016. *Marine sources* [Online]. Available: http://www.sercel.com/products/Lists/ProductSpecification/MarineSources_brochure_Sercel_EN.pdf [Accessed 23.05 2017].

SHARPE, J. A. 1942. The production of elastic waves by explosion pressures. I. Theory and empirical field observations. *Geophysics,* 7**,** 144-154.

SHOCKLEY, R. C., NORTHROP, J., HANSEN, P. G. & HARTDEGEN, C. 1982. SOFAR propagation paths from Australia to Bermuda: Comparison of signal speed algorithms and experiments. *The Journal of the Acoustical Society of America,* 71**,** 51-60.

SOCCO, L. V., FOTI, S. & BOIERO, D. 2010. Surface-wave analysis for building near-surface velocity models—Established approaches and new perspectives. *Geophysics,* 75**,** 83-102.

SOUTHALL, B. L., BOWLES, A. E., ELLISON, W. T., FINNERAN, J. J., GENTRY, R. L., GREENE JR, C. R., KASTAK, D., KETTEN, D. R., MILLER, J. H. & NACHTIGALL, P. E. 2007. Marine Mammal Noise Exposure Criteria: Initial Scientific Recommendations. *Aquatic mammals,* 33**,** 411-509.

STEEPLES, D. W., SCHMEISSNER, C. M. & MACY, B. K. 1995. The evolution of shallow seismic exploration methods. *Journal of Environmental and Engineering Geophysics,* 1**,** 15-24.

STEIN, P. J., EUERLE, S. E. & PARINELLA, J. C. 1998. Inversion of pack ice elastic wave data to obtain ice physical properties. *Journal of Geophysical Research: Oceans,* 103**,** 21,783-21,793.

STEWART, R. R., GAISER, J. E., BROWN, R. J. & LAWTON, D. C. 1999. Converted-wave seismic exploration: a tutorial. *CREWES Res Rep,* 11.

TEN KROODE, F., BERGLER, S., CORSTEN, C., DE MAAG, J. W., STRIJBOS, F. & TIJHOF, H. 2013. Broadband seismic data—The importance of low frequencies. *Geophysics,* 78**,** 3-14.

TOLSTOY, M., DIEBOLD, J., WEBB, S., BOHNENSTIEHL, D., CHAPP, E., HOLMES, R. & RAWSON, M. 2004. Broadband calibration of R/V Ewing seismic sources. *Geophysical Research Letters,* 31.

TOUGAARD, J., HENRIKSEN, O. D. & MILLER, L. A. 2009. Underwater noise from three types of offshore wind turbines: Estimation of impact zones for harbor porpoises and harbor seals. *The Journal of the Acoustical Society of America,* 125**,** 3766-3773.

TRUPP, R., HASTINGS, J., CHEADLE, S. & VESELY, R. 2009. Seismic in arctic environs: Meeting the challenge. *The Leading Edge,* 28**,** 936-942.

UNIVERSITY OF RHODE ISLAND & MARINE ACOUSTICS INC. 2013. *Cylindrical vs. Spherical Spreading* [Online]. Available: http://www.dosits.org/science/advancedtopics/spreading/ [Accessed 12.04 2017].

VENOSA, A. & HOLDER, E. 2007. Biodegradability of dispersed crude oil at two different temperatures. *Marine pollution bulletin,* 54**,** 545-553.

WARD, W. D. 1968. Proposed damage-risk criterion for impulse noise (gunfire). DTIC Document.

WEF & CERA 2012. Energy for Economic Growth Energy Vision Update 2012. World Economic Forum & IHS CERA.

ZIOLKOWSKI, A., PARKES, G., HATTON, L. & HAUGLAND, T. 1982. The signature of an air gun array: Computation from near-field measurements including interactions. *Geophysics,* 47**,** 1413-1421.

Appendix I – MATLAB scripts

A number of MATLAB scripts were written specifically for use in the work with this thesis. The scripts included functions included in the MATLAB add-on SeisLab 3.01. The scripts that were written were the following:

'shotplot.m': Plots a common shot plot for a specified shot. Also plots frequency spectrum if requested.

'receiverplot.m': Plots a common receiver plot for a specified receiver. Also plots frequency spectrum if requested.

'shotdepths.m': Plots common shot plots and frequency spectra for shots from several depths to be able to compare these.

'receiverdepths.m': Plots common receiver plots and frequency spectra for receivers at several depths to be able to compare these.

'pressuretime.m': Converts amplitudes to pressure values and plots pressure versus time for specified shots.

'receiverpressure.m': Converts amplitudes to pressure values and plots pressure versus time for specified receivers.

'SPL.m': Computes maximum and minimum pressure values at all receivers for all detonating cord shots, and uses this p-p pressure to compute sound pressure level at each receiver for each detonating cord shot.

'SPLairgun.m': Computes maximum and minimum pressure values at all receivers for all air gun shots, and uses this p-p pressure to compute sound pressure level at each receiver for each air gun shot.

'SEL.m': Computes rms pressure at all receivers for all detonating cord shots. Uses this to compute the sound exposure level at each receiver for all detonating cord shots.

'SELairgun.m': Computes rms pressure at all receivers for all air gun shots. Uses this to compute the sound exposure level at each receiver for all air gun shots.

'AlogR.m': Uses linear regression to compute a source level P(s) and a propagation loss constant A for each node 17 air gun shot. Plots a figure showing the best fit values, versus the recorded sound pressure levels P(r) and distances from source to receiver.

Anyone interested in gaining access to these scripts are welcome to contact: helene_stemland@hotmail.com.

Appendix II – Shot list

Parts of the Excel file SP-list-Svea-2016. Only ordinary detonating cord and air gun shots are included in this table. Shots that did not fire properly (internal time break) are excluded.

Shot number (of total)	Ordinary det.cord/air gun shot number	Timebreak	Comment	Source position	Source depth	Source size	Air gun pressure (bar)
54	1	Sat Mar 12 10:54:31 CET 2016	Ordinary line, shooting through the spread	Node 1	0 m	Det.cord 5 m	
55	2	Sat Mar 12 10:59:43 CET 2016	"	Node 2	0 m	"	
56	3	Sat Mar 12 11:04:07 CET 2016	" time error (shot at 6 s)	Node 3	0 m	"	
57	4	Sat Mar 12 11:06:59 CET 2016	" time error (shot at 4 s)	Node 4	0 m	"	
58	5	Sat Mar 12 11:20:17 CET 2016	"	Node 5	0 m	5 m	
59	6	Sat Mar 12 11:23:09 CET 2016	"	Node 6	0 m	"	
60	7	Sat Mar 12 11:24:54 CET 2016	" time error (shot at 3 s)	Node 7	0 m	"	
61	8	Sat Mar 12 11:26:51 CET 2016	"	Node 8	0 m	"	
62	9	Sat Mar 12 11:28:33 CET 2016	" time error (shot at 4 s)	Node 9	0 m	"	
63	10	Sat Mar 12 11:30:35 CET 2016	" time error (shot at 4 s)	Node 10	0 m	"	
64	11	Sat Mar 12 11:34:17 CET 2016	"	Node 11	0 m	"	
65	12	Sat Mar 12 11:43:14 CET 2016	"	Node 12	0 m	"	
67	13	Sat Mar 12 11:46:25 CET 2016	"	Node 13	0 m	5 m	
68	14	Sat Mar 12 11:49:37 CET 2016	" time error (shot at 5 s)	Node 14	0 m	"	

69	15	Sat Mar 12 11:51:47 CET 2016	"	Node 15	0 m	"	
70	16	Sat Mar 12 12:02:38 CET 2016	" 25 m offline	Node 16	0 m	"	
71	17	Sat Mar 12 12:04:41 CET 2016	" 25 m offline	Node 17	0 m	"	
72	18	Sat Mar 12 12:09:00 CET 2016	" 25 m offline	Node 19	0 m	"	
73	19	Sat Mar 12 12:11:44 CET 2016	"	Node 20	0 m	"	
74	20	Sat Mar 12 13:35:21 CET 2016	"	Node 21	0 m	"	
75	21	Sat Mar 12 13:37:14 CET 2016	"	Node 22	0 m	"	
76	22	Sat Mar 12 13:39:36 CET 2016	"	Node 23	0 m	"	
77	23	Sat Mar 12 13:48:31 CET 2016	"	Node 24	0 m	"	
78	24	Sat Mar 12 13:50:51 CET 2016	"	Node 25	0 m	"	
79	25	Sat Mar 12 13:52:41 CET 2016	"	Node 26	0 m	"	
81	26	Sat Mar 12 13:56:42 CET 2016	"	Node 27	0 m	5 m	
82	27	Sat Mar 12 14:00:15 CET 2016	" time error (shot at 9 s)	Node 28	0 m	5 m	
83	28	Sat Mar 12 14:04:40 CET 2016	"	Node 29	0 m	5 m	
84	29	Sat Mar 12 14:07:04 CET 2016	"	Node 30	0 m	"	
85	30	Sat Mar 12 14:09:10 CET 2016	"	Node 31	0 m	"	
86	31	Sat Mar 12 14:11:15 CET 2016	" time error (shot at 6 s)	Node 32	0 m	"	
87	32	Sat Mar 12 14:13:40 CET 2016	"	Node 33	0 m	"	

88	33	Sat Mar 12 14:17:55 CET 2016	"	Node 34	0 m	"	
89	34	Sat Mar 12 14:21:03 CET 2016	"	Node 35	0 m	"	
90	35	Sat Mar 12 14:23:59 CET 2016	"	Node 36	0 m	"	
91	36	Sat Mar 12 14:26:27 CET 2016	"	Node 37	0 m	"	
92	37	Sat Mar 12 14:29:09 CET 2016	"	Node 37 + 50 m	0 m	Det.cord 10m	
93	38	Sat Mar 12 14:32:15 CET 2016	"	Node 37 + 100 m	0 m	"	
94	39	Sat Mar 12 14:34:33 CET 2016	"	Node 37 + 150 m	0 m	"	
95	40	Sat Mar 12 14:37:01 CET 2016	"	Node 37 + 200 m	0 m	"	
96	41	Sat Mar 12 14:39:57 CET 2016	"	Node 37 + 250 m	0 m	"	
97	42	Sat Mar 12 14:46:26 CET 2016	"	Node 37 + 250 m	0 m	Det.cord 12.5m	
98	43	Sat Mar 12 14:52:51 CET 2016	"	Node 37 + 250 m	0 m	"	
99	1	Sat Mar 12 15:48:40 CET 2016	Air gun shots	Node 17	5 m	30 cu.inch	122
100	2	Sat Mar 12 15:49:20 CET 2016	"	Node 17	5 m	30 cu.inch	118
101	3	Sat Mar 12 15:50:34 CET 2016	"	Node 17	5 m	30 cu.inch	110
102	4	Sat Mar 12 15:51:16 CET 2016	"	Node 17	5 m	30 cu.inch	100
103	5	Sat Mar 12 15:55:25 CET 2016	"	Node 17	5 m	30 cu.inch	160
104	6	Sat Mar 12 15:57:17 CET 2016	"	Node 17	3 m	30 cu.inch	160
105	7	Sat Mar 12 15:58:10 CET 2016	"	Node 17	3 m	30 cu.inch	160

106	8	Sat Mar 12 15:58:45 CET 2016	"	Node 17	3 m	30 cu.inch	160
107	9	Sat Mar 12 15:59:35 CET 2016	"	Node 17	3 m	30 cu.inch	160
108	10	Sat Mar 12 16:00:14 CET 2016	"	Node 17	3 m	30 cu.inch	160
109	11	Sat Mar 12 16:08:22 CET 2016	"	Node 17	3 m	30 cu.inch	150
110	12	Sat Mar 12 16:09:22 CET 2016	"	Node 17	3 m	30 cu.inch	145
111	13	Sat Mar 12 16:10:16 CET 2016	"	Node 17	3 m	30 cu.inch	140
112	14	Sat Mar 12 16:11:10 CET 2016	"	Node 17	3 m	30 cu.inch	130
113	15	Sat Mar 12 16:11:53 CET 2016	"	Node 17	3 m	30 cu.inch	130
114	16	Sat Mar 12 16:19:15 CET 2016	"	Node 17	5 m	30 cu.inch	150
115	17	Sat Mar 12 16:20:18 CET 2016	"	Node 17	5 m	30 cu.inch	150
116	18	Sat Mar 12 16:20:59 CET 2016	"	Node 17	5 m	30 cu.inch	150
117	19	Sat Mar 12 16:22:12 CET 2016	"	Node 17	5 m	30 cu.inch	150
118	20	Sat Mar 12 16:23:03 CET 2016	"	Node 17	5 m	30 cu.inch	150
119	21	Sat Mar 12 16:24:27 CET 2016	"	Node 17	5 m	30 cu.inch	130
120	22	Sat Mar 12 16:25:22 CET 2016	"	Node 17	5 m	30 cu.inch	100
121	23	Sat Mar 12 16:26:35 CET 2016	"	Node 17	5 m	30 cu.inch	90
122	24	Sun Mar 13 12:39:51 CET 2016	"	Node 1 - 50 m	3 m	30 cu.inch	150
123	25	Sun Mar 13 12:43:05 CET 2016	"	Node 1 - 50 m	3 m	30 cu.inch	150

124	26	Sun Mar 13 12:45:01 CET 2016	"	Node 1 - 50 m	3 m	30 cu.inch	150
125	27	Sun Mar 13 12:47:34 CET 2016	"	Node 1 - 50 m	1.5 m	30 cu.inch	150
126	28	Sun Mar 13 12:48:22 CET 2016	"	Node 1 - 50 m	1.5 m	30 cu.inch	150
127	29	Sun Mar 13 12:50:47 CET 2016	"	Node 1 - 50 m	1.5 m	30 cu.inch	150
128	30	Sun Mar 13 12:56:42 CET 2016	"	Node 1 - 50 m	1.5 m	30 cu.inch	140
129	31	Sun Mar 13 12:58:17 CET 2016	"	Node 1 - 50 m	1.5 m	30 cu.inch	135
130	32	Sun Mar 13 12:59:05 CET 2016	"	Node 1 - 50 m	1.5 m	30 cu.inch	130
131	33	Sun Mar 13 13:00:58 CET 2016	"	Node 1 - 50 m	3 m	30 cu.inch	120
132	34	Sun Mar 13 13:02:00 CET 2016	"	Node 1 - 50 m	3 m	30 cu.inch	118
133	35	Sun Mar 13 13:02:43 CET 2016	"	Node 1 - 50 m	3 m	30 cu.inch	110
134	36	Sun Mar 13 13:05:11 CET 2016	"	Node 1 - 50 m	3 m	30 cu.inch	110
135	37	Sun Mar 13 13:05:55 CET 2016	"	Node 1 - 50 m	3 m	30 cu.inch	100
136	38	Sun Mar 13 13:10:11 CET 2016	"	Node 1 - 50 m	3 m	30 cu.inch	155
137	39	Sun Mar 13 13:12:25 CET 2016	"	Node 1 - 50 m	1.5 m	30 cu.inch	160
138	40	Sun Mar 13 13:13:07 CET 2016	"	Node 1 - 50 m	1.5 m	30 cu.inch	160
139	41	Sun Mar 13 13:13:50 CET 2016	"	Node 1 - 50 m	1.5 m	30 cu.inch	160
140	42	Sun Mar 13 13:23:32 CET 2016	"	Node 1 - 50 m	1.5 m	30 cu.inch	160
141	43	Sun Mar 13 13:28:01 CET 2016	"	Node 1 - 50 m	1.5 m	30 cu.inch	160

142	44	Sun Mar 13 13:37:51 CET 2016	"	Node 1 - 50 m	1.5 m	30 cu.inch	160
143	45	Sun Mar 13 13:38:42 CET 2016	"	Node 1 - 50 m	1.5 m	30 cu.inch	150
144	46	Sun Mar 13 13:40:13 CET 2016	"	Node 1 - 50 m	1.5 m	30 cu.inch	150
145	47	Sun Mar 13 13:42:23 CET 2016	"	Node 1 - 50 m	3 m	30 cu.inch	140
146	48	Sun Mar 13 13:43:12 CET 2016	"	Node 1 - 50 m	3 m	30 cu.inch	135
147	49	Sun Mar 13 13:43:57 CET 2016	"	Node 1 - 50 m	3 m	30 cu.inch	130
148	50	Sun Mar 13 13:47:07 CET 2016	"	Node 1 - 50 m	3 m	30 cu.inch	130
149	51	Sun Mar 13 13:47:53 CET 2016	"	Node 1 - 50 m	3 m	30 cu.inch	120
150	52	Sun Mar 13 13:48:38 CET 2016	"	Node 1 - 50 m	3 m	30 cu.inch	110
151	53	Sun Mar 13 13:51:27 CET 2016	"	Node 1 - 50 m	1.5 m	30 cu.inch	110
152	54	Sun Mar 13 13:55:34 CET 2016	"	Node 1 - 50 m	1.5 m	30 cu.inch	160
153	55	Sun Mar 13 13:56:19 CET 2016	"	Node 1 - 50 m	1.5 m	30 cu.inch	160
154	56	Sun Mar 13 13:58:38 CET 2016	"	Node 1 - 50 m	1.5 m	30 cu.inch	160
155	57	Sun Mar 13 13:59:25 CET 2016	"	Node 1 - 50 m	1.5 m	30 cu.inch	160
156	58	Sun Mar 13 14:00:06 CET 2016	"	Node 1 - 50 m	1.5 m	30 cu.inch	160
157	59	Sun Mar 13 14:01:48 CET 2016	"	Node 1 - 50 m	3 m	30 cu.inch	160
158	60	Sun Mar 13 14:02:43 CET 2016	"	Node 1 - 50 m	3 m	30 cu.inch	160
159	61	Sun Mar 13 14:03:57 CET 2016	"	Node 1 - 50 m	3 m	30 cu.inch	160